# ZnO-based nanostructures by PLD: growth mechanism, doping and geometry

Von der Fakultät für Physik und Geowissenschaften

der Universität Leipzig

genehmigte

DISSERTATION

zur Erlangung des akademischen Grades

*Doctor rerum naturalium*

Dr. rer. nat.

vorgelegt

von M.Sc. Alexander Shkurmanov

geboren am 09.06.1991 in Seryshevo, Russland

Gutachter:  Prof. Dr. Marius Grundmann (Universität Leipzig)

Prof. Dr. Ullrich Pietsch (Universität Siegen)

Tag der Verleihung: 23.04.2018

# Bibliographic Record

Referat:

The present work covers investigation of the growth mechanism and growth kinetics of the ZnO nanowires and nanoneedles fabricated by using high-pressure pulsed laser deposition. The growth model based on the combination of four different flows of the interfacial particles is introduced. A variation of the free energy is given as a major reason of the change of the growth mechanism which appears by using different doped seed layers, growth temperature and the doping of the deposited material. A fabrication of the ultrathin nanowires with a diameter of $d \leq 10$ nm at CMOS compatible growth temperature of $T \approx 400\,°\text{C}$ is demonstrated. The diameter of these nanowires is comparable with the Bohr radius. The growth of the Al and Ga doped and undoped ZnO nanoneedles with a sharp tip was shown. The doping of the nanowires and nanoneedles can be promising for their applications. By using a patterned sapphire substrate, an unidirectional growth of the nanowires and nanoneedles was achieved. These nanostructures are tilted by $58\,°$ with respect to the surface normal.

# Contents

# CONTENTS

# Chapter 1

# Introduction

ZnO is a wide-bandgap II-VI transparent semiconductor which attracts a lot of scientific interest for more than sixty years. Its optical, electrical and piezoelectrical properties as well as its self-organized growth of quasi 1D, 2D and 3D nanostructures allow ZnO to be implemented in a variety of applications [1, 2, 3]. For ZnO, lasing is possible even for temperatures above 300 K [4]. Furthermore, ZnO can be easily etched by the technologically simple wet-chemical etching method which allows structuring of the material [5]. ZnO is non-toxic and has biocompatible properties [6] which are favorable for its application in numerous commercially available devices.

Additionally, the variety of the ZnO nanostructures supports their applications. For instance, for the piezoelectric, piezotronic and piezophototronic devices $c$-oriented elongated nanostructures such as nanowires (NWs) and nanoneedles (NNs) are required [3]. The usage of ZnO NWs for the devices is supported by the high piezoelectric constant of this material [7]. The NWs and NNs have a small diameter and high surface-to-volume ratio which is also important for a fabrication of the nanocantilevers [8], NW logic circuits [9] and field-effect transistors [10]. Quantum confinement effect is expected in the NWs with a diameter of less than 10 nm and fabrication of such ultrathin NWs is promising for quantum research applications [11]. Doping of the ZnO nanostructures allows to significantly change their properties [1, 2, 4], e.g. controlling of the band gap from 2.8 eV to 4.0 eV [12, 13]. Moreover, there are reports about an impact of the doping on the changes of the optical properties, e.g. an increase of the luminescence

# 1. INTRODUCTION

intensity of the NWs by several times [14], electrical properties, e.g. a decrease of the dopant efficiency with increasing of the doping concentration, changes of the conductivity and the transport properties [15, 16]. Some kind of dopants can change the geometrical shape of the NWs, e.g. Na-doped ZnO NWs have a narrowed tip compared to the cylindrical undoped NWs [17]. A variation of the NW fabrication temperature is important for the integration of the NWs into different devices. For instance, a fabrication temperature of $T \leq 550\,^{\circ}\mathrm{C}$ is CMOS compatible [18], i.e. this temperature does not damage the metallic contact lines.

The functionality of the NW or NN based devices strongly depends on the geometrical shape, orientation and density of the nanostructures. For instance, for the pressure sensor fabrication, thick NWs are preferred for the compressive strain, whereas thin NWs would be bend by an applied force in such device, i.e. different working principles are using for the NWs with different thickness [19]. For controlling the field emission characteristics of the NWs or NNs a tilt with respect to the surface normal is desired [20, 67]. Additionally, tilted NWs are favorable for a fabrication of asymmetric hyperbolic metamaterials [21]. For such of the application as pressure and imaging sensors, a high density array of the unidirectional NWs is desired [22].

Despite the need of ZnO NWs for different applications and a requirement of the high level of variation of the NW geometry and doping concentration, there are limited reported growth techniques and approaches for such variation [3, 25]. Among other growth techniques, the pulsed laser deposition (PLD) offers the best compromise between technical simplicity and manipulations of the NW properties [23, 24, 25]. For the PLD growth, three different free energies occur - free energy of the incoming particles, interface of the adatoms and surface of the substrate. Any change of the free energy leads to a change of the growth mechanism and kind of the obtained nanostructures [26]. Understanding of the origin of such changes is important for the tuning of the NW properties. Additionally, a model of the growth process is required for the understanding of the NW development.

A thermodynamic explanation of the difference in the growth mechanism can be done by the Gibbs model and a free energy consideration of the catalyst-free epitaxial growth [26, 27, 28, 29]. Since there are three different free energies in the PLD growth process, a change of the free energy of any of these system leads to

a shift of the epitaxial growth mechanism mode, i.e. from the Volmer-Weber one which is apparently responsible for the NW growth, to the Stranski-Krastanov, which is responsible for the growth of the honeycomb- and nanowall-like structures [26, 27, 29]. The shift of the growth mode causes the change of the growth velocity between the vertical velocity and the lateral one. The doping concentration of the income material and number of the laser pulses [2, 79], growth temperature and surface characteristics of the substrate [33, 96] are influential on the material, interfacial and surface free energies respectively [27, 28]. A development of the shape of the NWs or rather NNs can be attributed by a combination of the different flows of the particles which are deposited on the substrate but not yet crystallized. Controlling of the combination of the free energies of the different systems allows to tune a diameter of the grown NWs and therefore their optical properties [34, 35] and an increased impact of the surface near region on the luminescence properties of the ZnO NWs is observed with decreasing of the NW diameter. Controlling of the NW tilt with respect to the surface normal can be achieved by self-tilted growth of the NWs on the $m$-plane sapphire substrate [37] or by structuring of the substrate [36, 38]. The main advantage of the substrate structuring is an opportunity to obtain an unidirectional growth of the NWs or NNs.

The purpose of this work is to analyze the growth kinetics of the doped and undoped NWs and NNs and an understanding of the impact of the different growth parameters on the growth process in the terms of free energy. The NW diameter, aspect ratio and density are presented as a function of the growth temperature and the doping concentration of the seed layer. Both of these parameters have a significant influence on the growth kinetics and the results of the growth, e.g. a low density array of the NWs is observed at the growth temperature of $T \approx 950\,°\mathrm{C}$ on the undoped seed layer whereas doping of the seed layer by $x = 1\,\mathrm{at\%}$ of Ga and reduction of the growth temperature to $T \approx 400\,°\mathrm{C}$ leads to a fabrication of the high density array of well-oriented ultrathin NWs with a diameter of d $\leq$ 10 nm. A pre-structured $r$-plane bulk sapphire has been chosen as an approach in order to achieve unidirectionally grown NWs or NNs tilted with respect to the surface normal. The CL-measurements revealed the high crystalline quality of such NWs.

# 1. INTRODUCTION

The presented research is part of the project PiezoMAT in the FP7 Framework Program (grant no. 611019) funded by the European Commission. The project involves a collaboration of 8 european research institutions and companies in order to develop a high spatial resolution fingerprint sensor based on ZnO NWs. In the frame of the project, ZnO(Al,Ga) thin films prepared by chemical vapor deposition at CEA LETI (Grenoble, France) were used as seed layers for the NW growth. The growth was performed and investigated at the Universität Leipzig, Semiconductor Physics Group. The ceramic ZnO targets were prepared by Gabriele Ramm, the seed layers were deposited by low-pressure PLD chamber by Dipl.-Ing. Holger Hochmuth, the EDX measurements were done by Dipl.-Phys. Jörg Lenzner. A structuring of the $r$-plane sapphire was performed by Guy Feuillet (CEA LETI, Grenoble, France), Florian Tendille and Philippe De Mierry (CNRS-CRHEA, Valbonne, France).

In this work, the own publications are labeled as E[X] where X denotes the corresponding reference number.

# Part I

# Basics and Methods

# Chapter 2

# Basic properties and growth concept

ZnO mostly crystallizes in the hexagonal wurtzite structure at ambient pressure and temperature. In this lattice structure each Zn ion is encircled by a tetrahedra of O ions, and vice-versa. Such tetrahedral coordination causes a polar symmetry along the hexagonal axis, i.e. ZnO tends to form $c$-oriented structures with Zn-terminated (0001) or O-terminated (000$\bar{1}$) polar faces [40] (Fig. 2.1). The polarity is responsible for most of ZnO properties, i.e. piezoelectricity and spontaneous polarization [40, 41, 22]. Additionally, growth, etching and defect generation of the ZnO are determined by its polar $c$-orientation [1, 40]. These properties of the ZnO in a combination with its wide bandgap of about 3.37 eV, optical transparency in the visible spectrum range, large exciton binding energy of about 60 meV at room temperature [1], self-grown properties, opportunities for wet chemical etching, radiation hardness, biocompatibility and high melting point of $T = 1950\,°$C make the ZnO favorable semiconductor material for the fabrication of the numerous nanostructures with further integration of them in different applications [40].

There are a variety of ZnO nanostructures with different shapes which can be fabricated [2, 36], for instance:

- *Nanorings* which are are single-crystal nanoobjects with a circular shape [43]

7

## 2. BASIC PROPERTIES AND GROWTH CONCEPT
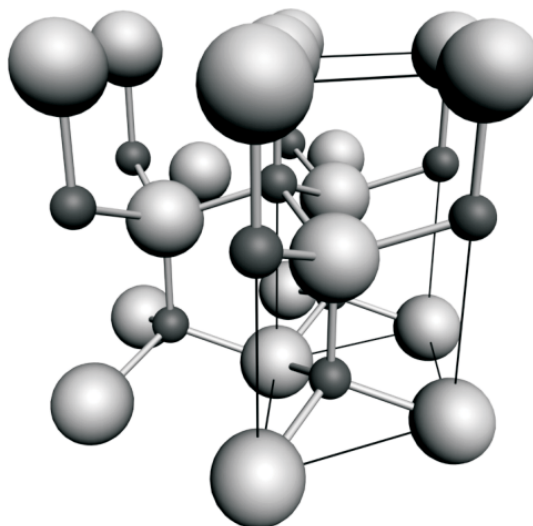
Figure 2.1: The hexagonal wurtzite structure of ZnO. Large white spheres are O atoms, small black speres - Zn atoms. Taken from [40].

- *Nanopropellers*, the dendrite-like structures which represents itself a combination of the "trunk" nanowire grown along the surface normal with perpendicular to it "branch" nanowires [43]

- *Nanotubes*, i.e. hollow tubular ZnO structures [44, 45, 46]

- *Nanohoneycombs*, the macroporous nanostructures made of a combination of the nanowalls with a pores between them [47, 48]

Nanowires (NWs) and nanoneedles (NNs) are of special interest in this work and their properties will be described later. These nanostructures can be grown by different growth methods which will be mentioned briefly later. For this research the NWs and NNs have been fabricated by using high-pressure pulsed laser deposition growth technique which will be descibed in details further. The growth can be carried out with or without catalyst. The catalytic material supports the growth process, but its presence has an impact on the purity of the nanostructures and their properties [2, 49]. Additionally, a catalyst changes the growth mechanism [26]. The different NW/NN properties, purity, geometrical shape and density is crucial for their applications. The most important NW/NN-based

applications will be discussed further in this Chapter.

## 2.1   ZnO nanowires and nanoneedles

*Nanowires*

Nanowires (NWs) or also nanorods, nanowhiskers and nanocolumns are elongated crystalline nanostructures with an aspect ratio much larger than 1. Typically, NWs have a shape of a prism or a cylinder [25]. The most of the using for the NWs fabrication growth techniques allows to obtain NWs almost without dislocations, with a high crystalline quality [25, 36, 98]. The *c*-oriented NWs are polar and can be used in the piezoelectrical applications [50].

The NW diameter plays an important role for the NW application. For instance, for the piezoelectrical investigations, thick NWs are favorable pressure application based on the compression of the NWs while thin NWs are favorable for bending application [3, 36]. At the same time, for the thin NWs the surface-to volume ratio is higher than for the thick NWs and therefore optical properties of the NWs are determined by the surface-near-region [34], E[32]. If the diameter of the NWs is $d < 10$nm, then a quantum confinement effect might appears in such wires and they are promising for quantum effects researches, e.g. topological qubits [51].

Beside the diameter and aspect ratio, the NW density is an important parameter, which determines their prospective application. A high density of the NWs is desired for the imaging sensors since the tips of the NWs are pixels of the image [22]. Also a closely packed NW array can improve light trapping and charge separation in the NW-based solar cell [38, 52]. However, for the applications based on the bending of the NWs, contacts to their facets should be performed. For these applications a low density NW array is favorable [53]. Tilting of the NW array with respect to the surface normal allows to increase a number of prospective applications of the NWs. For instance, tilted conductive NWs can be used for a fabrication of the asymmetric hyperbolic metamaterials and for optical absorbers [21]. Additionally, optical and electrical properties of the NWs might be tuned by doping [16]. If a conductive seed layer is used for the NWs growth, it might be used as a back electric contact and NWs might be applied for the CMOS

structures [3].

*Nanoneedles*

Nanoneedles (NNs) are a special kind of NWs with a pyramidal shape, i.e. they have a sharp tip and broadened base. The tip is usually observed in a few atoms in diameter [54]. Due to this shape, the NNs have high flexibility and hardness resulting from the defect-free lattice [55]. However, in contrast to the NW growth, a fabrication of the NNs is rarely reported in the literature [54]. Fabrication of the NNs is technologically challenging because of a requirement of the nonuniform growth conditions for the obtaining narrowed shape of the NNs, i.e. a gradient of the ZnO concentration in the phase from which a crystallization takes place should reduces along the seed surface normal. Remarkably, for further description of the NN geometric characteristics in the next Chapters, their diameter has been taken from the middle of the nanostructure.

A variation of the NW or rather NN geometric shape, density and the tilting angle is required for their usage in applications. However, there are numerous challenges for such obtaining different geometric properties. The ZnO particles which were crystallized on the surface of the substrate in the beginning of the growth process create a nucleation seed. This seed can be developed in two growth directions - in the vertical one or in the lateral one. The vertical growth rate should be larger than the lateral one, otherwise a thin film, a honeycomb-like or a nanowall-like structure will be fabricated instead of elongated NW or NN. For this requirement, the growth mechanism should be adjusted and a variation of the growth mechanism can be carried out in different ways which will be described in the Chapters 6 and 7.

### 2.1.1 Applications

There are numerous applications which are based on the exploitation of different properties of the doped and undoped NWs or rather NNs [2, 3]. The most typical of these application can be highlighted:

- *Light emitting diode*

  Each single NW can act as a single light emitter [36]. For instance, such device was demonstrated in Ref. [57]. The NW array grown on the p-GaN

and covered by a $SiO_2$, thin bimetallic layer of Ni/Au and a layer of indium tin oxide. This light emitting diode (LED) gives an external quantum efficiency of 2.5% and the blue and near-UV emission occurs because of distinct electron-hole recombination processes.

- *Pressure and 3D imaging sensors*

  The above mentioned LED based on ZnO NW can be implemented as a pressure sensor and reconstruct image of the distributions of strain with a high spatial resolution (Fig. 2.2). In this device, each single NW is a pixel and reading out of the electroluminescent signal from each pixel in the array allows to obtain a pressure image [22].
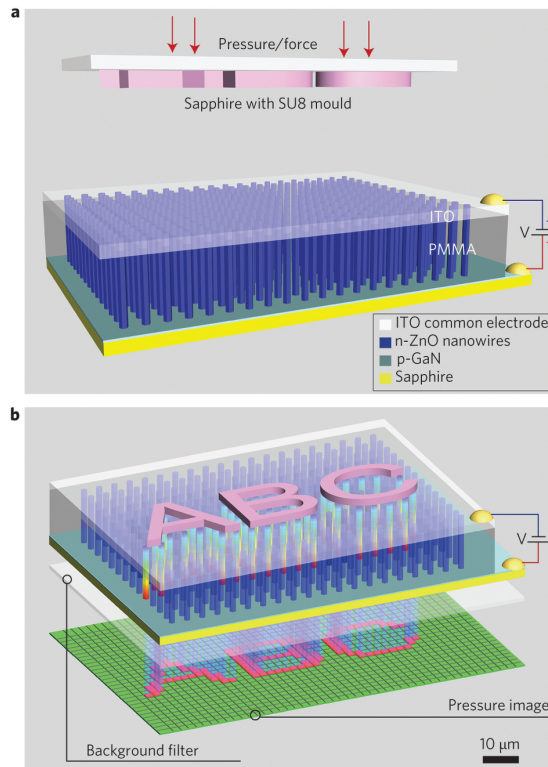


Figure 2.2: Design of the pressure sensor based on the ZnO NWs array before (a) and after (b) applying a compressive strain. Taken from [22].

A local deformation of the NWs and reconstruction of the image from the generated potentials allow to fabricate a high-resolution fingerprint sensors

11

which was the aim of the PiezoMAt project [59]. In this structure the ZnO charges are collected with top-bottom contacts. For performing such contacts, the ZnO NWs were fabricated on the conductive Ga-doped ZnO seed layer and encapsulated with a conductive polymer [60].

- *Energy harvesting cells*

  ZnO NWs can be integrated into the hybrid cell which harvests two different kinds of energy - the solar one and the energy of the ultrasonic wave simultaneously [3]. The hybrid cell integrates a dye-sensitized solar cell (DSSC) and a piezoelectric nanogenerator (NG) which should be connected face to face [62]. The main advantages of this hybrid cell are an absence of liquid electrolyte and an opportunity to transfer two different kinds of energy into the electric power.

- *Gas sensors*

  The gas sensing is a surface sensing process. In contrast to the conventional gas sensors based on thin films, the sensors based on the NWs are much sensitive even to few gas molecules because of high surface-to-volume ratio of the NWs which allows to change their electrical characteristics [63, 64]. In this sensor the ZnO NWs are integrated into the field-effect transistor (FET) as n-channel [65] (Fig. 2.3). Different gases change the conductance of the NWs differently and determination of the certain gas is possible. Efficiency of the gas sensor increases with reduction of the NW diameter.
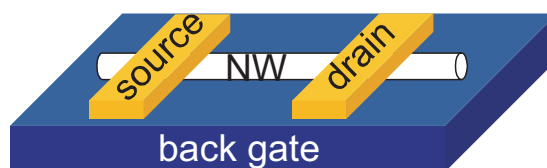


Figure 2.3: A scheme of the FET based on the ZnO NWs.

- *Probing tips for scanning probe microscope with high spatial resolution*

  The NNs are promising for the development of the probing tips since electrons are more easily emitted from sharp tips of NNs than from cylindrical

NWs as was demonstrated for the devices based on the Ga-doped NNs [55, 66, 67]. The NN fabrication temperature and the Ga-doping concentration have a strong impact on the field enhancement factor of the device [54].

## 2.2 Nanowire and nanoneedle fabrication

ZnO can be achieved by chemical or physical processes, i.e. with or without chemical reaction. Recently, the most of the known growth methods use a vapor to solid phase transfer. The growth mechanisms for the fabrication of the NWs or rather NNs can be divided by two main groups - mechanisms which require the presence of a catalyst or a catalyst free group [29]. A catalytic material change the melting and evaporation point, phase and supports a chemical reaction. However, the main disadvantage of using a catalyst are its diffusion and incorporation into the NW. In the further subsections both growth mechanisms with and without catalyst are described.

### 2.2.1 Growth mechanisms which require a catalyst

One of the most often used mechanism which requires the presence of a catalyst is the vapor-liquid-solid (VLS) one. The VLS mechanism is historically the first growth mechanism which was implemented for the growth of Si thick wires with high crystalline quality in the 1960s by Wagner and Ellis [68]. Such wires were $0.1 - 0.2$ mm thick. However, with developing of this mechanism, using of different materials including ZnO and a decrease of the diameter became possible [49]. The diameter of the NW can be controlled by a size of the metallic droplet [2, 49]. In contrast to the first experiments with the VLS mechanism for a wires fabrication, recently not only gold catalytic particles can be used but also other metals [2, 48, 69, 70, 71]. It was observed that a catalyst was essential for the growth of the wires and a small sphere was present at the tip of each wire [49]. In the VLS growth mechanism, the metallic catalyst supports the crystallization of the ZnO from the vapor phase, forming a liquid alloy at a high temperature and adsorbing ZnO vapor components. At a certain temperature and pressure

## 2. GROWTH MECHANISMS WHICH REQUIRE A CATALYST

of the vapor, the liquid alloy becomes supersaturated, i.e. concentration of the ZnO in the liquid metal is higher than the equilibrium concentration [49]. By reaching a supersaturation, the ZnO is diffused through the metal to the substrate and becomes crystallized there. However, a high applied temperature for this mechanism allows the material of catalyst to thermally diffuse into the NW. A presence of the catalytic material in the NWs can change electrical and optical properties of the NWs compared to undoped NWs [72].

Beside the VLS growth mechanism the vapor-solid-solid (VSS) one is based on the same principle of the continuous saturation and diffusion through the catalytic material, but for this mechanism the catalyst remains in the solid state, i.e. without melting of the metal [26]. The VSS mechanism allows to reduce a fabrication temperature and at the same time, makes a diffusion of the catalytic material into the growing NW difficult. However, a diffusion of the ZnO from the vapor into the catalytic material is difficult too and it might leads to a growth of non arranged structures [49]. A thermodynamical description of the VSS growth mechanism is more difficult compared to the VLS mechanism [26].

For both growth mechanisms, VLS and VSS, the saturation of the interface of the catalyst is more important for the NW fabrication than the kind of the substrate on which the NW grown. The ZnO NWs can be grown on substrates with high crystalline quality [69], polycrystalline [49] and amorphous as well [2]. However, the crystalline quality of the substrate reflects the orientation of the NW, i.e. the NWs are typically growing well-oriented vertically on the bulk substrates whereas they are frequently growing tilted with different angles with respect to the surface normal on the amorphous substrate or on the substrate with bad crystalline quality [2]. Also, the VLS and the VSS growth mechanisms are independent on the growth method - the NW can be brown by pulsed laser deposition (PLD) [23], molecular beam epitaxy (MBE), chemical vapor deposition (CVD), carbothermal growth [49]. However, a presence of the metalic sphere on the top of the NW makes an application of the NWs difficult if there is a requirement of the non-conductive tip of the NW [3].

Beside using a catalyst as an additional intermediate phase, it can also support the chemical reaction in order to obtain ZnO material. For instance, in the hydrothermal growth method mentioned in Ref. [73], a salt of $Zn(NO_3)_2$ was

mixed with different organic catalytic solutions. The ZnO particles as a product of the chemical reaction were deposited on the substrate and developed an array of NWs. For a such growth method, the VSS growth mechanism can be used as well, however the obtained NWs would be doped by materials of catalysts. For the physical growth processes such as carbothermal growth, a graphite powder is used in order to reduce the melting point of ZnO which makes a low growth process temperature possible [2, 25].

## 2.2.2   Catalyst-free epitaxial growth mechanism

In order to avoid an undesired diffusion of the catalytic material into the NWs, a catalyst free epitaxial growth mechanism can be used. Such mechanism is the most compatible with the PLD and MBE growth techniques [2, 24, 29]. In contrast to the mechanisms which require a presence of a catalyst, in the catalyst free one, an impact of the interface is significantly reduced and the result of the NW fabrication strongly depends on the type of the substrate, i.e. its surface and thermodynamical characteristics of the vapor [24, 25, 27, 29]. However, the epitaxial growth of the NWs is much complicated than the growth driven by the VLS or VSS growth mechanisms. In the case of the growth from the vapor phase which is attributed to the PLD method, the ZnO particles should be deposited on the surface of the substrate and create a crystalline cluster for the subsequent developing of it into the NW. The deposited ZnO particles (the so-called adatoms [26]) can be in one of the following states and can easily switch their state from one to another (Fig. 2.4):

1) Adatoms near the surface of the substrate or transferred from the substrate back to the vapor

2) Adatoms which are moving on the surface of the substrate

2) Adatoms which are developing a crystalline cluster

For the catalyst free epitaxial growth, the interface is all ZnO particles which were deposited on the substrate but not yet crystallized. Additionally, adatoms which are near the surface but still are in the vapor phase, might be directly transferred to the crystalline cluster i.e. being crystallized. However, due to the temperature driven diffusion, atoms in the crystalline cluster might be diffused
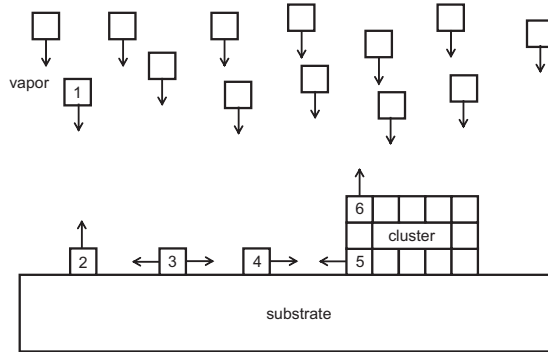
to the interface [26].



Figure 2.4: Possible positions of the interface atoms (adatoms) and transfers of the atoms from the vapor to the crystalline cluster and from the cluster to the interface: (1) deposited ZnO particles from the target, (2) transfer of the adatom to the vapor phase, (3) a moving adatom on the surface of the substrate, (4) adatom which joins the crystalline cluster, (5) a particle of the crystalline cluster which is transfered to the interface and(6) a particle of the cluster which is transfered to the vapor

## 2.3   Free energy and the growth mechanism

Since the growth process strongly depends on the properties of the vapor (pressure, temperature), surface of the substrate and the interface (kinetic energy of the moving particles), the free energy consideration should be taken into account [26, 27, 29]. However, this consideration requires the non-equilibrium thermodynamic conditions of the vapor and the interface [27]. Otherwise a phase transfer would be impossible. This requirement means that the ZnO vapor should be supersaturated for a deposition of the particles on the substrate. At the same time, the number of the particles which are deposited on the substrate should be larger than the number of the particles which are returned back to the vapor [26]. For the growth of the NWs by PLD process, these requirements are satisfied.

According to Ref. [29] and [74], the free energy determines the type of the developing nanostructure and the resulting epitaxial growth mechanism. The difference between the free energies can be written as

$$\Delta F = F_m + F_i - F_s, \tag{2.1}$$

where $F_m$ represents the free energy of material which is deposited on the substrate, $F_i$ - the free energy of the interface and $F_s$ - the free energy of the surface.

There are three different epitaxial growth mechanism modes which depend on the sign of the free energy. These growth mechanism modes are schematically presented in Fig. 2.5. In the case of $\Delta F < 0$ the Frank-van der Merwe mode will dominate (Fig. 2.5a). The effect of this mode leads to the consecutive step-by-step growth of relatively smooth thin films [75, 76]. For this mode, the free energy of the surface is larger than the sum of the interfacial free energy and the free energy of the deposited material. This situation might occur if the number of the adatoms is small and almost all particles which are deposited on the substrate are integrated into the crystalline cluster and only a negligible number of the clustered particles escapes from the interface. The Frank-van der Merwe mode is typically observed if the temperature of the surface of the substrate is low and thus the probability to create a crystalline seed for further developing of it into the crystalline cluster is increased [26, 27, 74]. In this case, for most of the deposited particles the crystallization is energetically much favorable than remaining at the interface. For the Frank-van der Merwe growth mode, the lateral growth rate is much larger than the vertical one, i.e. a covering of the surface is more attractive for the crystalline structure than the growth in vertical direction.
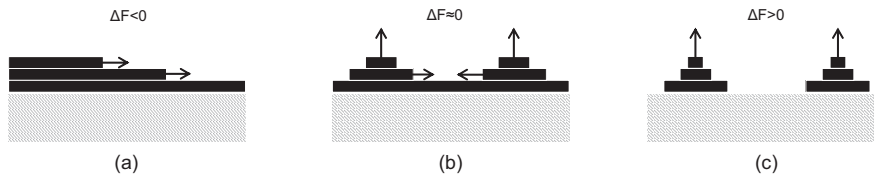


Figure 2.5: The epitaxial growth modes and the structures which can be grown by them: (a) The Frank-van der Merwe mode and step-by-step growth of the thin films (b) the Stranski-Krastanov mode and interconnected islands (c) Volmer-Weber mode and the separated islands

In the case of $\Delta F \approx 0$, a sum of the material free energy and interfacial free

## 2. FREE ENERGY AND THE GROWTH MECHANISM

energy is almost equal to the surface free energy and the Stranski-Krastanov epitaxial growth mode takes place (Fig. 2.5b). This growth mode can be described as the development of the crystalline cluster in both vertical and lateral directions. This situation occurs if the vapor is more saturated than the vapor in the Frank-van der Merwe mode. A movement of the deposited particles on the substrate is supported. Such support might be achieved if the surface of the substrate is smooth with a low number of the surface defects and does not disturb a movement of the interfacial particles. Furthermore, the interfacial movement can be enhanced by increasing of the thermal energy ($E = k_B T$), i.e. by increasing of the growth temperature. After the deposition, adatoms receiving the thermal energy from the substrate which is transfered into their kinetic energy and the adatoms start to move on the surface. Such movement is possible until they will lose an excess of the kinetic energy and will be integrated into the crystalline cluster. Since the Maxwell-Boltzmann distribution of the kinetic energy, some deposited particles have a quite low energy compared to the most of the particles [126]. The low energy particles can be chemisorbed immediately after the deposition and create the crystalline clusters. These clusters are the nucleation seeds for further development into the nanostructures [29]. However, these seeds are obstacles for the movement of the rest of the particles and after collisions with the seeds the moving particles lose their energy and can also crystallize. Some of the high energy particles are able to reach the top of the seeds and crystallize there. After continuous collisions and movements, the initial crystalline clusters are developing in both vertical and lateral growth direction simultaneously. The Stranski-Krastanov mode might be a possible reason of the growth of the honeycomb- and nanowall-like structures [47, 77]. Note, the vertical growth might have a limit and with continued deposition of the particles they prefer to connect the 3D structures together and the growth of relatively smooth thin film is fabricated [78]. This limit might occur since the energy which is required for the deposited particle to reach the top of the nanostructure enhances with the length of the nanostrucure.

In the case of the positive sign of the free energy ($\Delta F > 0$, i.e. $F_m + F_i \gg F_s$), the Volmer-Weber mode is appearing in the growth process (Fig. 2.5c). For this mode the nucleation seeds are developing mostly in the vertical diraction rather

the lateral one. This growth mode is typical for the VLS growth since a catalyst plays a role of the interface and thus supports the NW growth. For the catalyst-free epitaxial growth, this situation might be achieved by using a smooth substrate with high crystalline quality and non-tilted grains. Additionally, the Volmer-Weber mode can be obtained by increasing of the material and/or interfacial free energy. However, for the PLD technique there are limitations for the pressure and temperature of the vapor of the deposited material [29]. Thus, an increase of the impact of the interface on the growth process seems the most prominent way in order to achieve growth process governed by the Volmer-Weber mode. Thereby, increase of the interfacial free energy might indicate an increase of the number of adatoms which are deposited on the surface of the substrate. These adatoms should have a high kinetic energy for their movement on the substrate. At the same time, the moving particles should be able to climb over the seeds and be crystallized there. It is important that a number of the adatoms which are leaving the substrate and returning back to the vapor should be neglectable small [26, 29]. Probably, the NWs and the NNs are growing by the Volmer-Weber mode, since these nanostructures are developed mostly in the vertical direction.

For a consideration of the material free energy, a thermodynamic explanation by the Gibbs model can be used [26]. Such model associates the free energy of the depositing material with thermodynamic parameters of the vapor (pressure, temperature). In the simplest growth process, where particles of the vapor are deposited on the substrate and immediately crystallized without having an interface, the the vapor is supersaturated, i.e. the non-equilibrium thermodynamic requirement of the crystallization is satisfied. This situation can be described by a difference of the chemical potential

$$\Delta\mu = \mu_v - \mu_c = k_B \Delta T ln\zeta, \tag{2.2}$$

The $\mu_v$ is a chemical potential of the vapor and the $\mu_c$ is a chemical potential of the crystalline seed, $\Delta T$ represents a supercooling of the vapor and $\zeta$ represents a supersaturation. The difference of the chemical potential $\Delta\mu$ is the driving force of the crystallization [26]. This difference of the chemical potential is related to the free energy and for the desired Volmer-Weber mode (i.e. with small $F_s$) can

## 2. FREE ENERGY AND THE GROWTH MECHANISM

be written by

$$\Delta F^* \sim N \Delta \mu, \tag{2.3}$$

where $\Delta F^* = F_m + F_i$, N is the number of the particles which were crystallized from the vapor and created a nucleation seed. For the crystallization from the vapor the logarithm of the supersaturation is $ln\zeta \approx \zeta$ [26]. The supersaturation can be written by

$$\zeta = \frac{(p - p_0)}{p_0}, \tag{2.4}$$

with the equilibrium pressure of infinitely large condensed phase $(p_0)$ and the partial pressure of the system $(p)$.

The supercooling is related to the temperature of the surface $(T)$ and the temperature of the vapor $(T_0)$, i.e.

$$\Delta T = \frac{T - T_0}{T_0} \tag{2.5}$$

By using Eq. 2.4 and 2.5 the chemical potential can be written as

$$\Delta \mu = k_B \frac{T - T_0}{T_0} \frac{p - p_0}{p_0} \tag{2.6}$$

Therefore, by using Eq. 2.6 the free energy can be related to the temperature and pressure as

$$\Delta F^* \sim N k_B \frac{T - T_0}{T_0} \frac{p - p_0}{p_0} \tag{2.7}$$

According to Eq.2.7, required for the NW growth the Volmer-Weber mode appears in the case of both positive or both negative factors. The supersaturation can be adjusted by a variation of the volume or mass of the vapor. Since for the PLD growth which is used in this work, the volume of the vapor is constant, the supersaturation strongly depends on the mass of the particles in the vapor. There are numerous growth parameters which can change the supersaturation, however, adding of the atoms which have different mass than Zn or O is the most promising way to enhance the supersaturation. The supercooling of the vapor in

the PLD process can be changed by a variation of the energy of the laser pulses. However, there are limits for applied energy of the pulses since the NWs can be fabricated by using a narrow range of the pulse energy [2, 23, 79]. Thus, a change of the growth mechanism mode is difficult by a variation of the supersaturation and/or the supercooling.

The surface free energy seems responsible for the lateral growth rate if the sum of $F_m + F_i = const$. The choice of the substrate material [28], its crystallographic orientation [80], surface defects, surface roughness, unperfect crystalline quality of the substrate or non-crystalline substrate, tilted grains [26, 29] are obstacles for a moving deposited particles which can collide with the surface defects. However, such defects are potential places for a crystallization and play a sufficient role for a creation of the crystalline nucleation seeds [81].

The interfacial free energy strongly depends on the number of the adatoms on the surface [82]. Most of the growth techniques based on the growth from a vapor phase including PLD technique, allow to enhance or reduce the number of moving particles via tuning of the temperature of the substrate. High growth temperature probably leads to an increase of the interface component of the free energy and the Volmer-Weber mode is possible. A low growth temperature reduces the thermal energy and the kinetic energy of the adatoms. The adatoms with low kinetic energy cannot reach the top of the nucleation seeds and crystallized on the sides of them, i.e. lateral growth rate is more significant than the vertical one. At the same time, a small number of the adatoms and their low kinetic energy indicates a small impact of the interfacial free energy on the growth process.

The epitaxial growth driven by any growth mode starts from the nucleation process. There are two main kinds of the nucleation - homogeneous one and the heterogeneous process [26, 83]. The schemes of the different nucleations are shown in Fig. 2.6. The homogeneous nucleation is a creation of the nucleation seeds with the same material and the same purity as the substrate. This kind of nucleation is typical for the growth of undoped ZnO NWs on the undoped ZnO seed layer. Such process requires high energy and involves the most of the deposited particles in formation of the nucleation seed. The heterogeneous process is a formation of the seeds with presence of two or more different phases. This kind of nucleation is typical for the growth of undoped ZnO NWs on the doped seed layers (since

the dopants can be located on the surface as shown in Fig. 2.6e), doped NWs on the undoped seed layers (since the dopants of the deposited material can form the clusters of the additional phase with respect to the ZnO phase) and doped NWs on the doped ZnO seed layers. The presence of the additional phase reduces the required nucleation energy and the seeds in the heterogeneous nucleation are usually smaller than for the homogeneous process [26, 83].
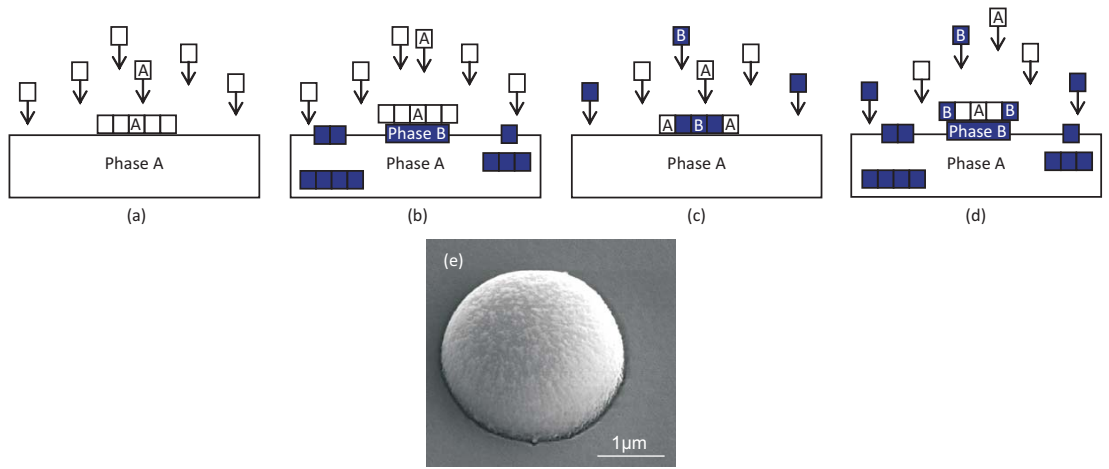


Figure 2.6: Homogeneous nucleation of the undoped material on the substrate made of the same material (a), Heterogeneous nucleations: undoped deposition on the the doped substrate (b), a deposition of the doped material on the undoped substrate (c) and deposition of the doped material on the doped substrate (d). An example of the dopant on surface of the Al-doped ZnO seed layer (e)

## 2.4 NW growth techniques

NWs can be grown by different growth techniques which involve chemical or physical principles of the NW fabrications. The desired growth mechanism, supersaturation and supercooling are achieved in different ways for different growth techniques by using catalyst, background pressure, transport gas, temperature [26, 29]. In this work PLD was used for a fabrication of the NWs and the seed layers. This growth technique represents a trade off between technical simplicity and the opportunities to adjust the NW properties [23, 24, 25] and will be

described in details in the Chapter 3. In this Section several other growth techniques will be discussed such as carbothermal evaporation, hydrothermal growth and molecular beam epitaxy which are the most typical growth techniques for the NW fabrication. The typical geometric parameters of the ZnO NWs fabricated by different growth techniques are presented in Table 2.1

*Carbothermal evaporation*

The growth of the micro- and nanowires via vapor-phase reactions is well known since several decades [84, 85]. The carbothermal evaporation is a vapor-phase transport technique when a carbon is used for a reduction of the melting point [2]. Thus, a phase transfer from vapor to crystalline structure is possible and crystallization occurs at the temperature of $T \approx 1000\,°C$ when the reaction of the carbon with ZnO takes place [86]. Usually, a mixture of ZnO with carbon (usually as a graphite) with a mass ratio $1:1$ is located in a horizontal quartz tube with a furnace. In this chamber the temperature, pressure and the evaporation time are controlled. The particles can be transfered with an Ar flow to the substrate and be crystallized there into the micro- and nanowires or the wires can be grown directly in the source [2]. Adding of the dopants such as Al into the mixture allows to grow nanobridges and nanonails [88] or nanosheets and nanowalls [48].

In the Fig. 2.7 a scheme of the setup for the NWs growth by carbothermal evaporation is presented which is based on the chamber used in the Universität Leipzig [2, 87]. The chamber consists of a heater with a quartz tube inside. The main advantages of the carbothermal growth is technical simplicity and accessibility whereas using of the carbon and its diffusion into the NWs is the disadvantage of this growth method.
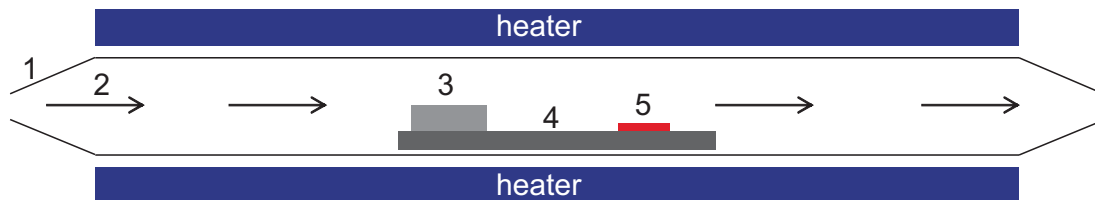


Figure 2.7: Schematic setup of the chamber for the NWs growth by carbothermal evaporation technique. (1) the quartz tube inside the heater, (2) transport gas flow, (3) source, (4) ceramic slat, (5) substrate.

## 2. NW GROWTH TECHNIQUES

*Hydrothermal growth*

This technique is based on the decomposition or hydrolysis of zinc salts with further formation of ZnO colloids in aqueous solution with further deposition on the substrate and fabrication of the NWs [52, 89, 90]. The hydrothermal growth allows to obtain NWs at relatively low temperature (in a range from room temperature to $T \approx 100\,°$C) using atmospheric pressure on crystalline or amorphous kinds of substrate [91]. There are a lot of different zinc salts which can be used for the NWs fabrications, e.g. zinc nitrate hexahydrate [91], zinc acetate dihydrate [52], zinc chloride [92]. The choice of the salt is crucial for the aspect ratio of the NWs [89]. An aqueous solution of the salt with a distilled water should be performed and the substrate should be located in the solution. However, this process is time consuming and can take several days [52]. Moreover, a presence of other chemical elements in the process can be reflected on the purity of the NWs and their doping concentration is uncontrolled.

*Molecular beam epitaxy*

The NW growth by Molecular Beam Epitaxy (MBE) is a process based on the physical deposition, i.e. this technique does not use any chemical reaction of the components [93]. For achieving epitaxial growth by this method, a high vacuum is required in order to avoid the presence of other substances in the chamber and collision of them with ZnO particles during the process. Moreover, in contrast to the PLD, the source materials are not initially mixed, i.e. Zn, $O_2/O_3$ sources and doping material (Al, Ga, etc. if required) are located separately and a fabrication of the ZnO or doped ZnO occurs in the vapor phase. Pure Zn metal, which is evaporated from an oven toward the substrate is mixed with atomic oxygen derived from a plasma or ozone source [94]. The substrate should be warmed up to $T \approx 700\,°$C and the deposited ZnO particles receive a sufficient energy for their movement on the surface with further creation and developing the nucleation seeds [95]. However, the disadvantage of the MBE technique is its technological complexity of controlling of the molecular beams.

## 2.5 Aligned tilted growth

There are few reported approaches which allow to grow NWs tilted with respect to the surface normal (Fig. 2.8):

*Self-tilted growth*

In Ref. [37] a growth of tilted NWs on the $m$-plane sapphire substrate of it is reported (Fig. 2.8a). For this growth no catalyst was used and the fabrication was done by pulsed laser deposition. The obtained NWs are tilted with an angle of about $\pm 30°$ with respect to the surface normal. However, these NWs are bidirectionally tilted. The diameter, aspect ratio and crystal quality of such NWs are controllable during the growth process by variation of the growth parameters (number of applied pulses, contain and pressure of the ambient gas, etc [2, 23]).

*Growth of laterally horizontally NWs*

Structuring of the substrate and covering of it by a combination of the material which suppress and support NW growth allow to fabricate them with a horizontal alignment [36, 56] (Fig. 2.8b). In doing so, a Si wafer is covered by ZnO stripes with Cr layer on the top of them. The obtained structured substrate was located in a reservoir with zink salt aqueous solution for a hydrothermal growth. The Cr layer is incompatible for the NW growth and no NWs are observed on the top of this layer. Also, almost no NWs were grown on the Si parts of the substrate. At the same time, the underlying ZnO stripes supports the NW growth. Thus the NWs were obtained parallel to the surface of the substrate.

*Unidirectional growth on the pre-structured substrates*

Yang *et al*[38] reported about a method which allows to grow locally unidirectional and tilted NWs. For this method, the Si (100) substrate was be preliminarily structured. In doing so, the substrate was etched in order to achieve a periodic set of tilted Si facets. Furthermore, the entire substrate was covered by a thin ZnO film which is a seed layer and support the NW fabrication. Thus on these structures a high density NW growth is observed. However, the obtained facets are equally compatible for the NW growth. An application of these NWs can be difficult. A selective unidirectional growth on the pre-structured substrate is desired. This growth in mentioned in the Chapter 8.
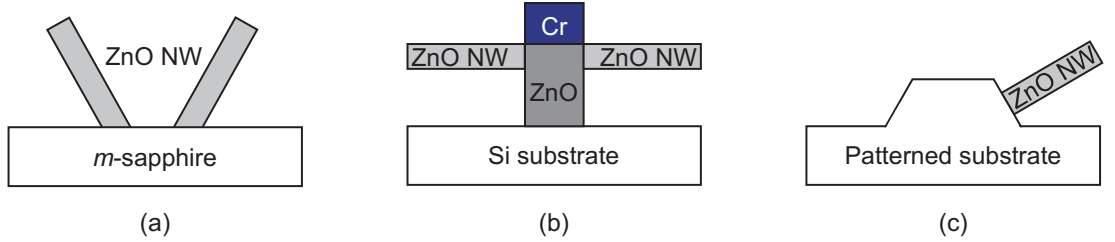
Figure 2.8: Approaches for the tilted NW growth: (a) self-tilted growth on $m$-plane sapphire substrate, (b) structuring of the substrate and using a combination of the materials which can suppress and support the NW growth, (c) unidirectional growth of tilted NWs on the pre-structured substrate

Table 2.1: Typical geometric parameters of the ZnO NWs grown by different methods

| Parameter | Carbothermal [2] | Hydrothermal [52] | MBE [95] | PLD E[32] |
|---|---|---|---|---|
| Diameter (nm) | $\geq 100$ | $\geq 100$ | $\geq 15$ | 7 - 550 |
| Aspect ratio | $\geq 20$ | $\geq 5$ | 80 - 130 | 3 - 450 |
| Density ($\mu m^{-2}$) | 3 - 50 | 1 - 40 | 50 - 100 | 1 - 300 |

# Chapter 3

# Growth and characterization

A two-step growth process was used in order to obtain NWs or rather NNs. The first step is a fabrication of the ZnO(Al) and ZnO(Ga) seed layers with different concentration of the dopants, surface roughness, surface polarity and the crystalline quality. A variation of the seed layer properties gives an opportunity to control the NW growth [33, 96], E [32]. For the fabrication of the seed layers, two different growth techniques was exploited - the chemical vapor deposition (CVD) fabricated by CEA LETI within the PiezoMAT project and the low pressure pulsed laser deposition (LP PLD) used at the Universität Leipzig. The characterization techniques used for the investigation of the surface morphology, surface roughness, polarity and thickness will be discussed in this Chapter. The measurements revealed that the seed layers grown by LP PLD are smooth with high crystalline quality, whereas seed layers grown by CVD have high average surface roughness and almost all of them are polycrystalline. The characterization techniques used for the investigation of the surface morphology and the surface properties will be mentioned in the Section 3.4.

The second step is the growth of the NWs/NNs by using high-pressure pulsed laser deposition (HP PLD). The main difference between this technique and the LP PLD one is the presence of a background gas flow [23]. The geometric characteristics of the obtained nanostructures were investigated by scanning electron microscopy (SEM). In this Chapter the growth and characterization techniques are will be discussed.

## 3.1  Preparation of the seed layers by CVD

The fabrication of the Ga-doped ZnO seed layers was performed by CEA LETI by CVD in the framework of the PiezoMAT, european research project. Using of the CVD growth technique for a fabrication of the doped ZnO thin films represents a deposition from the vapor a product of the chemical reaction of Zn with oxygen by using a catalyst [99]. For this research a modified CVD process, such as a pulsed-injection plasma-assisted metal-organic CVD method was used (PE-MOCVD) was used in order to achieve the layers with a homogeneous thickness and doping concentration [97]. A scheme of the experimental setup is shown in Fig. 3.1. A pulsed-liquid-injection source is required for a generation of the vapor. The droplets of the liquid source (liquid Zn-Ga-organic solution) are provided to the evaporator. The precise amount of the liquid is controlled by the injection opening time and injection frequency. The reaction chamber is additionally filled by a mixture of Ar and oxygen. The pressure of the vapor and the supersaturation of the ZnO are controlled by using the plasma and the homogeneous deposition of the ZnO is possible. The Ga-doped ZnO film was deposited on 8" Si wafer which was covered by a 500 nm thick $SiO_2$ layer. After the growth process the wafer was diced into $1 \times 1 cm$ pieces. The choice of the underlying material and the deposition parameters of the ZnO were determined by the requirement of the PiezoMAT project. Moreover, the amorphous $SiO_2$ layer enhances the number of the nucleation seeds for the ZnO(Ga) thin film growth [98, 100].

## 3.2  Preparation of the seed layers by low pressure PLD

Low pressure pulsed laser deposition (LP PLD) is a well-established growth technique for the fabrication of thin films [29]. It allows to obtain thin films with good crystalline quality, controllable purity and high growth rate [24]. The growth of the seed layers with different concentration of Al or rather Ga dopants as well as undoped ZnO seed layers were performed in the Semiconductor Physics Group in Universität Leipzig by Dipl.-Ing. Holger Hochmuth. A scheme of the exper-
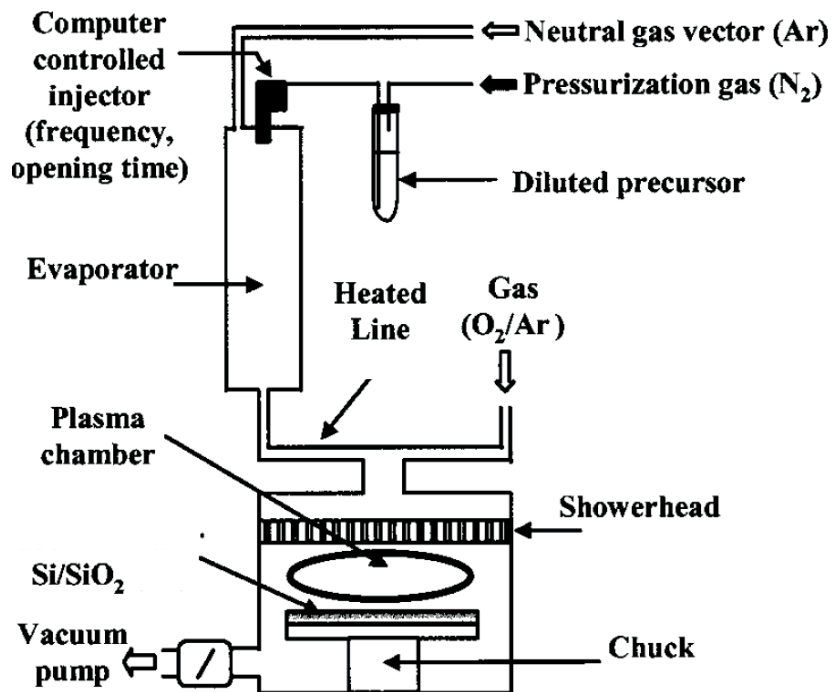
Figure 3.1: Schematic setup of the PE-MOCVD chamber. Taken from [97].

## 3. PREPARATION OF THE SEED LAYERS BY LOW PRESSURE PLD

imental setup is presented in the Fig. 3.2. A pulsed high-power KrF UV laser beam with a wave length of $\lambda = 248$ nm is focused by a UV lense on a target surface. The power density on the target is about 108 W/cm$^2$. Upon absorption of the laser energy, the target material is evaporated, excited and ionized [24]. A plasma plume is formed and expands perpendicular to the heated substrate surface which is mounted vis-à-vis to the target. This position of the plasma plume allows to obtain seed layers with a low surface roughness. An applied rotation of the substrate leads to a homogeneous thickness of the deposited films [2].

The doped and undoped ZnO seed layers were fabricated on $a$-plane sapphire substrate with a typical size of $1 \times 1$cm which allows to obtain a high crystalline quality of the thin films [24]. The sapphire single crystals are chemically stable in air, hard and available by reasonably price. Also, Al- and Ga-doped seed layers were fabricated on the Si with thermal Si (100) layer by LP PLD in order to compare their surface morphology and the crystalline quality with seed layers performed by PE-MOCVD.
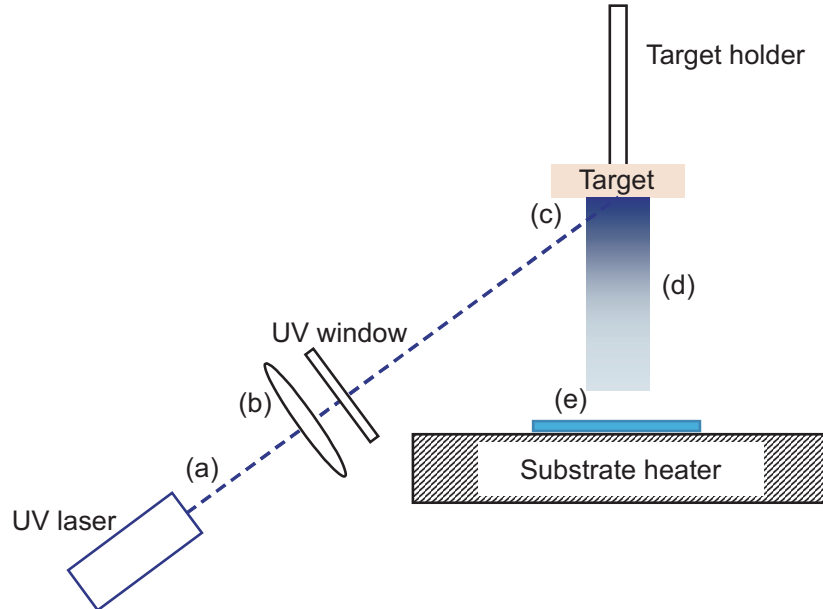


Figure 3.2: Scheme of the low-pressure PLD process: (a) laser beam, (b) UV lense, (c) surface of the target, (d) plasma plume, (e) substrate.

For the fabrication of the seed layers an oxygen partial pressure of about

$p = 0.01$ mbar and a growth temperature of about $T = 720\,°\mathrm{C}$ was used. For the seed layer growth the ceramic targets were sintered: ZnO (with a purity of $x = 99.997\,\mathrm{wt\%}$), ZnO(Al) with a concentration of the $Al_2O_3$ powder of $x = 0.4, 0.75, 1.5, 3.5\,\mathrm{wt\%}$ and ZnO(Ga) targets with $x = 0.4, 0.75, 1.5, 3.5, 4, 9\,\mathrm{wt\%}$ of $Ga_2O_3$ powder.

## 3.3  HP PLD for the NW and NN growth

For growth of the doped and undoped ZnO nanowires (NWs) and nanoneedles (NNs) a modified PLD chamber was used for this research [2, 25]. Such chamber is different to the conventional LP PLD since the pressure used for the growth of NWs and NNs is in the range of a hundred of mbar, i.e. in several orders of magnitude larger than the pressure for the thin film growth. The Ar flow of 50 sccm with pressure of 150 mbar used in the modified high-pressure PLD chamber (HP PLD) leads to a change of the grown structures from planar thin films to the quasi 1D or 3D nanostructures [2, 23, 25, 79, 101]. This change is possible since the increase of the pressure leads to the enhanced supersaturation of the ZnO deposited particles and supports their transport to the substrate. In the HP PLD chamber the substrate is tilted with respect to the the plasma plume direction. In contrast to the LP PLD technique, for the HP PLD, the deposition occurs from the vapor instead of plasma, i.e. the ions of the plasma are forming the molecules and clusters of molecules during their transport with the flow [29].

A scheme of the high-pressure PLD chamber is shown in Fig. 3.3 and described in details by Lorenz et al. [23]. Such chamber was constructed at the Universität Leipzig and consist of a $T$-shape quartz tube with rotated ceramic target. The design of the chamber supports the transport gas flow and the particles of the plasma plume can be easily transfered to the substrate. A pulsed high-power excimer laser beam with a wavelength of $\lambda = 248$ nm is focused by a UV lens onto the target surface, which is evaporated, excited and ionized as mentioned for the LP PLD. The plasma plume propagates with angle of about $30\,°$ towards the substrate surface. The argon particles are mixed with ZnO particles near the plasma plume, transport them to the substrate and were removed in the end of the quartz chamber. The pressure of the chamber is controlled by mass flow
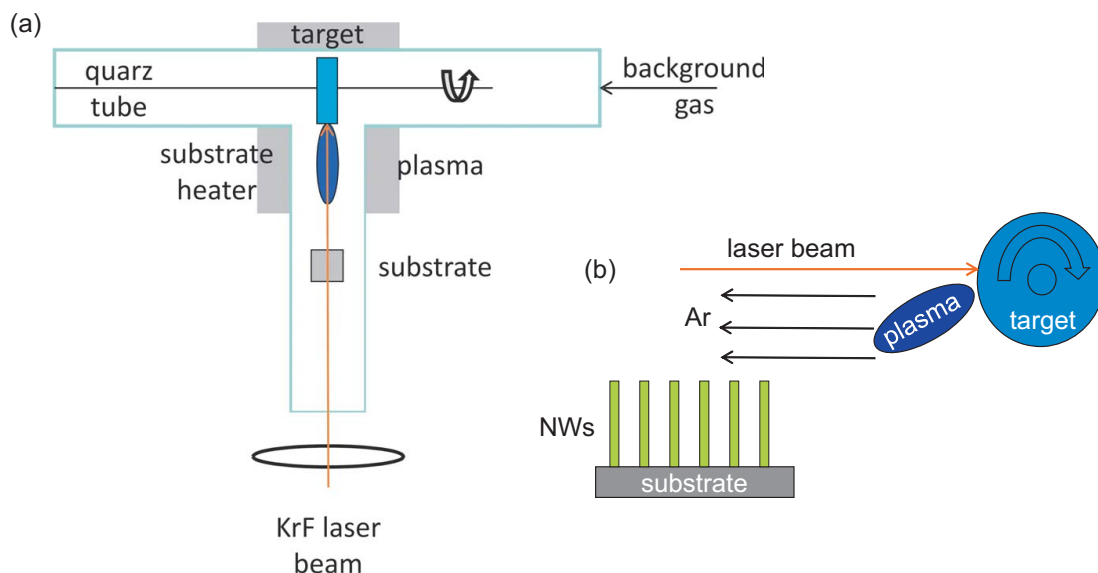
control (MKS type 146 system).



Figure 3.3: Scheme of the high-pressure PLD process: (a) top view, (b) side view

The growth process can be controlled by a variation of the growth temperature, pressure of the background gas, energy and number of the laser pulses and the surface characteristics of the seed layer, e.g. surface roughness, kind of the doping material, crystalline quality. The impacts of these variations on the NW growth and their geometric characteristics will be mentioned further. For a confirmation of the reproducibility of the obtained results, each growth experiment was repeated several times.

## 3.4 Characterization techniques

### 3.4.1 X-ray Diffraction

The crystalline structure of the seed layers was characterized by X-ray diffraction. For these measurements the wide angle goniometer of a Philips Analytical Materials Research Diffractometer (type XPert) with a copper anode ($Cu - K_\alpha$: $\lambda = 0.15406$ nm) was used. The X-rays were scattered at the three-dimensional lattice of the crystalline film and substrate. A fulfilling of the Laue condition

is a requirement for the occurring of constructive interference. The geometric interpretation of the Laue condition allows to consider the path difference of X-rays which are diffracted at two lattice planes as presented in the Fig. 3.4a and therefore, the Bragg equation is given by [102, 103, 104]:

$$2d_{hkl}sin\theta = n\lambda \qquad (3.1)$$

where $d_{hkl}$ is the spacing between adjacent lattice planes, n is the diffraction order, and $\theta$ the angle of incidence [105].
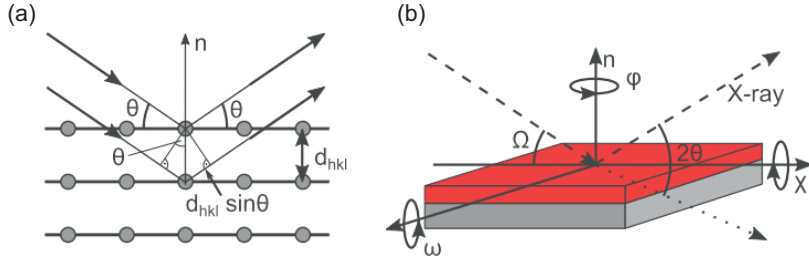


Figure 3.4: (a) Geometry describing the Bragg condition. (b) Euler angles $\omega$, $\theta$, $\chi$ and $\phi$, used to access the reciprocal lattice points. $\Omega$ is the angle between surface and incident beam. Taken from Ref. [104]

During the measurements, the sample is rotated with an $\omega$ angle, and the angle between source and detector is $2\theta$ (Fig. 3.4b). In order to obtain a $2\theta - \omega$-scan, the detector is rotated with doubled speed than the sample. By this scan the different crystalline planes of the film can be detected. The size of the grains can be estimated by the full width at half maximum (FWHM) of the rocking curves. These rocking curves can be obtained from the $\omega$-scan and the angle between source and detector is fixed, i.e. the rocking curve can be taken for the crystalline plane which was determined by the $2\theta - \omega$-scan [104]. A sharp rocking curve with small FWHM of $\omega$ indicate a large size of the crystallites [105].

## 3.4.2 Atomic Force Microscopy

The atomic force microscopy (AFM) was demonstrated for the first time in 1986 by Binnig *et al* and represents a combination of the principles of the scanning

tunneling microscope and the stylus profilometer. Importantly, the probe in the AFM does not damage the surface of the sample [106]. In Fig. 3.5 a scheme of the AFM setup is presented. An AFM XE 150 supplied by Park Systems with non contact Nanosensors PointProbePlus-NCHR cantilever was used for this research [107]. The AFM technique is based on the electromagnetic interactions between a sharp tip and the surface of a sample. The tip is made of Si and mounted on a cantilever. The interactions can be detected by the deflection of a control laser beam, which is reflected on the upper side of the cantilever and can be detected by an photodiodes. It allows to investigate the surface morphology. The so-called intermittent or tapping contact mode was used for the investigations in this research. The intermittent mode is based on the analysis of a sinusoidal oscillation of the cantilever which are close to the resonance frequency of the cantilever. Such oscillations lie in the range from 200 to 400 kHz [105]. It allows for the tip to touch the surface with every oscillation and lift off again. The high oscillation energy prevents the tip from sticking of the surface due to meniscus forces caused by e.g. moisture [104].
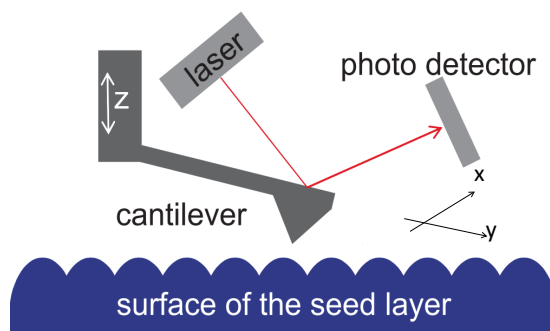
Figure 3.5: Schematic of the AFM setup.

A $20\times20\mu$m scan was performed and the surface roughness was analyzed by using the open source software Gwyddion [108]. The average surface roughness was obtained which is defined by:

$$R_a = \frac{1}{N} \sum_{i=1}^{n} |z_i - \bar{z}| \tag{3.2}$$

here $z_i$ is the height of the $i$-th data point, $\bar{z}$ represents the average height and $N$ is the number of acquired data points.

### 3.4.3 Scanning electron microscopy

A dual beam microscope FEI NanoLab Nova 200 was used for scanning electron microscopy (SEM) in order to obtain the images of the grown structures with a high-resolution. A focused electron beam with a typical spot size of several nanometers scans over a part of the sample surface. The typical acceleration voltage which was used for in order to obtain a high quality SEM image of the fabricated nanostructures was 15 keV. The electrons interact with the material, scattere and the resulting secondary electrons are detected [104]. The number of secondary electrons determines the brightness and the contrast of each single pixel. Incident beam electrons are also backscattered by elastic interaction with the sample atoms. The used Everhart Thornley Detector (ETD) allows to detect all backscattered electrons since their low kinetic energy and attracting them to a charged grid, i.e. keep the contrast of the image stable [104].

### 3.4.4 Energy Dispersive X-ray Spectroscopy

The dual beam microscope FEI NanoLab Nova 200 was also used for the Energy dispersive X-ray spectroscopy (EDX) in order to determine the concentration of the Al or Ga dopants in each seed layer. The layers were irradiated by electron beam with a typical voltage in the range from 5 to 15 keV which removes the inner shell electrons from the atoms of the sample. The vacancies are filled by outer shell electrons and such transition leads to an emission of the X-rays. Since the energies of the emitted X-rays are different for different elements, an analysis of the emission, the elements of the sample can be defined [104, 109].

### 3.4.5 Spectroscopic Ellipsometry

The NW growth is strongly depends on the thickness of the seed layer, i.e. the thin seed layers with a thickness of less than 100 nm have a rough surface which can suppress the NW growth [96]. Additionally, an impact of the underlying material on the thin film surface morphology can occur [110]. In order to exclude these effects on the NW growth, the seed layer should be thick enough. The seed layer thickness in the range of $200 - 250$ nm is considered as an appropriate for the NW fabrication [2, 96]. However, the larger thickness might lead to an increase of the dislocations [24, 29]. A determination of the thickness of the seed layers was performed by a spectroscopic ellipsometry. Ellipsometry based on the change of polarization of light which is reflected from the sample surface [111]. For the thickness determination a M2000 ellipsometer was used which is produced by J.A. Woollam Co., Inc. The white light in the spectral range of $E = (0.73 - 3.24)$ eV passes through a rotating compensator and a fixed polarizer. The reflected light from the sample is analyzed in its polarization state and guided to a monochromator with a CCD camera. The spectral resolution is limited by number of pixels of the CCD row. For this device the CCD has 512 points [112].

### 3.4.6 Cathodoluminescence

For the cathodoluminescence (CL) characterization technique is an analysis of the luminescence spectra of the material which is excited by an electron beam [2]. The CL allows to investigate the optical properties of the NWs and was performed by using the SEM setup. As will be discussed in the Chapters 6 and 7, the fabricated NW have a diameter in a range from d = 7 nm to more than 300 nm and thus a strong impact of the surface properties on the NW emission characteristic is expected. In comparison to other optical methods like conventional photoluminescence spectroscopy (PL), CL has the advantage of a much higher spacial resolution due to a size of the exciting electron beam. The luminescent region is generally of several hundred nm since the beam is broadening in the NW and occurring of the carrier diffusion [2, 87].

The CL measurements were performed by Dipl.-Phys. Jörg Lenzner, Universität Leipzig by using CAMScan CS44 SEM. The spectral resolution of this setup

is about 0.9 meV. The low temperature of $T \approx 10\,K$ was reached by using a heatable helium-flow cryostat [2]. The measurements were performed from the side of the sample, along the vertical direction of the NWs. It allows to reduce the signal from the seed layer E [32]. The NWs were excited by using an electron current of about 400 pA for the thick NWs (with a diameter of more than 180 nm) and 200 pA for the thin NWs ($d \leq 180\,nm$). The enhancement of the current for the thin NWs was necessary due to their low photon emission. The luminescence was collected by an ellipsoid mirror and was spectrally analyzed by a monochromator with a focal length of 320 mm, a grating of 600 lines/mm. The entrance slit width is $50\mu$m. The NW luminescence was detected by using a CCD camera with a spectral resolution of 0.9 meV [2].

## 3.4.7  Angle-varied X-ray photoelectron spectroscopy

Since the seed layers are polar, an impact of their polarity on the NW growth is expected according to Ref. [33]. One of the method for the surface polarity determination is the Angle-varied X-ray photoelectron spectroscopy (AVXPS) which was performed by the group of X-ray and photoelectron spectroscopy and surface analysis at Wilhelm-Ostwald-Institute for Physical und Theoretical Chemistry, Universität Leipzig. This technique is based on irradiating the sample with X-rays and measuring the kinetic energy and number of electrons that escape from the top surface of the sample. It allows to measure the O 1s and Zn $2p_{3/2}$ core level spectra at different photoemission angle ($\theta$) between the surface normal and the detector axis (usually $\theta = 0\,°$ and $\theta = 70\,°$). The surface polarity determines the intensity ratio at these angles ($\chi$) [113]:

$$\chi = \frac{(I_{O1s}/I_{Zn2p3})_{\theta=0}}{((I_{O1s}/I_{Zn2p3})_{\theta=70})} - 1 \tag{3.3}$$

In Eq.3.3 the $\chi$ parameter has different sign for Zn- and O-terminated ZnO(0001), i.e. $\chi < 0$ corresponds to O-termination and $\chi > 0$ corresponds to Zn-termination of the surface. However, the AVXPS method is very sensitive to a contamination of the surface of the sample.

### 3.4.8 Etching of the seed layers

Another method for the determination of the polarity was mentioned by Mariano and Hanneman [114] in 1963. This method highlights the differences of the polar surfaces with response to the chemical etching which is well known for different wurtzite structures [115]. It was found that the O-polar surface surface can be etched more rapidly in the oxidizing etchants than the Zn-polar surface. The rapidly attacked O-polar surface is etched with more uniformly distributed etch figures such as hills. For the Zn-polar surface the etching is primarily located where dislocations intersect that surface and the etching pattern for such surface is usually pits [114].

A thick ZnO layer can be etched by a wide range of different etchants [116, 33]. For this research a diluted HCl acid was used in order to obtain a distinct etching pattern. For the investigation, the tested samples were dipped in the 1:100 concentrated solution for 30 s with further rinsing in deionized water. For such concentration of HCl the etching rate was found to be about 1 nm per second and was determined by spectroscopic ellipsometry. The etching pattern were investigated by laser microscopy and SEM.

# Chapter 4

# Seed layer characterization

The doping concentration, surface morphology, crystalline quality and polarity of the seed layers have a strong impact on the NW growth [33, 96], E [32]. The doping material and its concentration as well as the growth method have a significant impact on the seed layer properties. Thereby, by a variation of these properties the surface free energy and the growth mechanism of the NWs can be changed [26]. In this Chapter the seed layers obtained by LP PLD and CVD growth techniques are discussed. The surface properties of the seed layer are presented in the Table 4.1.

## 4.1 Doping concentration

The seed layers fabricated by the LP PLD and the CVD growth technique were investigated by EDX in order to determine the Al or Ga doping concentration. For the seed layers grown by LP PLD growth technique, the measurements revealed a doping concentration of $x = 1, 2, 3.5, 7 \, \mathrm{at}\%$ of Al and $x = 1, 2, 3.5, 7, 9, 15 \, \mathrm{at}\%$ of Ga dopants. An undoped ZnO seed layers was fabricated as well. For the Al-doped seed layers a set of the reference films grown on Si (100) is required in order to avoid an incorrect determination of the Al concentration by sapphire substrate. The reference films are comparable to the seed layers performed on sapphire and they were grown at the same growth conditions. Additionally, spectroscopic ellipsometry was used for the determination

of the thickness of the seed layers. All deposited seed layers have a thickness of about $200 - 250$ nm.

By using CVD growth technique, several ZnO(Ga) seed layers were obtained. These layers have a Ga doping concentration of x $= 9, 13, 16, 20$ at%. Notably, no seed layers with other doping concentration and the surface properties could be fabricated at CEA LETI.

## 4.2 Surface morphology

All seed layers prepared by LP PLD and CVD growth techniques were investigated with the AFM. In Fig. 4.1 the average surface roughness as a function of the doping concentration is shown. For the Al-doped layers grown by LP PLD a smooth surface which decreases from $R_a = 2.4$ nm to $R_a = 1.3$ nm with increasing of Al concentration is observed. For the ZnO(Ga) layers the average surface roughness fluctuates in the same range as the roughness of the Al-doped seed layers, however no clear dependence from the doping concentration is observed. Also, for the Ga-doped seed layers fabricated on Si substrate the surface roughness has no clear dependence from the doping concentration. The average surface roughness is $R_a = 4.5$ nm for the layer doped by x $= 1$ at%, then the roughness reduces to 0.7 nm for the layer with a doping concentration of x $= 2$ at% and slightly increases to about 1 nm for the layer doped by x $= 9$ at%. However, a fabrication of the seed layers by CVD on the Si/SiO$_2$ substrate leads to an enhanced surface roughness. The seed layer doped by x $= 9$ at% of Ga has a surface roughness of $R_a = 11.5$ nm and it decreases with a doping concentration to $R_a = 6$ nm what is observed for the seed layer with x $= 20$ at% of Ga dopants.

An increase of the surface roughness can lead to the increase of the surface free energy and thus, suppress the growth of the NWs [26, 96]. Additionally, the hills and pits on the surface are the obstacles for the movement of the deposited interfacial particles. Such particles can interact with the obstacles and lose their kinetic energy. Thereby, such suspended particles cannot reach the top of the nucleation seeds and they cannot be grown in the vertical direction. This situation leads to the Stranski-Krastanov growth mode instead of desired Volmer-Weber one.
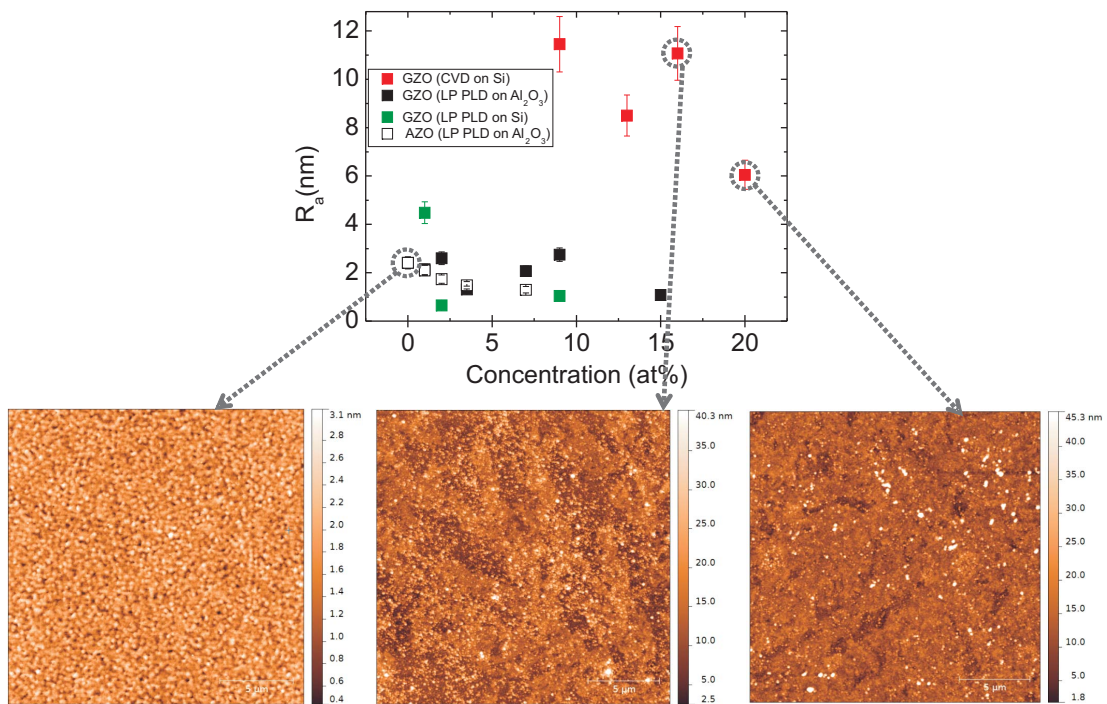
Figure 4.1: Surface roughness of the seed Al/Ga doped seed layers grown on sapphire or Si substrate by using LP LPD or CVD growth method as a function of the doping concentrations and some AFM topological scans.

Moreover, it seems that for both growth techniques - LP PLD or CVD, the average surface roughness tends to decrease with increasing doping concentration, since the smaller surface roughness is observed for the seed layers with the highest doping concentration (in dependence on the kind of the seed layers). This decrease is observed small for the seed layers fabricated by LP PLD, and sufficient for the seed layers grown by CVD. Thus, the growth method allows to enhance the surface roughness and therefore the surface free energy.

## 4.3   Crystalline quality

The crystalline quality of the seed layers was determined by the grain size and can be investigated by XRD. The FWHM of the rocking curves as a function of the doping concentration is presented in the Fig. 4.2a. Since all of the seed layers are $c$-oriented, the rocking curves were taken from the (0001) plane for further description of the crystalline quality of the seed layers. For the ZnO(Al) layers grown by LP PLD on sapphire, the FWHM of about $0.8°$ is observed for the undoped ZnO seed layer and it increases with increasing of the dopants concentration up to $2.4°$. For the Ga-doped seed layers fabricated on the sapphire substrate an increase of the FWHM with a doping concentration is also observed. The FWHM of the rocking curves increases from $0.8°$ to $3.2°$ for the seed layer doped by x = 15 at% of Ga. The ZnO(Ga) seed layers grown on Si substrate by LP PLD show an increase of the FWHM with a doping concentration in the range $1.8 - 7.2°$. For the layers fabricated by CVD technique, a much higher FWHM of the rocking curves are observed. They have no clear dependence from the Ga concentration and are in the range between $9.0 - 11.7°$.

Obviously, in contrast to the surface roughness, the FWHM of the rocking curves mostly depends on the doping concentration. Since the FWHM is inversely proportional to the grain size [117, 118], the grains of the investigated seed layers become smaller, e.g. for the undoped ZnO, ZnO(Al) layer with $x = 7$ at% grown on sapphire by LP PLD and for the seed layer with x = 9 at% of Ga doped fabricated on Si by CVD, the grain sizes are abou 55 nm, 50 nm and 39 nm respectively.

The grain boundaries are possible places for the nucleation sites [26, 83]. Since
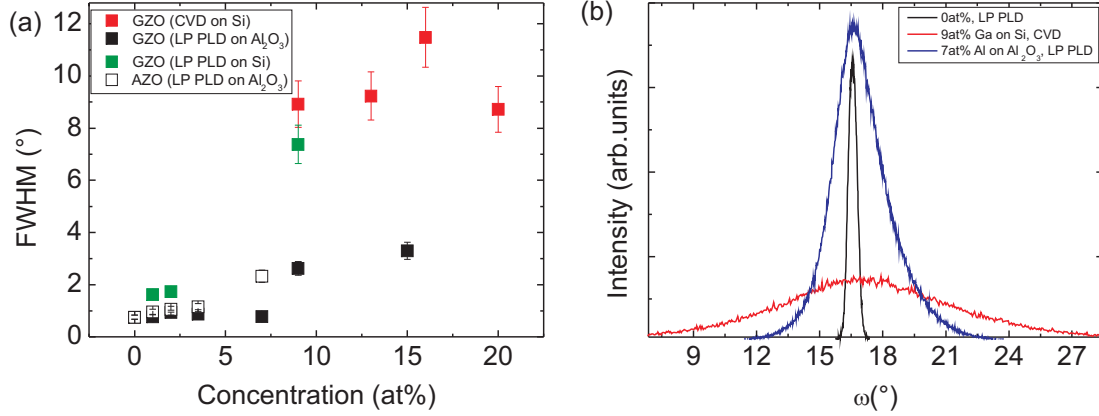
Figure 4.2: (a) The FWHM of rocking curves of ZnO (0001) plane for the seed Al/Ga doped seed layers grown on sapphire or Si substrate by using LP PLD or CVD growth method as a function of the doping concentrations, (b) examples of the rocking curves obtained from the different kinds of the seed layers. A gray dashed line is guide for the eyes.

the number of the grains increases with doping concentration, the density of the NWs is expected to be enhanced. Also the grain boundaries are the obstacles for the particle movement [26]. These obstacles can reduce the interfacial free energy and increase the surface one. Thereby, with increasing of the FWHM of the rocking curves the total free energy decreases and a switching of the growth mechanism mode from Volmer-Weber to the Stranski-Krastanov can occur.

## 4.4 Surface polarity

In order to investigate the surface polarity of the seed layers, an etching of the surface of the Al and Ga-doped seed layers was performed in 1% HCl solution during 1 $s$. Investigation of the etching pattern revealed O-polar surface for the undoped seed layer as well as for the seed layers with a doping concentration of x = 1 at% of Al and Ga. The SEM image of the etched surface of these seed layers show numerous pyramid-like hills on the entire etched surface as presented in Fig. 4.3a. Remarkably, all other doped seed layers have a Zn-polar surfaces, i.e. hexagonal-like pits (Fig. 4.3b). The characteristic patters are identical to all
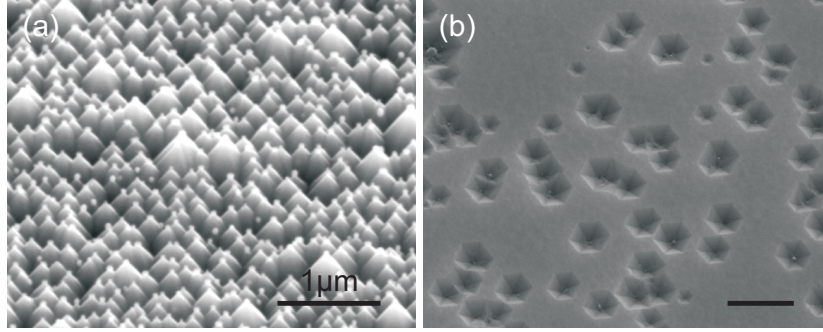
investigated surfaces.



Figure 4.3: SEM images of the O-polar seed layer (undoped ZnO) (a) and Zn-polar seed layers (Al-doped ZnO with a doping concentration of x = 3.5 at%) (b) after etching $1s$ in 1% HCl solution

The AVXPS measurement confirmed the O-polar surface of the seed layer doped by x = 1 at% of Al, however using of this characterization techniques for other seed layers is technically challenging due to a high sensitivity of the AVXPS to the surface contamination by carbon [113] and absorption of hydroxides due to hygroscopic properties of ZnO [120].

## 4.5   Summary of the Chapter

The fabricated seed layers have different surface properties such as surface roughness, crystalline quality, grain size, polarity which are strongly depend on the Al or rather Ga doping concentration, kind of the underlying material and growth technique. The seed layers fabricated on sapphire by LP PLD with small doping concentration of $x \leq 7$ at% have a crystalline quality close to that of bulk single crystals and the surface roughness of $R_a \approx 2$ nm. In contrast to that, the seed layers grown on Si/SiO$_2$ and grown on sapphire with a Ga doping concentration of $x \geq 7$ at% have an almost polycrystalline quality with a high surface roughness of $R_a \geq 10$ nm. Such different surface properties allow to change the NW growth mechanism by a variation of the impact of the surface free energy. The number of the nucleation seeds is dependent on the number of the surface defects, e.g. grain boundaries [26]. The size of the grains might determine the density of the

NWs. The surface defects are also obstacles for the movement of the deposited ZnO particles and thus, they define the interfacial free energy. The polarity of the seed layer plays a significant role on the kind of the grown nanostructures and can change the growth mechanism mode from the Volmer-Weber one to the Stranski-Krastanov one [33].

Table 4.1: The seed layer surface properties, doping material and the concentration and the fabrication techniques

| Underlying material | Growth method | Doping material | Doping (at%) | $R_a$ (nm) | FWHM $\omega$ (°) | Surface polarity |
|---|---|---|---|---|---|---|
| $a$-sapphire | LP PLD | undoped | 0 | 2.41 | 0.753 | O |
| $a$-sapphire | LP PLD | Al | 1 | 2.10 | 0.96 | O |
| $a$-sapphire | LP PLD | Al | 2 | 1.74 | 1.06 | Zn |
| $a$-sapphire | LP PLD | Al | 3.5 | 1.48 | 1.16 | Zn |
| $a$-sapphire | LP PLD | Al | 7 | 1.30 | 2.32 | Zn |
| $a$-sapphire | LP PLD | Ga | 1 | 2.12 | 0.77 | O |
| $a$-sapphire | LP PLD | Ga | 2 | 2.60 | 1.04 | Zn |
| $a$-sapphire | LP PLD | Ga | 3.5 | 1.13 | 0.88 | Zn |
| $a$-sapphire | LP PLD | Ga | 7 | 2.07 | 0.78 | Zn |
| $a$-sapphire | LP PLD | Ga | 9 | 2.75 | 2.62 | Zn |
| $a$-sapphire | LP PLD | Ga | 15 | 1.08 | 3.30 | Zn |
| $S$i$(100) + $SiO$_2$ | LP PLD | Ga | 1 | 4.48 | 1.63 | Zn |
| $S$i$(100) + $SiO$_2$ | LP PLD | Ga | 2 | 0.65 | 1.74 | Zn |
| $S$i$(100) + $SiO$_2$ | LP PLD | Ga | 9 | 1.04 | 7.38 | Zn |
| $S$i$(100) + $SiO$_2$ | CVD | Ga | 9 | 11.45 | 8.92 | Zn |
| $S$i$(100) + $SiO$_2$ | CVD | Ga | 13 | 8.5 | 9.23 | Zn |
| $S$i$(100) + $SiO$_2$ | CVD | Ga | 16 | 11.07 | 11.48 | Zn |
| $S$i$(100) + $SiO$_2$ | CVD | Ga | 20 | 6.05 | 8.72 | Zn |

# Part II

# NW growth: results

# Chapter 5

# NW growth characteristics

By using the HP PLD growth technique for the NW fabrication, the sum of the $F_m + F_i$ defined by Eq. 2.1 can be changed by a variation of the growth parameters. Thus, different growth modes can occur by using the same kind of substrate. The shift of the growth mode can be achieved by a variation of the pressure and temperature of the vapor over the substrate, doping of the deposited material, energy, frequency and number of the laser pulses (for the material free energy [29]) and growth temperature, number of the obstacles for the particle movement (for the interfacial free energy [28]). In this Chapter the growth parameters which influence on the material free energy as well the growth kinetics will be discussed. The impact of the interfacial free energy on the growth process will be highlighted in the next Chapter 6.

## 5.1 Material free energy and the deposited material parameters

The material free energy strongly depends on the number of the particles which are arriving to the substrate and their energy. The number of the laser pulses, their frequency, doping of the deposited material and the content of the transport gas determine the number of the particles, whereas the energy of the laser pulses and the pressure of the background gas flow have an impact on the energy of the particles. However, these parameters have a limited range of the variations which

# 5. MATERIAL FREE ENERGY AND THE DEPOSITED MATERIAL PARAMETERS

allow to obtain the NWs, e.g. the NWs can be grown by using laser frequency in a range of $f = 5 - 10$ Hz only. For such growth parameters as laser energy and frequency, content of the gas and its pressure, the range of the possible variations is narrow and for further investigations of the NW growth, these parameters are fixed in order to investigate the impact of the more flexible parameters on the growth mechanism. These flexible parameters are the number of the laser pulses and the doping of the deposited material. However, in this Section an overview of all mentioned parameters which are influential on the material free energy and their impact on the NW growth is discussed.

*Doping of the deposited material*

Since Al or Ga dopants are much heavier than Zn or O and the volume of the vapor is unchanged during the growth process, the density of the vapor and its mass are increased because of doping. Thus, the pressure $p$ of the vapor and the difference of the chemical potential $\Delta\mu$ are increased too. In the Eq. 2.7 a relation of the the sum of the $F_m + F_i$ to the difference of the chemical potential is given. Since for the desired Volmer-Weber growth mode, which is apparently responsible for the NW growth [26], the free energy should be positive, the doping of the ZnO material increases chances of proceeding the process by the Volmer-Weber mode E[30]. Results of the doped NW growth on the doped seed layers will be presented in details in the Chapter 7.

*Energy of the laser pulses*

The typical energy of the laser pulses is about 600 mJ. This energy is optimum for the NW growth on the most of the substrates [2, 23, 79]. Since the laser pulses produce the ZnO plasma, the energy of the pulses determines the temperature of the vapor and the kinetic energy of the deposited particles. In Eq. 2.7 the temperature of the vapor is related to its supercooling and thus to the difference of the free energy. If the laser pulse energy will be $E \ll 600$ mJ, the particles would be crystallized immediately after the deposition. However, if the energy of E $\gg$ 600 mJ would be applied, the deposited particles can return back to the vapor and then deposited again, but with significantly lower energy than at their first deposition. Both situations of the higher or lower laser pulse energy can lead to the undesired Stranski-Krastanov mode and no NWs can be grown.

*Frequency of the laser pulses*

The frequency of the pulses defines the number of the particles which are deposited from the vapor during the deposition, i.e. the higher is frequency, the higher is density of the vapor and thus, more particles can be deposited on the substrate by the limited number of the pulses. The optimum frequency for the NW growth is 10 Hz [2, 23, 79]. As mentioned above, there are the upper and the lower limits for the frequency, i.e. no NWs are observed at the $f < 5$ Hz and $f > 15$ Hz for the most of the substrate [79].

Since the density of the vapor determines the supersaturation of it [26, 29], high laser frequency increases the pressure $p$ and thus supports the Volmer-Weber growth mode and the vertical growth rate of the NWs. However, if the frequency is higher than the optimum value, the particles can return back from the substrate to the vapor. A decreased laser pulse frequency supports the lateral growth rate, as shown in the Fig. 5.1. By using a laser frequency of $f = 7$ Hz, the NWs have a two times larger diameter than by using the optimum frequency of $f = 10$ Hz, e,g, d = 70 nm for optimum laser pulse frequency and d = 200 nm for the f = 7 Hz. With further decrease of the frequency, the Stranski-Krastanov growth mode can be supported instead the Volmer-Weber one.
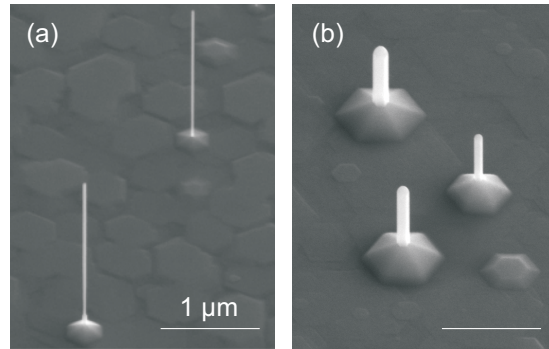


Figure 5.1: The undoped ZnO NWs grown on the undoped ZnO seed layer at $T \approx 950\,°C$ by applied laser pulse frequency of (a) f = 10 Hz and (b) f = 7 Hz

*Number of the laser pulses*

In the PLD growth technique, each single laser pulse produces an almost equal number of the ZnO particles [24, 29]. Thereby, by a variation of the laser pulses, a supersaturation of the ZnO vapor over the substrate can be achieved since the

supersaturation and the sum of the $F_m + F_i$ are strongly depend on the number os the particles as was given in Eq. 2.3. For the HP PLD growth, the NWs can be fabricated by the Volmer-Weber growth mode in a wide range of the laser pulses, from 3000 to several hundreds of thousands [2, 24, 29, 79]. Using a higher number of the pulses might lead to the growth of rough thin film by the Volmer-Weber mode [29]. In the next Section 5.2 an impact of the number of the laser pulses on NW shape will be discussed in details.

*Transport gas*

As mentioned in Chapter 3, in contrast to the LP PLD technique, for the HP PLD, a background transport gas is needed [23, 25]. There are several requirements for the kind of the gas: as it should not react with the ZnO and size of the atoms of the gas should not be larger than Zn or O, otherwise, the large atoms can significantly reduce the kinetic energy of the deposited particles by the numerous interactions. Obviously, oxygen or rather neutral gases are promising to be used in the HP PLD chamber. The pressure of the background gas supports the supersaturation of the ZnO vapor and increases an impact of the material surface energy on the growth process. The best results of the NW growth have been obtained by pressure of $p = 150$ mbar of the Ar gas flow. Reduction of the pressure leads to the growth of agglomerated nanostructures by $p = 1$ mbar and thin films at high vacuum [24].

## 5.2   Growth kinetics

For the growth of NWs two growth rates can be defined - the vertical one ($v_z$) and the lateral one ($v_r$). The Volmer-Weber growth mechanism mode requires that the vertical growth rate should be more larger than the lateral growth rate. It means that during the growth process, the most of the deposited ZnO particles are crystallized on top of the nucleation seeds. For this growth mode, the particles of the interface should have enough kinetic energy to move over the nucleation seeds but at the same time, they should not return to the vapor.

The number of the deposited particles determines the size of the NW. As it was mentioned in the previous Section 5.1, the number of the laser pulses determines the number of the ZnO particles. For the investigation of the development of

the NW geometrical shape by applying different number of the laser pulses, a well-known growth process at the growth temperature of $T \approx 950\,°C$ on undoped ZnO seed layers have been chosen [2, 23, 25, 77] since a low density of thick NWs can be grown. Several identical seed layers have been fabricated by LP PLD with a typical average surface roughness of $R_a \approx 2.4$ nm, FWHM of the rocking curves of about $0.75°$ and the thickness of about $200 - 250$ nm. Undoped ZnO NWs with different number of laser pulses, were fabricated with varying of the number of laser pulses from 1000 to 36000 in order to understand an impact of the number of particles on the geometric shape of the NWs.

All obtained NWs in this investigation were grown on the top of the nucleation seeds with a pyramidal shape (Fig. 5.2). Such nucleation seeds have a hexagonal base and are typical for the growth on the undoped ZnO seed layers by using a growth temperature of $T \approx 950\,°C$ [25]. However, no pyramidal-like nucleation seeds are observed for a high-temperature growth on any other seed layer E[32], as will be discussed in the next Chapter. The possible reason of fabrication of the large nucleation seeds is a homogeneous nucleation of the undoped ZnO seeds on the undoped ZnO seed layer. For the homogeneous nucleation, a higher energy of crystallization is expected than for the heterogeneous nucleation [26, 83]. Thus, a size of the nucleation seeds for the homogeneous nucleation should be larger than for the heterogeneous growth [26]. Moreover, since a lot of particles are required for the formation of the nucleation seed, a low density of several NW $\mu m^{-2}$ is observed. For the HP PLD growth, the fabrication of the pyramid-like nucleation seeds is take place between 1000 and 3000 applied laser pulses.
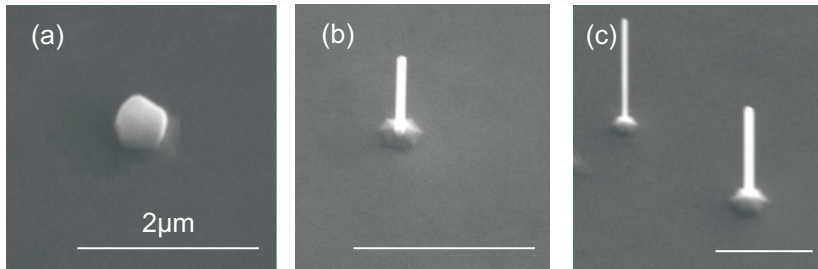


Figure 5.2: Scanning electron microscope images of the ZnO nanowires in different steps of its forming (a) at deposition of 3000 pulses, (b) 6000 pulses; (c) 24000 pulses. Note, the scale bar is the same for all three images

The median values of the NW length, diameter and aspect ratio as a function of the applied laser pulses are presented in the Fig. 5.3. Since growth of the NWs has a non-monotonic behavior, three different growth regimes can be introduced. In the first growth regime, i.e. for an applied range of pulses between 3000 and 12000 the length and aspect ratio of the NWs increases from 200 nm and 1 to $3\mu$m and 20 respectively, whereas the NW diameter is almost constant with a number of pulses and is about 200 nm. In the second regime, for applied $12000 - 24000$ pulses were applied, the length of the NWs slightly decreases to $2.5\mu$m, whereas the diameter decreases to about 120 nm and the aspect ratio increases to 23 with increasing number of pulses. For larger number of laser pulses in the third regime (over 24000 pulses) the length and diameter are increased to $4.4\mu$m and 330 nm respectively, whereas the aspect ratio decreases with a number of pulses to 12.
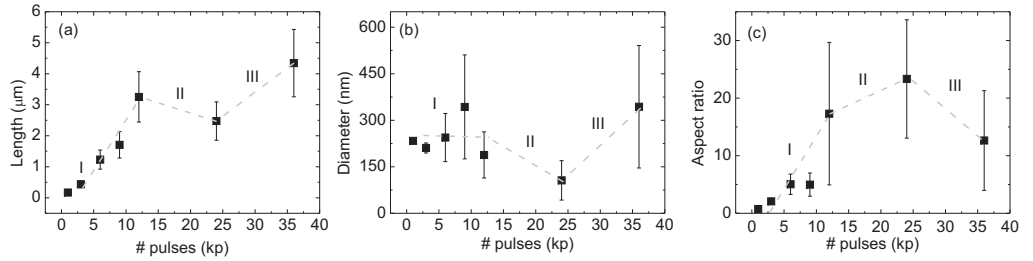


Figure 5.3: Median values of length (a), diameter (b) and aspect ratio (c) of the NWs grown on pure ZnO layer at the high temperature growth, as functions of number of laser pulses. First 3kP corresponds to formation of ZnO seeds for further growth of the NWs on the top of them.

All fabricated NWs have a sharp step-like tip as shown in the Fig. 5.4a independently of the number of laser pulses. Such tip has a length of about $50 - 70$ nm and broadens from the top to the bottom. Appearance of the tip might give possibility for the particles to be transferred from the side facets to the top if the tip. Such step-like tip might attract the moving particles, and allow them to move upward and downward or leave the tip. For an explanation of the observed NW growth, a growth model can be introduced. Such growth model is based on the interaction of several flows of the interfacial ZnO particles, as schematically shown in Fig. 5.4b E[31]. The first one ($f_1$) is the flow of the deposited particles

on the seed layer which are arriving to the NW. This flow can also move the particles to the step-like tip by the sides of the NW and return them from the NW sides to the surface of the substrate. This flow might dominates at the first growth regime. The second flow ($f_2$) is a movement of particles upward along the step-like tip to the top of the NW. The third flow ($f_3$) is an opposite flow to the second one and it represents the movement of particles downward, i.e. from the top of the NW to the sides of the NWs. The last fourth flow ($f_4$) is a flow of particles which are arrived from the target directly to the facets. A combination of the flows $f_2$ and $f_4$ can be responsible for the second growth regime whereas a combination of the third flow $f_3$ and the fourth flow $f_4$ might dominate on the third growth regime.
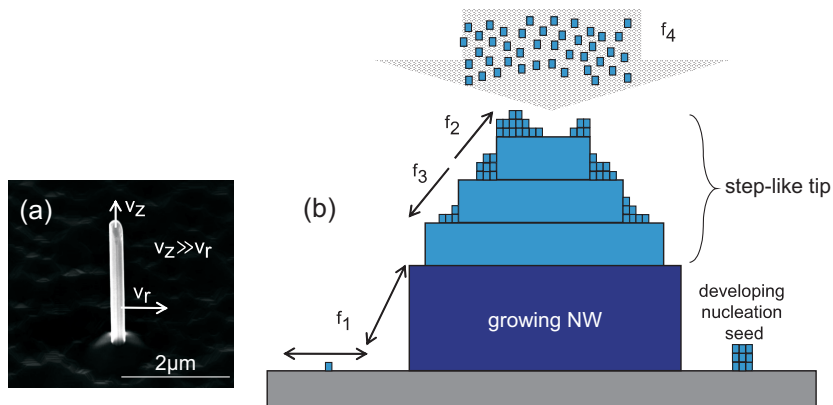


Figure 5.4: (a) ZnO nanowire grown by 6000 laser pulses on pure ZnO at the hight temperature process. (b) Schematic step-like tip of the nanowire with indicated ZnO flows  flow particles on the surface ($f_1$), moving particles uphill ($f_2$) and downhill ($f_3$) and flow of particles from the target to the NW facets ($f_4$).

A domination of the certain flow in the growth process is determined by the number of the particles. The particles which have arrived by the flow $f_4$ on the NW sides can be transfered upward to the top of the NW by the step-like tip and support the flow $f_2$. However, if the number of the particles on the step-like tip is large, a competition for the area on the top of the NW appears and particles with a high kinetic energy can leave the tip and return back to the vapor. Since the number of the deposited particles increases, a competition for the area on the top of the NW tip increases too. Thus, some particles which are arriving to the top

from the sides do not have enough energy to leave the NW back to the vapor, but can be transfered downward by the flow $f_3$. At the same time, the intensity of the flow $f_2$ decreases. The particles which were transfered from the step-like tip to the side lose their kinetic energy and cannot move anymore along the sides of the NWs. Such particles can crystallize there and thus, the NW diameter increases.

## 5.3   Summary of the Chapter

To summarize this Chapter, several points should be emphasized:

- Variation of the HP PLD growth parameters, e.g. doping of the deposited material, variation of the laser energy, frequency of the laser pulses, pressure and a composition of the transport gas flow reflects on the supersaturation of the ZnO vapor and thus, have the impact on the material free energy.

- A kind of the seed layer, i.e. doped or undoped ZnO plays a sufficient role in the nucleation process. Thus, a creation of the seeds by heterogeneous nucleation on the dopants of the surface requires less energy than the homogeneous nucleation of the undoped ZnO particles on the undoped seed layer [26, 83]. For the homogeneous nucleation, large pyramidal nucleation seeds are formed.

- The number of the deposited ZnO particles is strongly depends on the number of the laser pulses. The non monotonic behavior of the NW diameter, length and aspect ratio with increasing of the number of laser pulses is observed. There are three different growth regimes which occur with increasing of the number of deposited particles - increasing of the aspect ratio and diameter (i), decreasing of the diameter and increasing of the aspect ratio (ii) and increasing of the diameter and decreasing of the aspect ratio (iii).

- The observed behavior can be explained by an interaction of the flows of the moving particles. The step-like tip of the NW supports the movement of the particles upward from the NW sides to its top or downward, from the top to the sides. The particles which arrived to the NW and moving on

the sides of it form the flow $f_1$. The movement of the particles upward by the step-like tip is the flow $f_2$. The flow $f_3$ is opposite to the flow $f_2$. The flow $f_4$ is the deposition of the particles from the vapor to the sides of the NW.

- A domination of a certain flow in the growth process is determined by the number of the deposited particles. Since the area on the top of the NW is limited, a competition for the area appears with increasing the number of the particles. Thus, during the deposition the particles can move from the sides to the top with decreasing the diameter, or they can move downward to the sides and be crystallized there with increasing the diameter.

## 5. SUMMARY OF THE CHAPTER

# Chapter 6

# NW growth on doped seed layers

In this Chapter the growth of the undoped ZnO NWs on the Al or rather Ga doped ZnO seed layers is mentioned. For the NW fabrication, several growth temperatures in the range from $T \approx 400\,°C$ to $T \approx 950\,°C$ have been chosen. As will be discussed, the doping of the seed layers has a strong impact on the optimum growth temperature and a variation of the doping concentration allows to fabricate the ultrathin NWs with a diameter of $d < 10$ nm at a low growth temperature of $T \approx 400\,°C$. The geometrical properties such as diameter, aspect ratio and density of the obtained NWs are presented as a function of the doping concentration or growth temperature. Moreover, the optical properties of the fabricated NWs were investigated by cathodoluminescence spectroscopy which revealed a high crystalline quality. For the thin nanowires the emission characteristic is mainly determined by the properties of the surface near region.

## 6.1   Al doped seed layers

Scanning electron microscopy (SEM) images of the deposited nanostructures on the ZnO seed layers doped with Al with a doping concentration in the range of $0 \leq x \leq 7\,at\%$ are shown in Fig. 6.1. For the growth on the undoped ZnO seed layer a low density of vertically oriented NWs is obtained at $T \approx 950\,°C$. Such NWs have a diameter of about 70 nm and an aspect ratio of about 25. Note that the growth of the NWs with several times larger diameter by HP PLD is

possible on pure ZnO seed layer by varying of the growth conditions such as laser frequency, distance between target and substrate or structuring of the substrate [2, 77, 101, 122, 123]. With reduction of the growth temperature down to $T \approx 700\,^{\circ}\mathrm{C}$ the diameter of the NWs decreases from 70 nm to about 10 nm whereas the aspect ratio increases from 25 to 300. However, in contrast to the results obtained at $T \approx 950\,^{\circ}\mathrm{C}$ these NWs are randomly oriented and bent due to the large aspect ratio. Such long NWs are also observed in different works [72, 124, 125] and they can be also grown on the non-crystalline substrates. A further reduction of the growth temperature down to $T \approx 600\,^{\circ}\mathrm{C}$ leads to a suppression of the NW growth and only large sized parasitic effects such as agglomerated ZnO particles were grown. Very thin and short NWs with a diameter of 24 nm and aspect ratio of 6, were obtained for a growth temperature of $T \approx 400\,^{\circ}\mathrm{C}$.

By using a Al doping of the seed layers, the different dependences of the NW growth on the deposition temperatures were obtained. For the highest growth temperature of $T \approx 950\,^{\circ}\mathrm{C}$, only on the seed layer with a doping concentration of $x = 3.5\,\mathrm{at\%}$ NWs are observed. Such NWs have a diameter of about 80 nm and an aspect ratio of 30. However, for the other used doping concentrations the NW growth is suppressed and only honeycomb-like structures are obtained for this growth temperature. For a reduction of the growth temperature to $T \approx 700\,^{\circ}\mathrm{C}$ the NWs were obtained on the seed layer with an Al concentration of $x = 7\,\mathrm{at\%}$ whereas on the other doped seed layers the NW growth is suppressed. For this growth temperature the honeycomb-like structure was obtained on the seed layer with $x = 1\,\mathrm{at\%}$ of Al whereas for other concentrations different kinds of the parasitic effects were obtained. Further reduction of the growth temperature to $T \approx 600\,^{\circ}\mathrm{C}$ leads to the NW growth on the seed layers doped by $x = 2\,\mathrm{at\%}$ and $x = 3.5\,\mathrm{at\%}$. NWs with a diameter of about 10 and 17 nm and aspect ratio of about 65 and 22, respectively, were obtained. On the seed layers doped with the Al doping concentration of $x = 1\,\mathrm{at\%}$ and $x = 2\,\mathrm{at\%}$ NWs were obtained by using the lowest growth temperature of $T \approx 400\,^{\circ}\mathrm{C}$. Moreover, at this low growth temperature the NWs have typically diameter of $d < 7$ nm for both concentrations. The aspect ratio of the NWs fabricated on the layer with $x = 1\,\mathrm{at\%}$ is about 45 and 10 for the NWs grown on the layer with a doping concentration of $x = 2\,\mathrm{at\%}$.

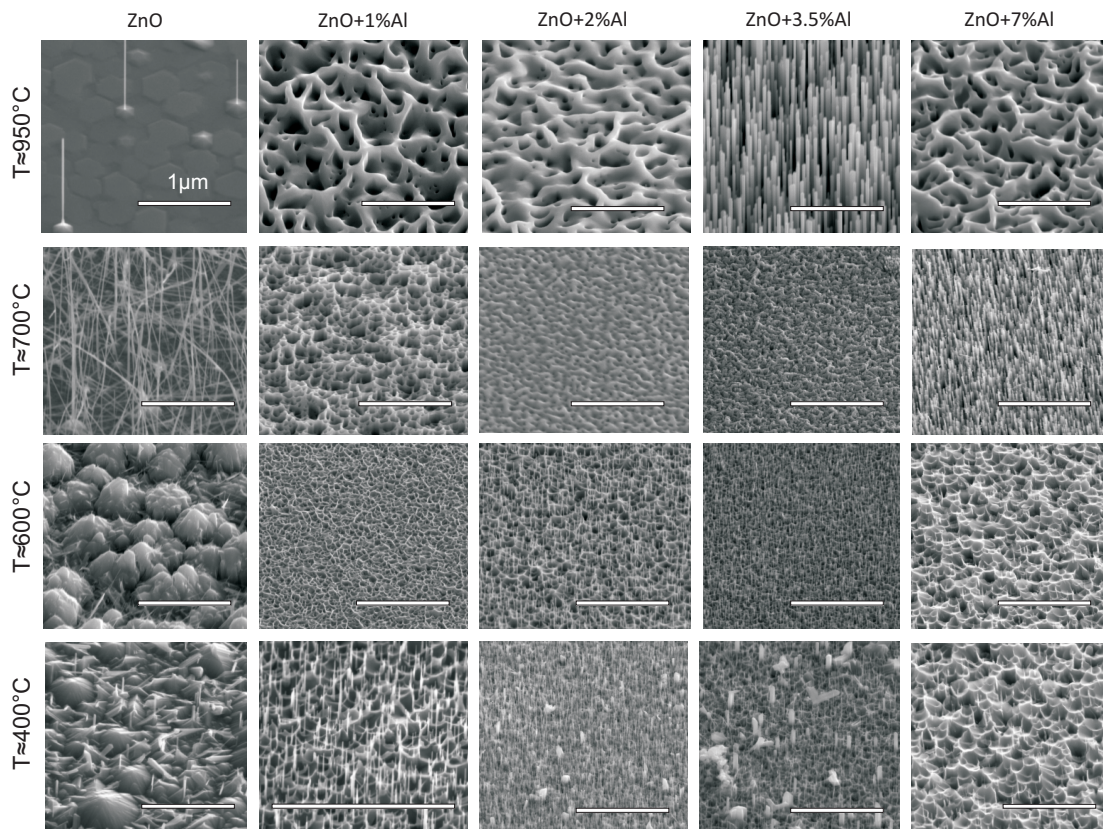The aspect ratio, diameter and density of the NWs grown on the Al-doped seed

Figure 6.1: The scanning electrone microscope (SEM) images of the NWs obtained on the ZnO(Al) seed layers with different doping concentration performed at different growth temperatures

layers as a function of the doping concentration and the growth temperatures are presented in the Fig. 6.2. Since the NW growth is not observed for all used growth temperatures and the seed layers, the NW geometric properties are presented not for all used temperatures and the doping concentrations and the overall behavior of the obtained geometric properties will be discussed. The aspect ratio of the NWs is almost constant with the doping concentration and is about 25 for the high temperature growth at $T \approx 950\,^{\circ}$C. For a growth temperature of $T \approx 700\,^{\circ}$C, the aspect ratio decreases from 400 to 150. A decrease of the aspect ratio is also observed for the growth at $T \approx 600\,^{\circ}$C and $T \approx 400\,^{\circ}$C, i.e. from 60 to 20 and from 45 to 10 respectively.

The NW diameter is almost constant with the Al doping concentration. For the high temperature process, the diameter is about $d \approx 70$ nm. For the growth at $T \approx 700\,^{\circ}$C and $T \approx 400\,^{\circ}$C the NWs are ultrathin and have a diameter of $d < 10$ nm. For the growth at $T \approx 600\,^{\circ}$C the diameter increases with a doping concentration from $d \approx 10$ nm for $x = 2\,\mathrm{at\%}$ to $d \approx 25$ nm for the seed layer doped by $x = 3.5\,\mathrm{at\%}$ of Al.

For the growth at $T \approx 950\,^{\circ}$C the NW density increases with increasing Al doping concentration from $1\mu\mathrm{m}^{-2}$ on the undoped ZnO seed layer to $100\mu\mathrm{m}^{-2}$ for seed layer doped by $x = 3.5\,\mathrm{at\%}$. For a growth temperature of $T \approx 700\,^{\circ}$C the density slightly increases from $70\mu\mathrm{m}^{-2}$ to $105\mu\mathrm{m}^{-2}$ with increasing doping concentration. For the growth at $T \approx 600\,^{\circ}$C and $T \approx 400\,^{\circ}$C the NW density is almost constant with an Al concentration and is about $110\mu\mathrm{m}^{-2}$ and $120\mu\mathrm{m}^{-2}$ respectively.

For the geometric properties as a function of the growth temperatures, the following behaviors are observed. The aspect ratio decreases with a growth temperature from 400 to 25 for a growth on the undoped seed layer. If the seed layer doped with $x = 2\,\mathrm{at\%}$ of Al is used, the aspect ratio increaes from 10 to 65 as a function of the growth temperature. For the growth on the seed layer with a doping concentration of $x = 3.5\,\mathrm{at\%}$ the aspect ratio is almost constant and is about 25.

An increase of the NW diameter with a growth temperature from $d \approx 7$ nm to $d \approx 70$ nm is observed for the growth on the undoped seed layer. For the seed layer with a doping concentration of $x = 2\,\mathrm{at\%}$ the diameter is almost constant

with a growth temperature and is about $d \approx 10$ nm. The NW diameter increases from $d \approx 25$ nm to $d \approx 90$ nm with increasing growth temperature for a seed layer doping concentration of $x = 3.5\,\mathrm{at\%}$.

A decrease of the NW density is observed as a function of the growth temperature. The density decreases from $70\mu\mathrm{m}^{-2}$ to $1\mu\mathrm{m}^{-2}$ for the growth on the undoped ZnO seed layer. A slight decrease for a temperature is observed from $120\mu\mathrm{m}^{-2}$ to $105\mu\mathrm{m}^{-2}$ and from $110\mu\mathrm{m}^{-2}$ to $100\mu\mathrm{m}^{-2}$ for the growth performed on the seed layers doped by $x = 2\,\mathrm{at\%}$ and $x = 3.5\,\mathrm{at\%}$ of Al, respectively.

As mentioned in the Chapter 5, a kind of the nucleation process - the homogeneous one or the heterogeneous nucleation plays a sufficient role on the density of the NWs, since the number of the nucleation seeds determines the number of the NWs. For the homogeneous nucleation, a higher energy is required in order to obtain a nucleation seed than for the heterogeneous nucleation [26, 83]. The homogeneous nucleation is typical for the deposition of the undoped ZnO particles with high kinetic energy, i.e. in the high-temperature process ($T \approx 950\,°\mathrm{C}$) on the undoped ZnO seed layer. In this case, a lot of particles are involved in creation of the large pyramidal nucleation seed. Thus, a density of the NWs is low compared with growth on other seed layers. If the doped seed layers are used, some of the dopants are located on the surface of the seed layer, i.e. the phase which is another with respect to the ZnO phase appears on the surface. Thus, the dopants support the nucleation process, i.e. the energy which is required for the nucleation is lower than the energy in the homogeneous process [26, 83]. The nucleation process is also depends by the kinetic energy of the particles, e.g. reduction of the growth temperature reduces the intensity of the particle movement and they can be crystallized immediately after the deposition [83]. Additionally, the surface defects can change the kinetic energy of the moving particles. Thus, the particles can be crystallized and create the nucleation seeds after their interaction with the surface defects.

For the high-temperature growth at $T \approx 950\,°\mathrm{C}$ on the ZnO(Al) seed layers, a doping concentration of $x = 3.5\,\mathrm{at\%}$ seems optimum for the NW growth. The Volmer-Weber mode is observed for this process whereas for other Al-doped seed layers the Stranski-Krastanov mode is taken place since the honeycomb-like structures are grown in the lateral and vertical growth directions simultaneously.
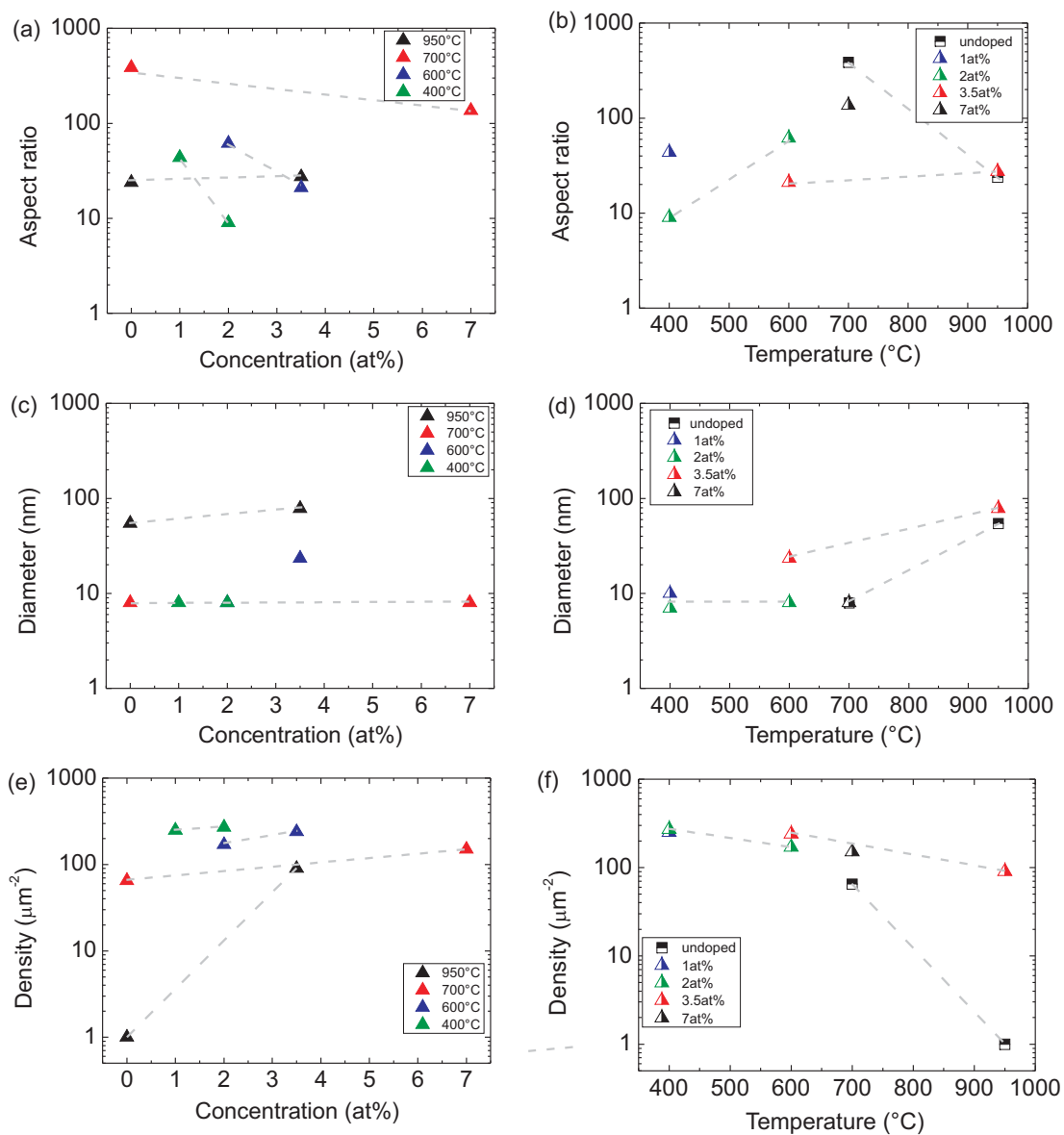
Figure 6.2: The geometrical characteristics of the ZnO NWs grown on the ZnO(Al) seed layer. The grey dashed line are the guide to the eye

The surface properties of the seed layer doped $x = 3.5\,\mathrm{at\%}$ of Al are optimum since this layer has low surface roughness of $R_a = 1.5$ nm and a low FWHM of the rocking curve of about $1°$. It means that the surface free energy is minimal for this seed layer and the Volmer-Weber growth mode is supported. Other Al-doped seed layers have higher surface roughness ($x = 1, 2\,\mathrm{at\%}$) or larger FWHM ($x = 7\,\mathrm{at\%}$) and their surface free energy is higher.

With reduction of the growth temperature to $T \approx 700\,°\mathrm{C}$ the interfacial free energy becomes lower than for the high-temperature process. The optimum doping concentration for the Volmer-Weber mode is shifted to $x = 7\,\mathrm{at\%}$ probably because the lower surface free energy and thus, the lower surface roughness of $R_a \approx 1.0$ nm are required. The crystalline quality of the seed layer and the grain size seems have no significant impact on the growth process at the reduced growth temperature.

For the low-temperature growth processes at $T \approx 600\,°\mathrm{C}$ and $T \approx 400\,°\mathrm{C}$ the optimum doping concentration is shifted to $x = 2\,\mathrm{at\%}$ and $x = 1\,\mathrm{at\%}$ and the size of the grains is more influential properties on the growth process than the surface roughness. It is probably because for these growth temperatures the particles can lose their kinetic energy more likely by the interaction with the grain boundaries than by the interaction with the hills or pits of the surface. Thus, for support of the particle movement, the grains should be large enough. Since for the low growth temperature, the particles with average kinetic energy can be crystallized immediately after the deposition, only few high-energy particles can move on the surface. These high-energy particles can probably easily overcome the obstacles on the surface. These high-energy particles are involved in the development of the NWs whereas all other deposited particles have created numerous nucleation seeds. The particles with high kinetic energy can move upward the nucleation seed and be crystallized on the top of them, i.e. $v_z \gg v_r$ and the ultrathin NWs are fabricated.

## 6.2 NW growth on Ga doped seed layers

The growth on the Ga-doped seed layers compared to the growth on the ZnO(Al) seed layers is slightly different. The NNs can be grown by using the Ga-doped

seed layers. In Fig. 6.3a the SEM images of the obtained structures grown on the seed layers fabricated by LP PLD technique are presented whereas in Fig. 6.3b shown structures grown by CVD method and shown. For comparison, the results obtained on the undoped ZnO seed layer, discussed previously, are also shown. For the highest growth temperature of $T \approx 950\,°C$ on the seed layer doped with $x = 7\,at\%$ of Ga separated and well-oriented vertically NNs were obtained. They are broadened on the bottom and narrowed to the top, such pyramids have a diameter in the middle of 380 nm and an aspect ratio of about 6. On the seed layers doped by $x = 9\,at\%$ and $x = 15\,at\%$ cylindrical NWs were grown. For a doping concentration of $x = 1\,at\%$ nanowall-like structures agglomerated with some NWs were fabricated, on the seed layer doped with $x = 2\,at\%$ of Ga a honeycomb-like structure was obtained and the growth of NWs or rather NNs is completely suppressed. There are no NWs are observed on the seed layers fabricated by CVD. With a reduction of the growth temperature to $T \approx 700\,°C$ the NWs were obtained on the layer with a doping concentration of $x \geq 3.5\,at\%$ and for the seed layer grown by CVD technique as well. For used here the highest doping concentrations the wires have a diameter of 40 nm and an aspect ratio of 70. These NWs are not well-oriented and slightly tilted in different directions with respect to the surface normal. At the same growth temperature the well-oriented and vertically aligned NWs were fabricated on the layer doped by $x = 3.5\,at\%$ of Ga. The diameter of these NWs is about 25 nm and the aspect ratio is 35. For other concentrations at this growth temperature no NWs were obtained and honeycomb-like structures only were fabricated. For the growth temperature of $T \approx 600\,°C$ the NW growth is observed on the seed layer with a concentration of $x = 2\,at\%$, $x = 9\,at\%$, $x = 15\,at\%$ of Ga. These NWs have the aspect ratio of 70, 100 and 110 respectively and the NWs diameter of $d = 8$ nm for all these NWs. A further reduction of the growth temperature to $T \approx 400\,°C$ leads to the growth of high density of the ultrathin NWs on the layer doped by $1\,at\%$ of Ga and on the seed layers grown by CVD, and agglomerated nanostructures on the seed layers doped by $x = 9\,at\%$ and $x = 15\,at\%$ of Ga whereas for the other doping concentrations the growth is suppressed. The obtained ultrathin NWs have a diameter $d \leq 7$ nm and an aspect ratio of about 100.

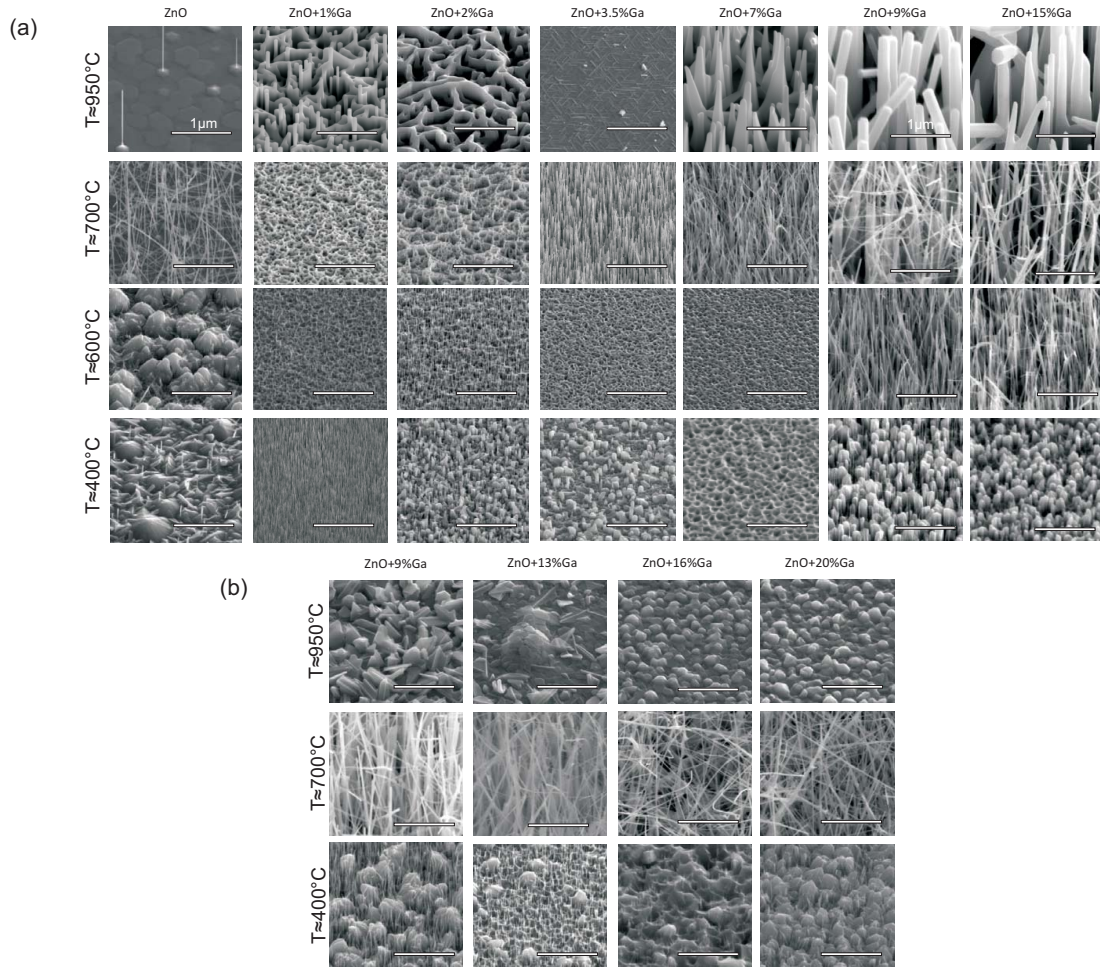In Fig. 6.4 an overall behavior of the geometric properties of the NWs grown

Figure 6.3: The scanning electron microscope (SEM) images of the NWs obtained on the ZnO(Ga) seed layers with different doping concentration performed at different growth temperatures and fabricated by (a) LP PLD or (b) CVD growth techniques

on the ZnO(Ga) seed layers are presented as a function of the doping concentration and the growth temperature. The aspect ratio of the NWs grown at high-temperature of $T \approx 950\,^\circ$C slightly decreases from 25 to about 10 with a Ga doping concentration. For the NWs grown at $T \approx 700\,^\circ$C and $T \approx 600\,^\circ$C the aspect ratio is almost constant with a doping concentration and is about 100 for both kinds of the NWs. The NW aspect ratio decreases with a concentration of the Ga dopants from 100 to about 5 for the NWs grown at $T \approx 400\,^\circ$C.

The diameter of the NWs grown on the seed layers performed by LP PLD increases with a doping concentration whereas for the seed layers fabricated by CVD, the NW diameter is almost constant. The diameter of the NWs obtained by LP PLD at $T \approx 950\,^\circ$C increases from 70 nm to 200 nm, for the growth temperature of $T \approx 700\,^\circ$C an increase is observed from about 10 nm to 25 nm, for $T \approx 600\,^\circ$C the diameter increases from 7 nm to 20 nm and for the fabrication temperature of $T \approx 400\,^\circ$C the increase of the NW diameter is observed in the range from 7 nm to 80 nm. For the seed layer obtained by CVD, the diameter of the NWs is about 30 nm for the processes performed at $T \approx 700\,^\circ$C and about 15 nm for the growth at $T \approx 400\,^\circ$C.

The NW density as a function of the Ga doping concentration increases from $1\,\mu$m$^{-2}$ to about $50\,\mu$m$^{-2}$ for the NWs fabricated at high growth temperature of $T \approx 950\,^\circ$C. For the NW grown at $T < 950\,^\circ$C the NW density is almost constant with a doping concentration and is about $150\,\mu$m$^{-2}$. The constant behavior of the NW density for the growth temperature of $T < 950\,^\circ$C is also independent on the growth technique which was used for the fabrication of the the seed layers.

For the dependence of the aspect ratio on the growth temperature, two main ranges can be introduced - from $T \approx 400\,^\circ$C to $T \approx 700\,^\circ$C and from $T \approx 700\,^\circ$C to $T \approx 950\,^\circ$C. For the NWs fabricated on the seed layers doped by $x = 9\,\mathrm{at}\%$ and $x = 15\,\mathrm{at}\%$ and performed by LP PLD, the aspect ratio increases in the first range from 4 to 100 and decreases in the second range from 100 to 10 with a growth temperature. NWs grown on the seed layers fabricated by CVD and doped by $x = 9\,\mathrm{at}\%$ and $x = 13\,\mathrm{at}\%$ are observed only in the first range and their aspect ratio is almost constant with the doping concentration and is about 50. NWs fabricated on the undoped seed layer and on the seed layer with a doping concentration of $x = 7\,\mathrm{at}\%$ are observed in the second range and their aspect

ratio decreases with increasing growth temperature from about 400 to 25 and from 70 to 6 respectively.

For the NW diameter as a function of the growth temperature the same two ranges of the growth temperature can be used as for the aspect ratio, i.e. from $T \approx 400\,°C$ to $T \approx 700\,°C$ and from $T \approx 700\,°C$ to $T \approx 950\,°C$. In the first temperature range, the diameter of the NWs grown on the seed layers doped by $x = 9\,at\%$ and $x = 15\,at\%$ of Ga and performed by LP PLD decreases from about 70 nm to about 15 nm and increases with increasing temperature in the second range from $d \approx 15$ nm to $d \approx 200$ nm. For the seed layers grown by CVD and having a doping concentration of $x = 9\,at\%$ and $x = 13\,at\%$ the NW diameter increases from 15 nm to 25 nm in the first temperature range only and no behavior is observed in the second range. For the undoped seed layer and the seed layer doped by $x = 7\,at\%$ of Ga, the NW diameter increases with a growth temperature in the second range from $d \approx 10$ to $d \approx 70$ and from $d \approx 25$ to $d \approx 350$ nm.

The density of the NWs obtained on all used seed layers, doped and undoped, monotonically decreases with increasing growth temperature. The decrease is observed from about $150\mu m^{-2}$ to about $10\mu m^{-2}$. The density of the NW grown on the undoped seed layer decrease significantly to $1\mu m^{-2}$ at $T \approx 950\,°C$.

The Ga doping of the seed layers leads to the heterogeneous nucleation process as was mentioned for the Al-doped seed layers. However, in contrast to the Al doping, the ZnO(Ga) layers require a higher nucleation energy and thick NNs can be grown on the layer doped by $x = 7\,at\%$. The NNs are broadened to the bottom, i.e. a large nucleation seed was developed on this layer. At the growth temperature of $T \approx 950\,°C$ more deposited particles are involved in the nucleation process than for the ZnO(Al) seed layers. However, the nucleation energy on the Ga-doped layers is probably lower than for the homogeneous nucleation since a higher NN density is observed.

For the doping concentration of $x = 9\,at\%$ and $x = 15\,at\%$ of Ga, the seed layers have a higher surface roughness and the FWHM of the rocking curves than for the ZnO(Ga) layers doped by $x \leq 7\,at\%$. These surface properties can support the nucleation since any surface defect is a potential place for a crystallization [26]. Thereby, the surface properties of these highly doped seed layers can reduce
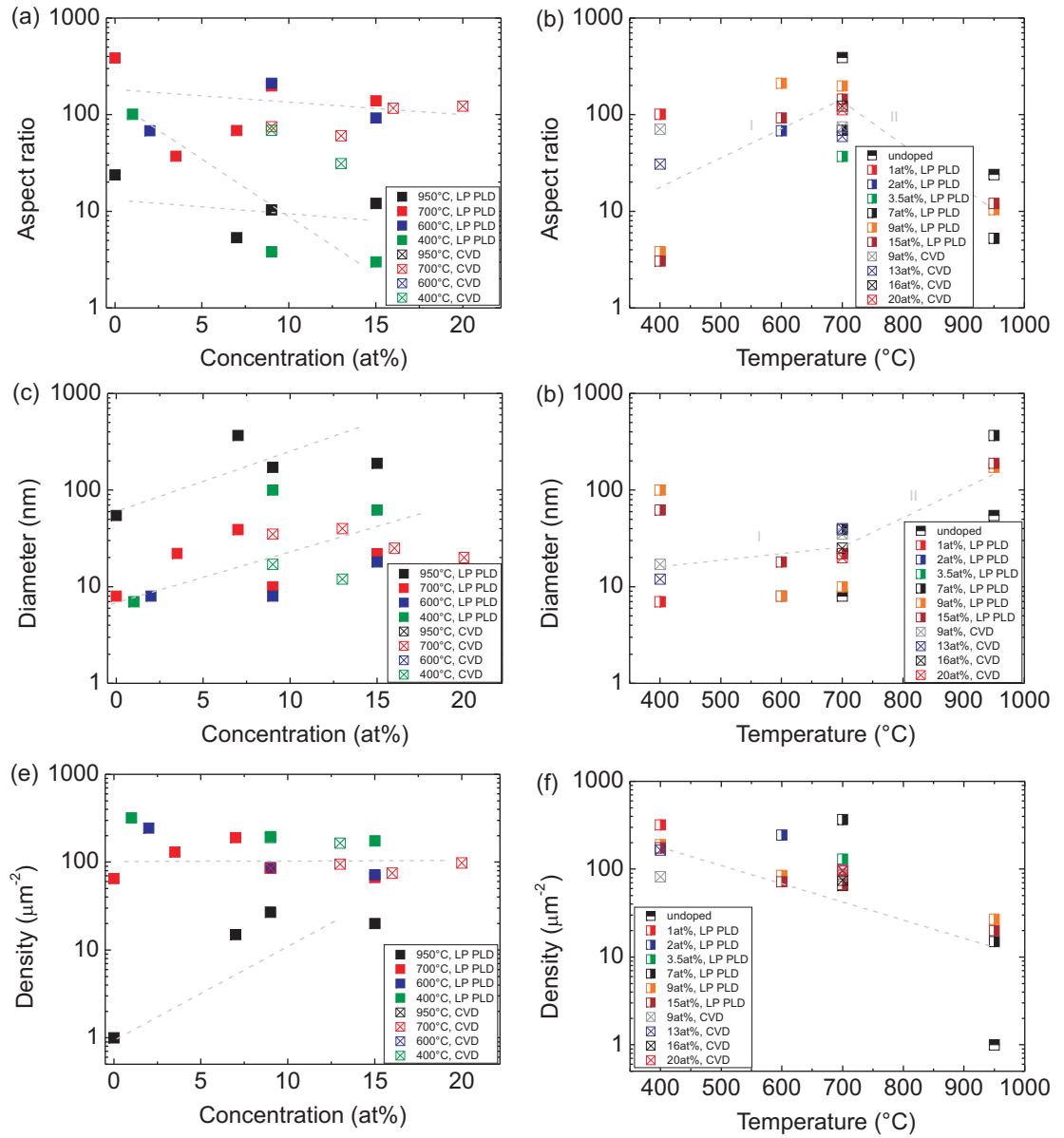
GZO



Figure 6.4: The geometrical characteristics of the ZnO NWs grown on the ZnO(Ga) seed layer. The grey dashed line are the guide to the eye

the required nucleation energy and the number of the particles which are involved in creation of the nucleation seeds [26, 83] and the NW growth can be supported. Such support of the growth is also observed for these seed layers at the growth temperature of $T \approx 600\,^{\circ}\mathrm{C}$. At the same time, for the seed layers with a doping concentration of $x \leq 7\,\mathrm{at\%}$ of Ga, which have a lower surface roughness and the FWHM of the rocking curve, the nucleation process is not supported and no NWs are observed.

The ultrathin NWs grown at the growth temperature of $T \approx 400\,^{\circ}\mathrm{C}$ on the seed layer doped with $x = 1\,\mathrm{at\%}$ of Ga can be explained by the same growth kinetics as mentioned for the Al-doped seed layer with the same doping concentration and the same growth temperature previously. These ultrathin NWs are fabricated because of a small number of the high-energy particles which can easily overcome the most of the surface defects and reach the top of the nucleation seeds for being crystallized there.

Interestingly, that for the seed layers with a doping concentration of $x \geq 9\,\mathrm{at\%}$ fabricated by CVD almost the same results of the NW growth are observed for all doping concentrations used at the growth temperature of $T \approx 950\,^{\circ}\mathrm{C}$ and $T \approx 700\,^{\circ}\mathrm{C}$. These results mean that the surface roughness of $R_a > 3$ nm and FWHM $> 8^{\circ}$ do not play a sufficient role on the seed nucleation and NW growth, but only the growth temperature. For the $T \approx 950\,^{\circ}\mathrm{C}$ the energy which is required for the nucleation can be higher than for the homogeneous nucleation and no NWs are observed. With a reduction of the growth temperature to $T \approx 700\,^{\circ}\mathrm{C}$ the most of the deposited particles are crystallized and they can play a role of the nucleation seeds and a high density of the NWs is observed. The ultrathin NWs fabricated at $T \approx 400\,^{\circ}\mathrm{C}$ on the seed layers doped by $x = 9\,\mathrm{at\%}$ and $x = 13\,\mathrm{at\%}$ of Ga can be grown because of the high energy particles which can overcome the most of the surface defects. However, for the seed layers with a doping concentration of $x \geq 16\,\mathrm{at\%}$ the number of the defects is too large and the high-energy particles are not able to move anymore.

## 6.3   Optical characteristics of the ZnO NWs

The observed NWs have a diameter in wide the range from $d \approx 400$ nm to $d \approx 7$ nm and thus, a strong increase of the surface-to-volume ratio appears with decreasing of the diameter. Increasing of the impact of the surface properties on the emission characteristics of the NWs is expected and in order to investigate the optical properties of the NWs with different diameters, the CL measurements were performed. For this measurements, the NWs with a diameter of $380, 180, 70, 40$ and 10 nm fabricated on the different seed layers and at the different growth temperatures have been chosen. In Fig. 6.5a results of the measurements of the grown NWs are presented. The NWs were investigated by cathodoluminescence (CL) at a temperature of $T \approx 10\,K$. In order to avoid a signal from the seed layer, each sample was cleaved in the middle and the measurements were performed along the vertical direction of the NWs E[32].

Several emission peak are observed for the thick NW with a diameter of $d = 380$ nm around $3.36\,\text{eV}$. These emission peaks mainly originates from the recombination of donor bound excitons [127]. The most prominent peak at E $\approx 3.361\,\text{eV}$ has a broadening of about $2\,\text{meV}$ which is close to the value determined on bulk single crystals of ZnO which is typical for the NWs grown by HP PLD [87].

With decreasing NW diameter the emission peaks at $3.36\,\text{eV}$ become broader and the broadening of 7.7 meV is observed for the NW with a diameter of $d = 40$ nm. With a further reduction of the NW diameter to $d = 10$ nm the observed peaks strongly overlap with each other and cannot be distinguished anymore. In this case the increase of the broadening is also reflected by an increase of the broadening of the entire emission peak (Fig. 6.5b).

Responsible for the observed increase of the broadening might be the bending of the energy bands at the surface near region [34, 35]. Since the surface states that are located within the band gap can be occupied by electrons, the band can be bent upward [128]. It reflects on the change of the electronic structure and emission characteristic. Also, decreasing of the exciton oscillator strength and increase of the surface defects can be attributed to be responsible for the broadening of the corresponding peak of the donor bound excitons [35, 105, 128]. By
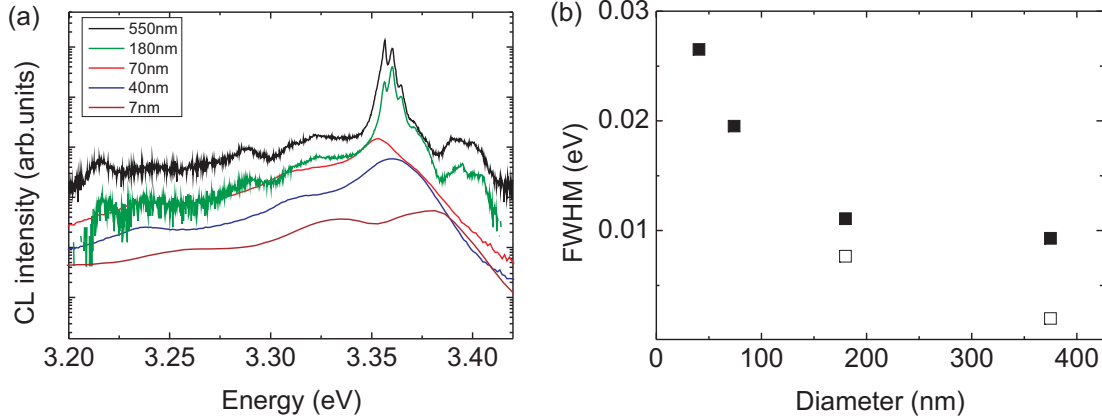
Figure 6.5: (a) CL spectra of ZnO NWs for different diameters. For a better clarity the spectra were shifted vertically. (b) Solid points - the FWHM from entire emission as a function of the diameter of the NWs, empty points - the FWHM from the single peaks for thick NWs

reducing the diameter of the NWs the surface-to volume ratio strongly increases and thus the emission characteristic of the surface near region becomes dominant.

## 6.4   Summary of the Chapter

In this Chapter the following points were discussed:

- Nucleation process is the most important step of the NW growth. The number of the nucleation seeds determines the density of the NWs and the movement of the deposited particles on the surface of the seed layer.

- There are two kinds of a nucleation processes - a homogeneous and a heterogeneous nucleation process [26, 83]. The first one is likely observed for the undoped ZnO NWs growth on the undoped ZnO seed layer whereas the second one is more typical for the growth on the doped seed layers.

- The homogeneous nucleation process requires a high energy of nucleation for a creation of the nucleation seed [83]. Thus, as was shown, the nucleation seeds are large for this process and the most of the deposited particles are

involved in the developing of the seeds. A low NW density is observed for this kind of the nucleation.

- The heterogeneous nucleation is a creation of the seeds on the dopants which are located on the surface or close to the surface of the substrate. For the heterogeneous nucleation process a lower nucleation energy is required compared with the homogeneous process [83]. As it was discussed, for the heterogeneous nucleation the NW seeds are smaller and their number is larger than for the homogeneous nucleation.

- Thick NNs can be fabricated at the high growth temperature of $T \approx 950\,°\mathrm{C}$ on the seed layer doped by $x = 7\,\mathrm{at\%}$ of Ga. This fabrication can probably be attributed to the higher nucleation energy which is required for the growth on the Ga-doped seed layers than for the growth on the Al-doped seed layers since the NNs are broadened on the foot. It means that for the formation of the NN nucleation seed, more deposited particles have been involved than for the formation of the nucleation seed on the ZnO(Al) seed layer with the same doping concentration.

- It was found that for the ZnO(Al) seed layers the surface characteristics have a stronger impact on the growth process than for the ZnO(Ga) seed layers. The surface defects are the obstacles for the particle movement, however they support the nucleation process since the surface defects are the most possible places for the crystallization [26]. A kind of the seed layer polarity seems has a minor and almost neglectable impact on the NW fabrication.

- With reduction of the growth temperature, the interfacial free energy reduces since a lot of deposited ZnO particles are crystallized immediately after the deposition and only few particles with high kinetic energy are able to move. However, for the growth at ZnO(Ga) seed layers with a doping concentration of $x > 2\,\mathrm{at\%}$ and at the growth temperature of $T \approx 700\,°\mathrm{C}$ the immediately crystallized particles form the nucleation seeds and the NW growth is supported. A high density array of $100\,\mu\mathrm{m}^{-2}$ NWs with an aspect ratio of 100 and diameter of $d \approx 25$ nm is observed for such growth.

- For the low-temperature growth at $T \approx 400\,°\mathrm{C}$ the most of the deposited particles are crystallized on the both kinds of the doped seed layers, independently on the growth technique. Only few particles with a high kinetic energy can move on the surface at this growth temperature. Also, only the seed layer with a low density of the grains can support this movement. Such particles can be crystallized as soon as they have reached the top of the nucleation seed or rather the developing NW. Since the high-energy particles is a small fraction of the deposited ZnO particles [126], there is a limited number of particles which are involved in the NW growth. As was demonstrated, the fabrication of the high density vertically oriented array of the ultrathin NWs, i.e. with a diameter of $d < 10$ nm can be obtained at the low growth temperature of $T \approx 400\,°\mathrm{C}$.

- The optical properties of the NWs with different diameters were measured by CL at low temperature of $T = 5$ K. For the thick NWs with a diameter of $d \geq 180$ nm, a broadening of the donor bound exciton of about 2 meV is observed. This reflects the high crystalline quality of the NWs. With decreasing diameter, the broadening of the emission peaks increases and it can be explained by the strong increase of the surface-to-volume ratio for the thin NWs.

## 6. SUMMARY OF THE CHAPTER

# Chapter 7

# Growth of ZnO(Al) and ZnO(Ga) NWs

As mentioned in the Chapter 2, the doping of the ZnO NWs changes their properties and opens new possibilities for their applications in different devices [16, 129]. For the investigation of the NW growth, doping of the deposited material by Al or rather Ga is important since it changes the supersaturation of the vapor and thus, the growth mechanism. The dopants of the deposited material can increase supersaturation of the vapor over the substrate and support the nucleation process. The increased material and interfacial free energies lead to the desired Volmer-Weber growth mode.

As mentioned in the previous Chapter 6, the NW can be grown well-oriented on the doped seed layers and their diameter can be decreased from $d \approx 400$ nm to $d \approx 7$ nm and at the same time, the growth temperature can be reduced. Thus, using of the same range of doping concentrations of $0 \leq x \leq 7$ at% of Al and $0 \leq x \leq 20$ at% of Ga for the NW doping seems promising. However, due to a technical and time limitations, the compromised doping concentrations have to be chosen. In this Chapter growth of Al-doped NWs with a doping concentration of $x = 3.5$ at% on the seed layers doped by $x = 0$ - 7 at% of Al and Ga-doped NWs doped by $x = 1$ at% on the seed layers with $x = 0$ - 7 at% of Ga dopants will be discussed. The geometrical properties of the obtained NWs (diameter, aspect ratio and density) as a function of the doping concentration

and the growth temperature will be presented as well.

## 7.1 Al-doped ZnO NWs grown on ZnO(Al) seed layers

The SEM images of the Al-doped NWs grown on the ZnO(Al) seed layers for different growth temperatures are presented in Fig. 7.1. The results on the un-doped ZnO seed layer at the growth temperatures of $T \approx 950\,°C$ and $T \approx 700\,°C$ exhibited by a high density of non oriented long NWs. These results are similar to the results obtained for undoped NWs on such seed layer at $T \approx 700\,°C$ but with higher length and density. The reduction of the growth temperature to $T \approx 600\,°C$ and $T \approx 400\,°C$ leads to a vanishing of the NW growth and only some agglomerated pyramids-like structures were grown.

For the seed layer doped by $x = 1\,at\%$ the results of the NW growth are similar to that obtained on the undoped seed layer at the temperatures of $T \approx 950\,°C$ and $T \approx 700\,°C$, i.e. a high density array of non-oriented NWs. For a growth temperature of $T \approx 600\,°C$ some agglomerated nanoparticles were grown and at $T \approx 400\,°C$ the pyramidal structures were obtained instead of a well-oriented array of the ultrathin undoped NWs which were observed in the previous Chapter and fabricated on the same seed layer with the same growth temperature.

With increasing of the doping concentration to $x = 2\,at\%$ the situation is changed. Almost no NWs were obtained for a high growth temperature of $T \approx 950\,°C$ and only a honeycomb-like structure was obtained for a growth temperature of $T \approx 700\,°C$. For $T \approx 600\,°C$ a low density array of thin NWs was grown and for the growth temperature of $T \approx 400\,°C$ a high density array of ultrathin NWs was fabricated.

For a doping concentration of $x = 3.5\,at\%$ some short nanocolumns were grown at low growth temperature of $T \approx 400\,°C$. A well-oriented array of NWs was obtained at the growth temperature of $T \approx 600\,°C$ and some NWs between nanowall- and honeycomb-like structures were fabricated at the $T \approx 700\,°C$. The vertically-aligned NWs were grown at the highest growth temperature and this result is similar to the result of undoped NW growth.

For the doping concentration of $x = 7 \, \text{at\%}$ of Al the results are similar to the undoped NW, i.e. agglomerated structure was grown at $T \approx 950\,^\circ\text{C}$, well-oriented NWs were achieved at $T \approx 700\,^\circ\text{C}$, almost no NWs were fabricated at the growth temperatures of $T < 600\,^\circ\text{C}$.
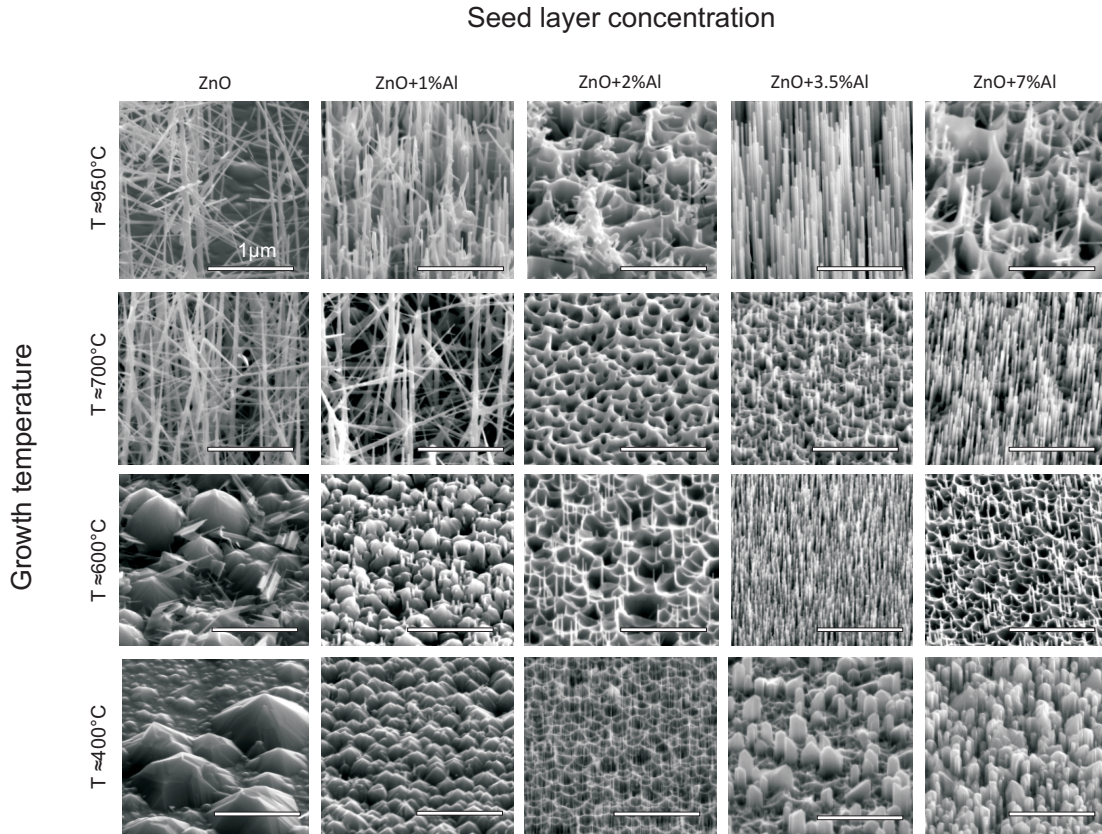
Seed layer concentration



Figure 7.1: The scanning electron microscope (SEM) images of the NWs doped by $x = 3.5 \, \text{at\%}$ of Al dopants obtained on the ZnO(Al) seed layers with different doping concentration performed at the different growth temperatures

The overall behavior of the aspect ratio, diameter and density of the ZnO(Al) NWs as function of the seed layer doping concentration or rather growth temperature are presented in Fig. 7.2. The behavior of the geometric properties of the Al-doped NWs is different to the behavior of the undoped NW properties. For instance, the aspect ratio of the NWs fabricated at high growth temperatures of $T \geq 700\,^\circ\text{C}$ decreases from about 80 to 10 with increasing doping concentration. The aspect ratio increases with an Al concentration from 20 to 60 for the NWs

grown at $T \approx 600\,°C$ and constant with a doping concentration and is about 5 for the NWs fabricated at $T \approx 400\,°C$.

The diameter of the Al-doped NWs does not change with the doping concentration. For the growth temperatures of $T \approx 950\,°C$ and $T \approx 700\,°C$ the diameter of the NWs is about 40 nm. The NWs grown at $T \approx 600\,°C$ have a diameter of about 10 nm. For the NWs fabricated at the growth temperature of $T \approx 400\,°C$ the diameter of 100 nm is observed. The NW density slightly increases from $20\mu m^{-2}$ to about $100\mu m^{-2}$ for all used growth temperature.

The aspect ratio increases with increasing growth temperature from 5 to 15 for the NWs grown on the seed layer doped by $x = 7\,at\%$ and from 5 to 80 for the growth on the seed layer with a doping concentration of $x = 3.5\,at\%$. For the higher growth temperature of $T \geq 600\,°C$ the aspect ratio is constant for these seed layers. If the seed layer is doped by $x = 2\,at\%$ of Al, the aspect ratio is constant with a growth temperature and is about 50. For the lowest doping concentration of $x = 1\,at\%$ and for the growth on the undoped seed layer, the NW aspect ratio is constant with a growth temperature and is about 20 and 70 respectively.

The diameter of the NWs grown on the undoped seed layer is constant with a growth temperature and is about 40 nm. For the NW fabrication on the seed layer with Al doping concentration of $x = 1\,at\%$ the diameter increases from 10 nm to 80 nm in the range of temperature from $T \approx 600\,°C$ to $T \approx 700\,°C$. For the seed layer doped by $x = 2\,at\%$ the diameter is constant with a growth temperature and is about 10 nm. An slight increase of the diameter with the growth temperature from about 10 nm to 30 nm is observed for the NWs obtained on the seed layer with $x = 3.5\,at\%$ of Al dopants. On the seed layer with a doping concentration of $x = 7\,at\%$ the NW diameter decreases from about 100 nm to 20 nm in the low temperature range from $T \approx 400\,°C$ to $T \approx 600\,°C$ and than remains constant in the high temperature range

The density of the NWs grown on the seed layers doped by $x = 2\,at\%$ decreases with increasing growth temperature from $200\mu m^{-2}$ to $30\mu m^{-2}$. For all other doping concentrations as well as for the undoped seed layers the NW density fluctuates in the range from $20\mu m^{-2}$ to $80\mu m^{-2}$ and no clear dependence on the growth temperature can be observed.
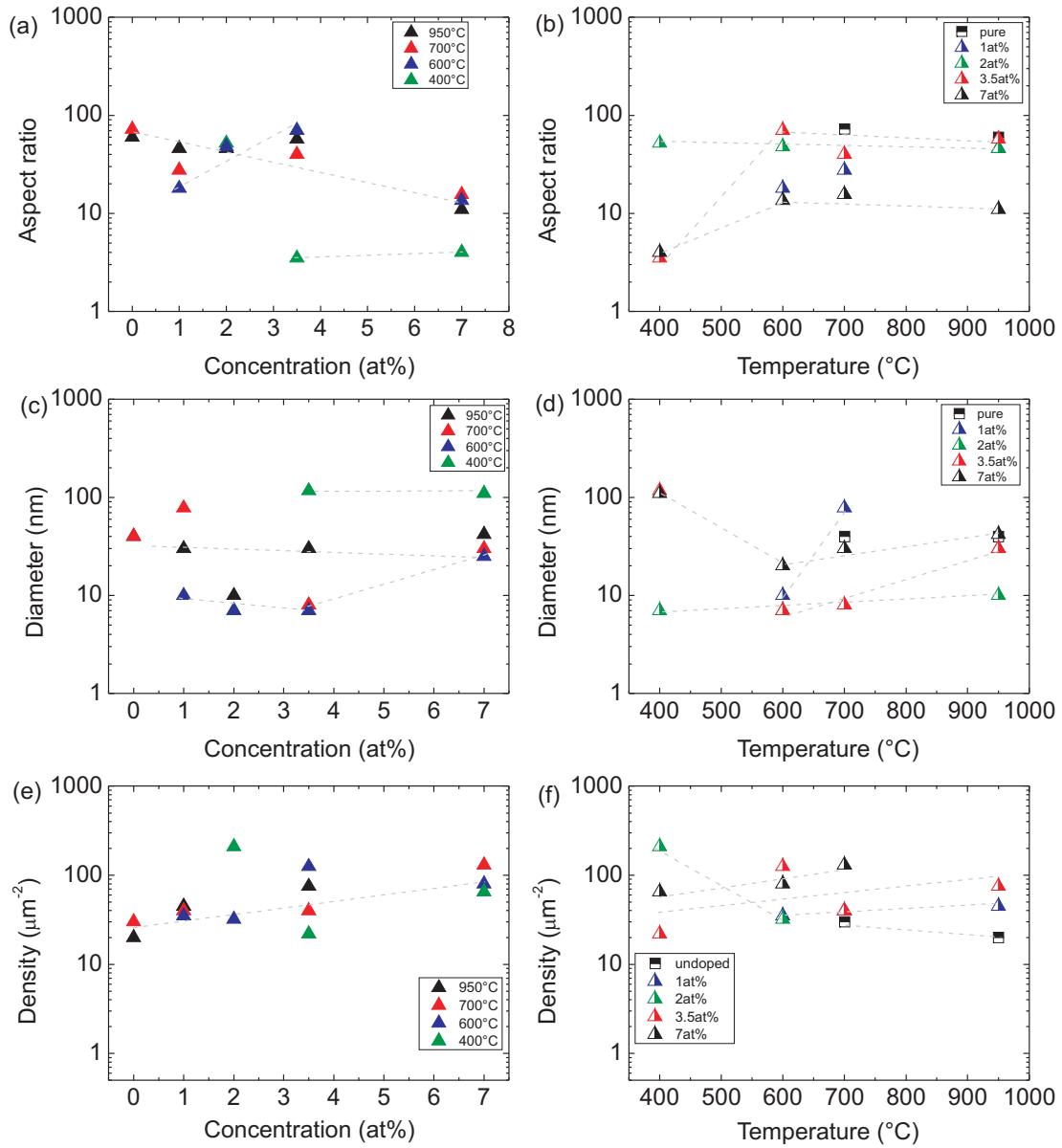
AZO NWs on AZO seed layers



Figure 7.2: Geometrical characteristics of the Al doped NWs fabricated on the ZnO(Al) seed layers as a function of the doping concentration and the growth temperature. The grey dashed line is a guide for the eye

## 7. AL-DOPED ZNO NWS GROWN ON ZNO(AL) SEED LAYERS

As mentioned previously in the Chapter 3, for the HP PLD growth technique, presence of the Ar flow leads to a formation of the ZnO and $Al_2O_3$ particles of the vapor instead of ions which are typical for the LP PLD [29]. Since the $Al_2O_3$ particles are heavier than the ZnO particles, the doped vapor is heavier compared to the undoped one. Thus, the pressure of the doped vapor is larger than the pressure of the undoped ZnO vapor and hence, the supersaturation of the vapor increases with a doping. Thereby, the material free energy is increased in comparison with the material free energy of the undoped vapor.

The deposited $Al_2O_3$ particles form a new phase on the surface of the seed layer [26, 29] and thus, the heterogeneous nucleation process is possible. It reflects on the growth of the high density array of the NWs which is observed on the undoped ZnO seed layer at $T \geq 700\,°C$. A slight increase of the FWHM of the rocking curve which is observed for the seed layer doped by $x = 1\,at\%$ of Al in comparison with the FWHM of the rocking curve of the undoped ZnO seed layer can be compensated by a slight decrease of the $R_a$ and no significant changes of the growth mechanism are observed for the high temperatures of $T \geq 700\,°C$. However, further increasing of the FWHM of the rocking curve which was determined for the seed layer doped by $x = 2\,at\%$ of Al cannot be compensated by decreasing of the surface roughness and no NWs were fabricated at the high growth temperatures.

For the Al doping concentration of $x = 3.5\,at\%$ the FWHM of the rocking curve is not increased significantly in comparison with the FWHM of the rocking curve of the seed layer doped by $x = 2\,at\%$ of Al. However, the reduction of the surface roughness to 1.2 nm can decrease the surface free energy and support the Volmer-Weber growth mode. The surface roughness of the seed layer doped by $x = 7\,at\%$ of Al is almost the same as for the layer with $x = 3.5\,at\%$ of dopants, however its FWHM of the rocking curve is increased by 1.2°. Such increase of the surface free energy does not lead to the NW growth at the growth temperature of $T \approx 950\,°C$. Reduction of the temperature to $T \approx 700\,°C$ can support the nucleation since more particles can be crystallized immediately after the deposition and moreover, a high density of grain boundaries can attract the deposited particles to be crystallized there. Thus, the high density array of the NWs is observed for the seed layer doped by $x = 7\,at\%$ of Al.

Reduction of the growth temperature to $T \approx 600\,°$C significantly reduces the interfacial free energy and deposited particles cannot move on the substrates with a supposed high surface free energy. Thus, no NWs are observed for the undoped seed layer as well as for the layers with a doping concentration of $x = 1\,$at% and $x = 2\,$at%. However, with reduction of the surface free energy, which was attributed for the seed layer doped by $x = 3.5\,$at% the NW growth is possible. The NW growth on the seed layer with $x = 7\,$at% of Al dopants can be explained by an impact of the small grains of this seed layers and the numerous grain boundaries can support the nucleation.

For the growth temperature of $T \approx 400\,°$C, growth of ultrathin NWs is observed on the seed layer doped with $x = 2\,$at% of Al instead of doping concentration of $x = 1\,$at% as was found for the undoped ZnO NWs. The shift of the optimum doping concentration can be explained by a reduction of the number of high energy particles with doping of the deposited material. However, the reduction of the surface roughness and the surface free energy can support the movement of the high energy particles and they can reach the top of the nucleation seeds, i.e. the NWs can be grown. Further increasing of the doping concentration can support the movement of the particles with average kinetic energy. These particles can interact with the particles with high kinetic energy and their movement can be stopped. For this situation the nanocolumns were grown, i.e. the Volmer-Weber growth mode is slightly shifted to the Stranski-Krastanov one, and the difference of the free energy $\Delta F \to 0$.

## 7.2 Ga-doped ZnO NWs grown on ZnO(Ga) seed layers

In Fig. 7.3 the SEM images of the Ga-doped ZnO structures are presented. Remarkably, high density array of the cylindrical NWs was obtained for a high growth temperature process of $T \approx 950\,°$C on the undoped ZnO seed layer. With decreasing the growth temperature to $T \approx 700\,°$C the NWs become thinner and tilted in different directions and in different angles with respect to the surface normal. However, with further decreasing of the growth temperature to $T \approx 600\,°$C

and $T \approx 400\,^\circ$C no NWs were obtained and only agglomerated particles were observable.

The NW growth on the doped seed layers with doping concentration of $x = 1\,\mathrm{at\%}$ leads to a change of the grown nanostructuress. For the growth temperature of $T \approx 950\,^\circ$C an array of NNs was obtained instead of cylindrical NWs. A reduction of the growth temperature to $T \approx 700\,^\circ$C suppresses the NW growth and only honeycomb-like structures were obtained. Surprisingly, NWs were fabricated for low growth temperature of $T \leq 600\,^\circ$C and the density of the NWs is increased with decreasing temperature.

For the seed layer with $x = 2\,\mathrm{at\%}$ of Ga dopants step-like non well-oriented NNs were grown. Notably these NNs are not well-oriented. For the growth temperature of $T \approx 700\,^\circ$C a combination of nanowall-like structure and cylindrical NWs was obtained and NWs only were fabricated at the growth temperature of $T \approx 600\,^\circ$C. However, at low growth temperature of $T \approx 400\,^\circ$C the NW growth was vanished. Similar results were obtained on the seed layer with Ga concentration of $x = 3.5\,\mathrm{at\%}$. However, for this doping concentration of the seed layers a nanowall-like structure at the growth temperature of $T \approx 600\,^\circ$C was not observable.

On the seed layer with a doping concentration of $x = 7\,\mathrm{at\%}$ the step-like NNs become more disoriented for the highest growth temperature. A high density array of the well-oriented NWs was obtained for the growth temperature of $T \approx 700\,^\circ$C. On this seed layer a nanowall-like structure is observable at the growth temperature of $T \approx 600\,^\circ$C and a combination of thick and thin NWs was fabricated at the low temperature growth of $T \approx 400\,^\circ$C.

The overall geometric properties (aspect ratio, diameter and density) of the ZnO(Ga) NWs fabricated on the Ga-doped seed layers as a function of the doping concentration of the seed layer and the growth temperature are presented in Fig. 7.4. For the NWs fabricated at $T \approx 950\,^\circ$C on the undoped seed layer the aspect ratio is about 30 and it decreases to 10 and remains constant for all doping concentrations of the seed layers. For the growth temperature of $T \approx 700\,^\circ$C the aspect ratio increases from 20 to about 150 with increasing doping concentration. The NWs obtained at $T \approx 600\,^\circ$C on the seed layer doped by $x = 1\,\mathrm{at\%}$ of Ga dopants have the aspect ratio of 10 and it increases to about 30 and remains
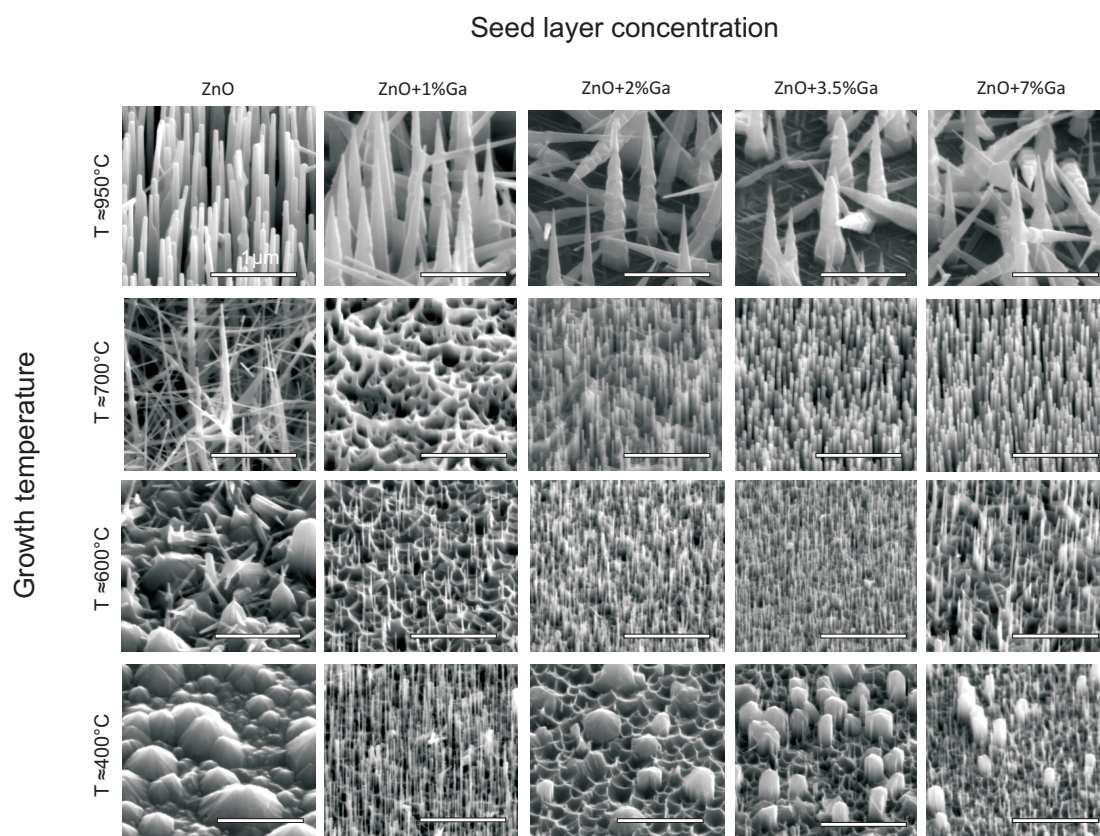
Figure 7.3: The scanning electron microscope (SEM) images of the NWs doped by $x = 1\,\text{at}\%$ of Ga dopants obtained on the ZnO(Ga) seed layers with different doping concentration performed at the different growth temperatures

constant with a doping concentrations. The aspect ratio of the NWs grown at $T \approx 400\,^{\circ}\mathrm{C}$ decreases with increasing Ga doping concentration from 100 to 50.

A constant NW diameter with a doping concentration of about 200 nm is observable for the highest growth temperature of $T \approx 950\,^{\circ}\mathrm{C}$. For the growth temperature of $T \approx 700\,^{\circ}\mathrm{C}$ the NW diameter decreases with increasing Ga concentration of the seed layer from 70 nm to 10 nm. For the doping concentrations of $x \leq 3.5\,\mathrm{at\%}$ the diameter of the NWs grown at $T \approx 600\,^{\circ}\mathrm{C}$ decreases from 30 nm to 7 nm and then increases to 20 nm with the doping concentration of $3.5 < x \leq 7\,\mathrm{at\%}$. For the NWs fabricated at the growth temperature of $T \approx 400\,^{\circ}\mathrm{C}$ the diameter is constant as a function of the seed layer doping concentration and is about 7 nm.

The density of the NWs fabricated at $T \approx 950\,^{\circ}\mathrm{C}$ slightly decreases from $30\mu\mathrm{m}^{-2}$ to $10\mu\mathrm{m}^{-2}$ in the range of the seed layer doping concentration of $x \leq 3.5\,\mathrm{at\%}$. In the range of the highest Ga doping concentration of $3.5 < x \leq 7\,\mathrm{at\%}$ the NW density slightly increases to $20\mu\mathrm{m}^{-2}$. For the NWs obtained at $T \leq 700\,^{\circ}\mathrm{C}$ the density is almost constant with the doping concentration and is about $150\mu\mathrm{m}^{-2}$.

The aspect ratio of the NWs obtained on the doped seed layers decreases with increasing growth temperature from about 70 to about 10. For the seed layer doped with $x = 7\,\mathrm{at\%}$ of Ga the aspect ratio is 150 for the growth temperature of $T \approx 700\,^{\circ}\mathrm{C}$. For the NWs fabricated on the undoped seed layer the aspect ratio is almost constant with the growth temperature and is about 30.

The NW diameter increases with increasing growth temperature from about 10 nm to about 250 nm. This behavior is observed for all used doped seed layers. However, for the NWs grown on the undoped seed layers the diameter is constant with the growth temperature and is about 70 nm.

The NW density is constant with increasing the growth temperature in the range from $T \approx 700\,^{\circ}\mathrm{C}$ to $T \approx 700\,^{\circ}\mathrm{C}$ and is about $150\mu\mathrm{m}^{-2}$. However, for the higher range of the growth temperature of $T > 700\,^{\circ}\mathrm{C}$ the NW density decreases to about $20\mu\mathrm{m}^{-2}$.

The heterogeneous nucleation process can be attributed to the ZnO(Ga) deposition on any kind of the used seed layer. Important, that on the all kinds of the Ga-doped seed layers at the highest growth temperature, the complex step-
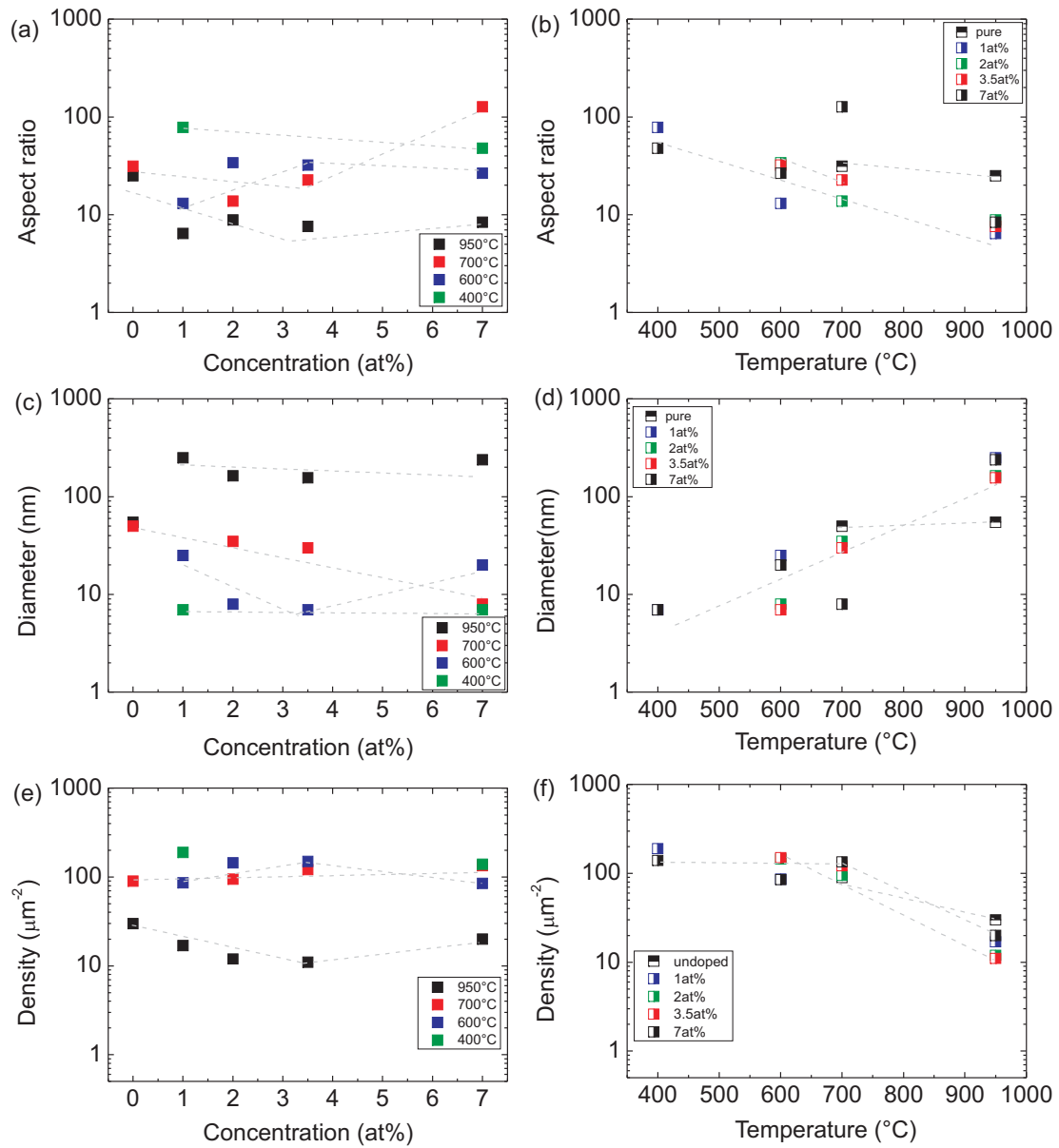
GZO NWs on GZO seed layers



Figure 7.4: Geometrical characteristics of the Ga doped NWs fabricated on the ZnO(Ga) seed layers as a function of the doping concentration and the growth temperature. The grey dashed line is a guide for the eye

like NNs were grown. Such growth might be caused by an increased nucleation energy compared to the Al-doped NW growth. As mentioned in the Chapter 6, the nucleation seeds on the Ga-doped layers have a larger size than the seeds on the Al-doped seed layers because the higher nucleation energy is required for the nucleation on the ZnO(Ga) layer than on the ZnO(Al) seed layer. Such nucleation seeds on the Ga-doped seed layers have probably a pyramidal shape as the undoped ZnO seeds formed on the undoped ZnO seed layer at high temperature of $T \approx 950\,°C$. The moving interfacial particles have a high kinetic energy and aspire to reach the top of the nucleation pyramid-like seed by the flows $f_1$ (which can deliver the particles to the sides of the seeds) and $f_2$ (which drives the particles to the top of the pyramid) as shown in Fig. 7.5a. However, the top of the nucleation seed has a limited place for the crystallization and the most of the particles can move downward by the flow $f_3$ (Fig. 7.5b). Since the moving particles are doped by the heavy Ga dopants, their movements consume a lot of energy and the particles cannot reach the surface of the substrate and become crystallized on the sides of the pyramidal seed. Further moving particles which are driven by the flows $f_1+f_2$ and also have reached the top of the pyramid and moved downward might be crystallized over the previously crystallized particles and a new pyramid-like structure is growing over the previous one and the growth of the step-like NNs is taken place (Fig. 7.5c).
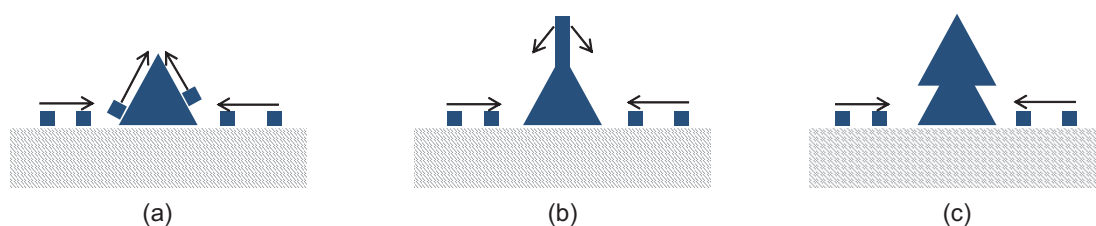


Figure 7.5: The possible scheme of the step-like NN growth: (a) particles reaching the top of the nucleation seed, (b) particles moving from the top of the nucleation seed downhill, (c) particles have been crystallized on the sides of the nucleation seed and next particles might be crystallized over the previously crystallized particles

With reduction of the growth temperature to $T \approx 700\,°C$ no NNs, neither conventional nor step-like, are presented. The growth of the high density array

of the NWs on the undoped seed layer is caused by a significant impact of the material free energy. As for the Al-doped ZnO deposition, the Ga doping enhances the supersaturation of the vapor and thus, the material free energy. However, due to difficult nucleation of the seeds on the Ga-doped seed layers, the interfacial free energy reduces with doping of the seed layer by $x = 1\,\mathrm{at}\%$ of Ga and the Volmer-Weber growth mode is shifted to the Stranski-Krastanov one. For the seed layer doped by $x = 3.5\,\mathrm{at}\%$ of Ga dopants, the small surface roughness of $R_a = 1.1$ nm and small FWHM of the rocking curve of $0.8°$ reduce the surface free energy and the growth of the NWs is possible. For the seed layer with a Ga doping concentration of $x = 7\,\mathrm{at}\%$ an impact of the increased surface roughness of $R_a = 2$ nm is compensated by small FWHM of $0.7°$ and the surface free energy is less influential on the growth process than a sum of $F_m + F_i$ and the NWs were fabricated.

The growth temperature of $T \approx 600\,°\mathrm{C}$ supports the nucleation since a lot of deposited particles have low kinetic energy, they cannot move and were crystallized soon after the deposition. Thus, numerous nucleation seeds were created. The growth of thin NWs is explained by the particles with a high kinetic energy. These particles can reach the top of the seeds and be crystallized there. However, a number of these high energy particles is limited and NWs cannot be developed well in the lateral direction.

A fabrication of the ultrathin NWs at the growth temperature of $T \approx 400\,°\mathrm{C}$ on the seed layer doped by $x = 1\,\mathrm{at}\%$ of Ga is similar to the undoped NWs grown at the same growth temperature and on the same seed layer. Probably, such low growth temperature determines the nucleation process instead of the kind of the doping material and thus the growth results are similar. However, for the higher doping concentration of $x = 2\,\mathrm{at}\%$ and $x = 3.5\,\mathrm{at}\%$ no NWs are observed probably due to an impact of the surface free energy and increasing of the FWHM of the rocking curves with the doping concentration. For these seed layers the grain boundaries are obstacles for the movement of the high-energy particles and the ultrathin NWs cannot be grown.

## 7.3 Summary of the Chapter

In this Chapter the following aspects were discussed:

- The Al or rather Ga dopants of the vapor increase its pressure and the supersaturation. Thus, the material free energy is supposed to be increased.

- Doped deposited material leads to the heterogeneous nucleation process, i.e. the required nucleation energy is lower than for the homogeneous nucleation and the numerous nucleation seeds can be formed.

- A nucleation process on the ZnO(Ga) seed layers requires a higher nucleation energy than for the Al-doped seed layers since the Ga dopants are heavier than the Al dopants. It reflects on the growth of the NNs on all kinds of the used Ga-doped layers at the high growth temperature of $T \approx 950\,°C$. For this growth process, the kinetic energy of the interfacial particles is supported by the high temperature and they can easily reach the top of the growing structure and move downward. The downward movement appears because of a competition between the particles for the place on the top of the pyramidal-like NN. The Ga-doped particles are also heavier than the undoped ZnO and the doped particles cannot be transfered to the surface of the substrate. Thus, the Ga-doped ZnO particles can be crystallized on the sides of the NNs forming the step-like structures.

- The low growth temperature can support the nucleation process since most of the deposited particles have a low kinetic energy, they cannot move on the surface and become crystallized. Thus, growth of the ultrathin Al or Ga doped NWs is possible at low growth temperature of $T \leq 600\,°C$.

- The doping of the NW material in a combination with the variation of the doping concentration of the seed layers and the growth temperature have a strong impact on the NW geometric properties, i.e. the NW diameter, length, aspect ratio and density.

# Chapter 8

# Growth of tilted ZnO NWs and NNs

In this Chapter an approach to obtain unidirectional growth of ZnO NWs is presented. For this purpose, the sapphire substrate was patterned. It is shown that, the growth of tilted structures can be realized in two ways: i) cylindrical NWs and ii) NNs. The type of the structures, NWs or NNs, can be controlled by the used substrate. Additionally, optical properties of the NWs and NNs are discussed.

## 8.1 Patterning of the substrates

A growth of the ZnO NWs on $a$- and $c$-facets of the sapphire is well-known (e.g. in the Ref. [25, 130]). On such surface orientations the NWs can be grown with a high density, large diameter and high aspect ratio. A bulk $r$-plane oriented sapphire contains a $c$-facet inside, which is tilted by 58° with respect to the surface normal of the $r$-facet [131]. However, the $c$-facet does not presented on the surface of the bulk $r$-plane oriented sapphire crystal. A patterning of the $r$-plane sapphire allows to achieve the $c$-facet of the surface and the NWs grown on the $c$-facet are expected to be tilted with respect to the $r$-plane normal.

The patterning of the $r$-plane sapphire was performed by the wet-chemical etching at CNRS-CRHEA, Valbonne, France and is presented in details in the

91

# 8. PATTERNING OF THE SUBSTRATES

Ref. [132] and [133]. A strong anisotropy of the etching rate of the different crystallographic planes is exploited and $c$-facets which are tilted with respect to the $r$-facet normal are obtained. The angle of the tilt is about $58°$. A 200 nm $SiO_2$ layer was sputtered on $r$-plane sapphire wafer by using a RF-sputtering and a patterning of the $SiO_2$ was performed by using a standard photolithography process. The $SiO_2$ stripes protect the sapphire areas from the etching since the $SiO_2$ does not react with the used acids. The stripes are 2 $\mu$m wide and oriented along the $\{1\bar{1}01\}$ direction with a period of 10 $\mu$m. For the etching process a mixture of $H_3PO_4$ and $H_2SO_4$ acids were used with a ratio of 3:1 and a temperature of $T \approx 270°$C was applied. The substrate was immersed in the mixture for 20 min and subsequent rinsing in deionized water. Remarkably, the ratio of the etching rates between $c$- and $r$-plane is about 10 which allows to achieve the tilted $c$-plane facets with respect to surface plane of the $r$-facet. The scheme of the obtained structure is presented in Fig. 8.1. The surface consist 8 $\mu$m wide trenches which have a depth of about 400 nm. Moreover, a 3 $\mu$m wide mesa with a desired tilted $c$-facet is presented between the trenches.
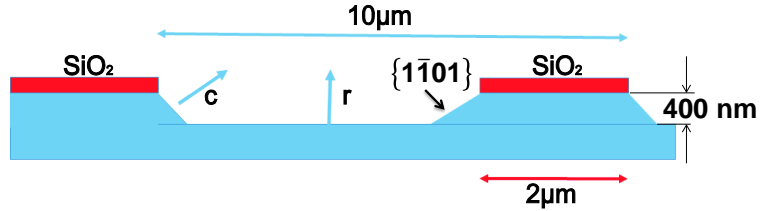


Figure 8.1: Scheme of the structured sapphire substrates.

In doing so the substrate consists of four differently oriented surfaces: a $c$-plane, $\{1\bar{1}01\}$ plane, $SiO_2$ on the mesa and the $r$-plane between the mesa. However, only on the $c$-facet an oriented NW growth is expected. The $SiO_2$ layer can support the movement of the particles due to its non-crystalline structure [134] and the particles which are deposited on the $SiO_2$ layer can easily be transfered to the sapphire planes where they can be crystallized. Thus, two promising ways will be presented in order to achieve the NW growth: remaining the $SiO_2$ layer

and it removing. For last case, some substrates were additionally etched in a buffered HF solution for 15 min at room temperature in order to remove the $SiO_2$ top layer before the growth of the NWs.

## 8.2 Growth of tilted NNs

For the growth of the undoped ZnO tilted nanostructures, a high-temperature growth at $T \approx 950\,°C$ has been chosen in order to support the interfacial free energy and the movement of the deposited particles. A reduction of the temperature to $T \leq 700\,°C$ leads to the growth of long and thin NWs with a diameter of $d \approx 20$ nm and aspect ratio of about 300 and the tilted nanostructures cannot be de defined among the other grown structures. The low temperatures of $T < 700\,°C$ suppress the NW growth.

The scanning electron microscope (SEM) images of the nanostructures obtained on the patterned sapphire substrate with a $SiO_2$ layer on top of the mesa are shown in Fig. 8.2. Here needle-like structures on the $SiO_2$ layer and on the $c$-plane, are observable. On the $c$-plane the NNs are well-oriented, with their c-axis perpendicular to this surface and therefore the NNs are tilted with respect to the substrate normal by $58°$. Furthermore, the high density of these NNs at this facet was expected. Here the density of about 5 NNs per $\mu m^{-2}$ is observed. The NN diameter is about 800 nm and the aspect ratio is 2.75 (the length of the NN was taken along the normal of the $c$-facet). In contrast to these NNs, the NNs observed on the mesa covered with $SiO_2$ layer are not well oriented vertically along the surface normal since the $SiO_2$ is amorphous and typically does not support the well-oriented growth. For the $r$-plane and $\{1\bar{1}01\}$ fecet no growth of NWs or NNs was observed. An occurrence of the undesired NNs on the $SiO_2$ layer might be a disadvantage for the applications of the tilted NNs.

A cross-sectional SEM image of the nanoneedles is shown in Fig. 8.2c. Remarkably, the $r$-facet between the mesa is covered by the ZnO layer with a thickness of about 250 nm, whereas the ZnO layer on the $SiO_2$ is only 50 nm thick. The NN has a complex shape, it becomes narrowing from the foot on the $c$-plane oriented facet. However, in the length of about 200 nm, the NN becomes broadening. After 200 nm more, the narrowing of the structure appears again. The supposed
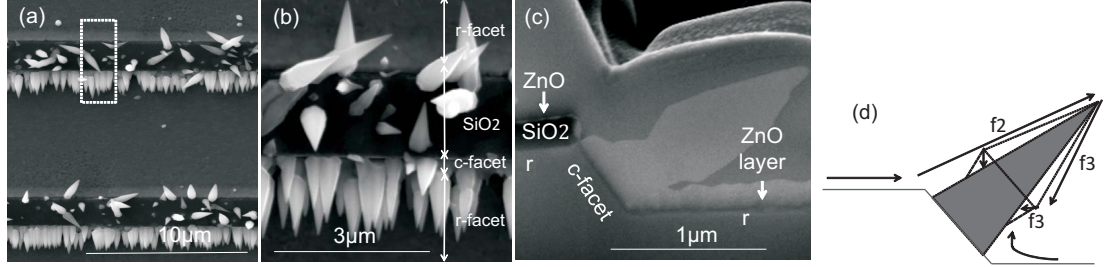
Figure 8.2: The scanning electrone microscope (SEM) images of NNs obtained on the patterned sapphire substrate with $SiO_2$ layer on the top of the mesa: (a) top view with low magnication, white dashed rectangle indicates area for high magnication and cross-section measurements (c). A scheme of the possible growth of the NN complex shape (d)

scheme of the NN growth is shown in Fig. 8.2d. Such complex shape of the NN is possible because of support of the ZnO particles which can be transfered from the $SiO_2$ and from the $r$-facet between the mesa to the $c$-facet. However, such transfer consumes the energy, and the transfered particles can have a lower kinetic energy than the particles which were directly deposited on the $c$-facet. The low energy particles are crystallized after their transfer and cover entire surface of the $c$-facet, whereas the high energy particles are able to move over the crystallized particles. The structure is growing as a pyramid here, and the moving particles which are driven by the flow $f_2$ aspire to reach the top of the pyramid. However, due to the limited space on the top of the pyramid, the particles are moving downward by the flow $f_3$. This flow meets new particles driven by the flow $f_2$ and because of a interaction of these two flows, the structure becomes broadening.

## 8.3 Growth of tilted NWs

The results obtained on the substrates without a $SiO_2$ layer on the mesa are shown in Fig. 8.3. Similar to the substrates with a $SiO_2$ layer, a well oriented growth of nanostructures is observable on the $c$-plane. However, in this case NWs were fabricated instead of NNs. Additionally, the thick ZnO layers with the thickness of about 200 nm are observed on the mesa and on the $r$-facet between the mesa. For the $r$-facet and for the $\{1\bar{1}01\}$ oriented facet some non-oriented

NWs are obtained. The NWs have a typical diameter of 150 nm and the aspect ratio of 12 which was taken along the normal to the $c$-facet.

A possible reason of the growth of the NWs instead of NNs is the absence of the $SiO_2$ layer. The uncovered $r$-plane oriented facet does not support the movement of the particles and at the same time, it does not support the NW growth. Thus, the particles which were deposited on $r$-plane are crystallized there as a layer which can be seen in Fig. 8.3a. The number of the particles on the $c$-plane is lower than in the case with presented $SiO_2$ layer and less particles are crystallized on the surface of the $c$-facet. Thus, the particles which are deposited directly to the $c$-facet can move upward with the flow $f_2$ and the thinner NW is growing on contrast to the thick NN. However, the interaction of the two flows, $f_2$ and $f_3$, is also presented here and a slight broadening of the NW in a length of about 200 nm from the foot is observed.
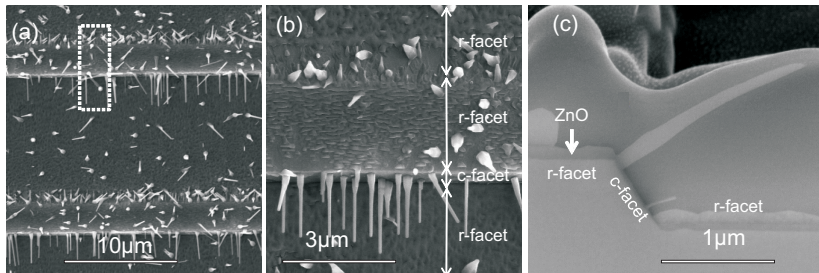


Figure 8.3: The scanning electron microscope (SEM) images of the NWs growth results on patterned sapphire substrate without $SiO_2$ mesa covering layer: (a) top view with low magnification, white dashed rectangle indicates area for high magnification (b) and cross-section measurements (c)

## 8.4 Optical properties of the tilted nanostructures

The optical properties of the obtained tilted nanostructures were investigated by cathodoluminescence spectroscopy (CL) at low temperature of $T = 5$ K. For this purpose, the sample was cleaved and the measurements were taken from the middle of each nanostructure. The CL spectra of NWs and NNs are presented in

Fig. 8.4. The NN has two pronounced emission peaks at $E = 3.357$ eV with the FWHM of about 2 meV and at $E = 3.60$ eV with the FWHM of 5 meV. These peaks belongs to the recombination of donor bound exciton emission [77, 127]. The broad peak at $E = 3.323$ eV originates from two-electron satellite emission. The weak peaks on the low energy range of $E = 3.320 - 3.330$ eV are the optical phonon replicas of the strong emission peak.

The NW has a less pronounced emission peak than the NN. This peak is observed at $E = 3.360$ eV and caused by recombination of donor bound excitons. The FWHM of the of the corresponding peak of the donor bound exciton is 12 meV which is comparable with the FWHM of the emission peak mentioned for the vertically oriented NWs in the Chapter 6. The emission peak of the tilted NW has two shoulders at $E = 3.355$ eV and $E = 3.371$ eV. Peaks of the two-electron satellite emission cannot be distinguished.

Since the NW is thinner than the NN in the middle, broadening of the emission peak of the NW can be caused by significant impact of the surface near region on the emission. This effect was also observed for the vertically oriented NWs mentioned in the Chapter 6. The emission of the narrowed tip of the NN can be determined by the surface defects and the broadening of the emission peak might be observed. However, for conforming this assumption a much higher spacial resolution of the CL is required. The decrease of the oscillator strength and bending of the energy bands at the surface near region can be responsible for the increasing of the FWHM of the emission peaks [105].

## 8.5  Summary of the Chapter

The following aspect were discussed in this Chapter:

- Patterned sapphire substrate with tilted $c$-plane oriented facets allows to grow NNs and NWs which are tilted by $58°$ with respect to the surface normal. This angle is determined by the tilt of the $c$-facet.

- The presence of the $SiO_2$ layer which covers the top of the mesa has a strong impact on the kind of the growing structure - NW or NN. For the growth
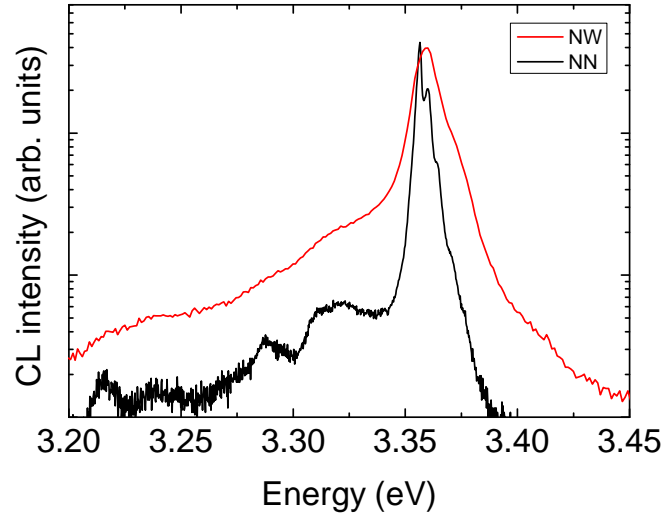
Figure 8.4: CL spectra of tilted ZnO NN (black) and NW (red). For a better clarity the spectrum of the NW was shifted vertically

of thick NN with a complex shape the presence the $SiO_2$ layer is required whereas its absence leads to the growth of the cylindrical thin NWs.

- The $SiO_2$ layer supports the movement of impinging particles on its surface and they can be transfered to the sapphire facets. Also, the particles deposited on the $r$-plane oriented facet between the mesa can be transfered to the $c$-facet. However, these transfers consume the kinetic energy of the particles and they can be crystallized on the entire $c$-facet. The high energy kinetic particles which are deposited directly on the $c$-facet are driven by intense flows $f_2$ and $f_3$ and interaction of the flows leads to the growth of the NNs.

- The particles which were deposited on the uncovered by $r$-facet are mostly crystallized there into the ZnO layer without transferring to the $c$-facet. Thus, less particles appear on the $c$-facet compared with the substrate with $SiO_2$ on the mesa. In this case, the high-energy particles develop thin cylindrical NWs.

- The low-temperature CL measurements revealed the pronounced emission peaks for the NN and less distinguished peak for the NW. A broadening of the corresponding peak of the donor bound exciton of 2 meV is observed for the NNs whereas for the NWs the broadening is increased to 12 meV. Such increasing of the broadening can be attributed to the decrease of the oscillator strength and bending of the energy bands at the surface near region.

# Chapter 9

# Summary and outloock

## 9.1 Summary

In this thesis the growth mechanism and growth kinetics of the undoped, Al or rather Ga doped ZnO NWs and a fabrication of the tilted NWs and NN were discussed.

The NWs are more likely grown by the Volmer-Weber mode of the epitaxial growth mechanism. The free energy which determines this growth mode is: $\Delta F = F_m + F_i - F_s > 0$, where $F_m$ is a free energy of the deposited material, $F_i$ - free energy of the interface and $F_s$ is a free energy of the surface of the substrate. The HP PLD technique allows to increase the pressure of the deposited material by using a transport gas. Thus, the supersaturation of the vapor is supported. The number of the laser pulses and doping of the deposited material are influential parameters on the material free energy. The interfacial free energy is strongly depends on the growth temperature which can be varied in the range from $T \approx 950\,°C$ to the CMOS compatible temperature $T \approx 400\,°C$ and thereby these NWs can be used as a building block for a variety of applications. The free energy of the surface depends on the surface roughness and the crystalline quality of the seed layers. The doping of the seed layers by Al with the range of the concentration of $1 < x < 7\,at\%$ or by Ga with the doping concentration of $1 < x < 20\,at\%$ as well as using different techniques for the seed layer fabrication (LP PLD or CVD) allow to vary the average surface roughness from $R_a \approx 1$ nm to $R_a \approx 11.5$ nm

and the FWHM of the rocking curves taken from the ZnO (0001) plane from $1°$ to $11°$ and thus the surface free energy is supposed to be changed.

There are two kinds of the nucleation - homogeneous one and the heterogeneous nucleation process. The homogeneous nucleation is more likely observed for the growth on the undoped ZnO nanostructures on the undoped ZnO seed layer. For this process a large nucleation energy is required and the nucleation seeds are formed larger than for the heterogeneous nucleation. For the deposition of the undoped ZnO nanostructures on the doped seed layers, doped structures on the undoped seed layers and for the fabrication of the doped nanostructures on the doped seed layers the heterogeneous nucleation can be attributed. The nucleation energy can define the density of the NWs by the number of the nucleation seeds and the shape of the nanostructures - NWs or NNs which are observed on the Ga-doped seed layers.

In the Chapter 5 was shown that there are several growth regimes which are observed with increasing of the laser pulses - growth of the NWs in the lateral and vertical directions, thinning of the NWs and increasing of its aspect ratio and increasing of the diameter with reduction of the aspect ratio. For explanation of this effect, following growth model can be introduced. The particles which were deposited on the seed layers but not yet crystallized can form different flows of the particles. Four main flows can be taken into account since their combination and interaction determine the growth process:

- The flow $f_1$ delivers the particles to the nucleation seeds and drives them on the NW sides. This flow can be responsible for the first growth regime when the NW growing in the vertical and the lateral direction

- The flow $f_2$ is associated with appearance of the step-like tip of the NWs. This flow drives the particles upward from the sides of the NWs to the top of the tip. This flow can be responsible for thinning of the NW and increasing of its length

- The flow $f_3$ is opposite to the flow $f_2$ and represents a moving of the particles downward from the top of the tip to the sides of the NWs. This flow appears when the number of the particles on the tip is quite large.

- A constant deposition of the particles on the sides of the NWs is the flow $f_4$. A combination of this flow with $f_3$ is responsible for increasing of the NW diameter with a slight decrease of its aspect ratio.

By using doped and undoped seed layers and different growth temperature, the NW diameter, aspect ratio and the density can be adjusted. For instance, it was demonstrated in the Chapter 6 that the growth of the ultrathin NWs with a diameter of $d \leq 10$ nm can be grown at $T \approx 400\,°C$. These NWs have the aspect ratio of about 100, density of about $350\mu m^{-2}$ and are well-oriented vertically. The diameter of these NWs is comparable with the Bohr radius leading to the presence of quantum effects [51]. Thereby such NWs can be used for the quantum research applications.

For the Al and Ga doped nanostructures a tuning of the optical and electrical properties are expected [16]. Thereby, growth of the doped nanostructures with a diameter in the range from $d \approx 250$ nm to $d \leq 10$ nm and aspect ratio between 100 and about 10 which was demonstrated in the Chapter 7 can be favorable for different applications. Moreover, the fabrication of the doped and undoped NNs which is rarely reported in the literature [54] can be promising for the development of the devices based on the electron emission since the NNs have a sharp tip.

In the Chapter 8 the unidirectional growth of tilted ZnO NWs or NNs was demonstrated by using a patterned substrate. For such growth, the NW/NN tilting angle of $58°$ is determined by the tilt of the $c$-plane with respect to the surface normal. The presence of the $SiO_2$ layer on the top of the mesa leads to the growth of NNs since the $SiO_2$ might support the particle movement and the particles can be transferred to the $c$-plane oriented facet. Such transfer consumes the kinetic energy of the particles and they are crystallized on the entire $c$-plane surface. The particles which were deposited directly on the $c$-facet can move upward the crystallized particles and develop the NN. Such NNs have a typical aspect ratio of 2.75 and the diameter in the middle of 800 nm. The mesa without the $SiO_2$ does not support the particle movement and the particles are crystallized into the ZnO layer on the $r$-plane. Thus, on the $c$-plane small seeds are formed which are developed into the cylindrical NW. These NWs have an aspect ratio of 12 and the diameter of 150 nm.

The optical properties of the vertically oriented and the tilted undoped nanostructures were measured by the CL at low temperature of $T \approx 5$ K. A broadening of corresponding peak of the donor bound exciton of about 2 meV is observed for the NWs with a diameter of $d \geq 180$ nm and the tilted NNs which reflects the high crystalline quality of the nanostructures. However, with decreasing of their diameter, a broadening is increased which can be attributed to the the strong increase of the surface defects [34] and/or to the decrease of the oscillator strength [105].

## 9.2   Outlook

The fabricated ultrathin NWs with a diameter of $d \approx 7$ nm and high aspect ratio of about 100 are promising for further investigations. Such ultrathin NWs mainly consist of surface atoms and a strong enhancement of the sensitivity of the NW based gas sensors and photocatalytic applications is expected. Additionally, the size of these devices can be strongly reduced.

For bending of these ultrathin NWs only few charges are necessary and thus the NWs can be easily used for piezoelectric applications and the magnitude of the bending should depend on the magnitude strength of the electric field. It is supported by the fact that the dipole moment in such NWs is predicted to be ten times larger compared to those of a bulk crystal [135]. The enhanced dipole interaction should be also reflected by the optical properties and an enhancement of the linear optical response as well as increased light-matter coupling strength is expected. The last one is interesting since due to the possibility to realize ultra-low threshold lasers and polaritonic circuits which combine the advantages of an electric system, i.e. the strong interaction with each other and with environment, with the long range propagation of the optical one. The diameter of these nanowires is comparable with the Bohr radius leading to presence of quantum effects [51].

Beside the NW applications, their growth kinetics can be deeply investigated in order to create a kinetic model for the growth process. Measurements of the properties of the vapor, i.e. its temperature and pressure are important for understanding of the supersaturation and supercooling of the vapor and the impact

of the material free energy on the growth process. Modeling of the deposited particles movement can support the investigation of the interfacial free energy. For this purpose more complex flows of the particles should be taken into account and the Monte Carlo modeling calculations should be used.

# Acknowledgements

- Anja Heck and Birgit Wendisch for organization help

- Dr. Elise Saoutieff, Marjolaine Allain and staff of CEA LETI (Grenoble, France) for the seed layer fabrication by CVD growth technique. Thanks to all members of the PiezoMAT consortium for the discussion of the selective growth of the NWs and their applications

- Dr. Guy Feuillet from CEA LETI (Grenoble, France), Dr. Florian Tendille and Dr. Philippe De Mierry from CNRS-CRHEA (Valbonne, France) for preparation of the patterned sapphire substrates and discussion of the tilted NW growth

- current and former members of the Ellipsometry Working group for the weekly discussions

# Curriculum Vitae

**Personal information**

| | |
|---|---|
| Name: | Shkurmanov, Alexander |
| Date of birth: | June 9, 1991 |
| Place of birth: | Seryshevo, Russia |
| Nationality: | Russian |

**Education and scientic activities**

| | |
|---|---|
| 1998 - 2001 | Primary school in Kharkiv, Ukraine |
| 2001 - 2008 | Secondary school in Severny, Belgorod oblast, Russia |
| 2008 | Graduation from Severny Secondary school, Severny, Belgorod oblast, Russia |
| 2008 - 2012 | Bachelor student, V.N. Karazin Kharkiv National University |
| 2012 | Bachelor thesis: *"Dynamics of sapphire growth by using Kyropoulos method"* |
| 2012 - 2013 | Master student, V.N. Karazin Kharkiv National University |
| 2013 | Master thesis: *"Bulk sapphires grown by Kyropoulos method"* |
| since 2013 | PhD student, Universität Leipzig |
| since 2013 | Scientific assistant, Felix-Bloch-Institut für Festkörperphysik, Universität Leipzig |

# List of own Articles

The following articles have been published in the course of this thesis or are submitted for publication:

1. A. Shkurmanov, C. Sturm, J. Lenzner, G. Feuillet, F. Tendille, P. DeMierry, and M. Grundmann, Selective growth of tilted ZnO nanoneedles and nanowires by PLD on patterned sapphire substrates, AIP Advances, **6**, 095013, 2016

2. A. Shkurmanov, C. Sturm, H. Hochmuth, and M. Grundmann, Growth kinetics of ultrathin ZnO nanowires grown by pulsed laser deposition, Procedia Engineering, **168**, 1156, 2016

3. A. Shkurmanov, C. Sturm, H. Franke, J. Lenzner, and M. Grundmann, "Low temperature PLD-growth of ultrathin ZnO nanowires by using $Zn_xAl_{1-x}O$ and $Zn_xGa_{1-x}O$ seed layers, Nanoscale Research Lett., **12**, 134, 2017

4. A. Shkurmanov, C. Sturm, H. Hochmuth, and M. Grundmann, Growth kinetics of the $Zn_xAl_{1-x}O$ and $Zn_xGa_{1-x}O$ nanowires in the PLD process" *the manuscript is in preparation*

# List of own Conference Talks and Posters

1. <u>A. Shkurmanov</u>, C. Sturm, H. Franke, M. Grundmann. *Low temperature PLD-growth of ZnO nanowires* (talk), TCO-2014, Leipzig (2014)

2. <u>A. Shkurmanov</u>, C. Sturm, H. Franke, H. Hochmuth, M. Grundmann. *Low temperature PLD-growth of ZnO nanowires on $Zn_xAl_{1-x}O$ films* (talk), DPG-Frühjahrstagung 2015, Berlin (2015)

3. <u>A. Shkurmanov</u>, C. Sturm, H. Hochmuth, M. Grundmann. *Growth of ultrathin ZnO nanowires* (poster), Minisymposium: Quantum Coherent Structures, Leipzig (2015)

4. <u>A. Shkurmanov</u>, C. Sturm, H. Hochmuth, M. Grundmann. *CMOS-compatible PLD-growth of ultrathin ZnO nanowires* (talk), DPG-Frühjahrstagung 2016, Regensburg (2016)

5. <u>A. Shkurmanov</u>, C. Sturm, G. Feuillet, F. Tendille, P. De Mierry, H. Hochmuth, M. Grundmann. *Growth of tilted ZnO nanowires by PLD on pre-structured sapphire substrates* (poster), DPG-Frühjahrstagung 2016, Regensburg (2016)

6. <u>A. Shkurmanov</u>, C. Sturm, G. Feuillet, F. Tendille, P. De Mierry, H. Hochmuth, M. Grundmann. *Growth of ultrathin ZnO nanowires at CMOS compatible temperature by pulsed laser depositions* (poster), E-MRS 2016, Lille (2016)

7. <u>A. Shkurmanov</u>, C. Sturm, H. Hochmuth, M. Grundmann. *Controlling of the geometrical shape of ZnO nanowires by pulsed laser deposition* (poster), NGPT 2016, Rome (2016)

8. <u>A. Shkurmanov</u>, C. Sturm, H. Hochmuth, M. Grundmann. *Growth of Ultrathin ZnO Nanowires by Pulsed Laser Deposition* (poster), Eurosensors XXX, Budapest (2016)

9. <u>A. Shkurmanov</u>, C. Sturm, G. Feuillet, F. Tendille, P. De Mierry, H. Hochmuth, M. Grundmann. *Tilted nanowires as building block for hyperbolic metamaterials* (poster), Scientific Module 2016-T6: Hybrid Systems - Metamaterials, Leipzig (2016)

10. <u>A. Shkurmanov</u>, C. Sturm, H. Hochmuth, M. Grundmann. *Al-doped ZnO nanowires grown by PLD* (talk), DPG-Frühjahrstagung 2017, Dresden (2017)

# Selbständigkeitserklärung

Hiermit erkläre ich, die vorliegende Arbeit selbständig und ohne unerlaubte fremde Hilfe angefertigt zu haben. Ich habe keine anderen als die in der Literatur angeführten Quellen benutzt und sämtliche der Literatur entnommenen Textstellen als solche kenntlich gemacht.

Ich versichere, dass keine weiteren Personen bei der geistigen Erstellung der vorliegenden Arbeit beteiligt waren, insbesondere weder mittelbar noch unmittelbar geldwerte Leistungen erhalten haben, die im Zusammenhang mit dem Inhalt der vorgelegten Dissertation stehen.

Die vorgelegte Arbeit wurde weder im Inland noch im Ausland in gleicher oder ähnlicher Form einer anderen Prüfungsbehörde zum Zwecke einer Promotion oder eines anderen Prüfungsverfahrens vorgelegt und ist in ihrer Gesamtheit noch nicht veröffentlicht. Darüberhinaus versichere ich, dass keine früheren Promotionsversuche stattgefunden haben.

Ich erkenne die Promotionsordnung in ihrer Fassung 23. März 2010 an.

Leipzig, den 06.07.2017

# References

[1] M Grundmann, *The Physics of Semiconductors*, Springer-Verlag, 2 edition, 2010. 1, 7

[2] Andreas Rahm, *Growth and Characterization of ZnO-based Nanostructures*, PhD thesis, Universität Leipzig, 2007. 1, 3, 7, 8, 10, 13, 14, 15, 21, 23, 25, 26, 30, 31, 36, 37, 50, 51, 52, 53, 60

[3] Z L Wang, "From nanogenerators to piezotronics - a decade-long study of ZnO nanostructures", *MRS Bulletin*, vol. 37, pp. 814, 2012. 1, 2, 9, 10, 12, 14

[4] Ü Özgür, Y I Alivov, C Liu, A Teke, M A Reshchikov, S Doğan, V Avrutin, S-J Cho, and H Morkoç, "A comprehensive review of ZnO materials and devices", *J. Appl. Phys.*, vol. 98, pp. 041301, 2005. 1

[5] M J Vellekoop, C C O Visser, P M Sarro, and A Venema, "Compatibility of zinc oxide with silicon IC processing", *Sensors and Actuators A: Physical*, vol. 23, pp. 1027, 1990. 1

[6] S C Minne, S R Manalis, and C F Quate, "Parallel atomic force microscopy using cantilevers with integrated piezoresistive sensors and integrated piezo-electric actuators", *Appl. Phys. Lett.*, vol. 67, pp. 3918, 1995. 1

[7] P M Verghese and D R Clarke, "Piezoelectric contributions to the electrical behavior of ZnO varistors", *J. Appl. Phys.*, vol. 87, pp. 4430, 2000. 1

[8] W L Hughes and Z L Wang, "Nanobelts as nanocantilevers", *Appl. Phys. Lett.*, vol. 82, no. 17, pp. 2887, 2003. 1

[9] W I Park, J S Kim, G-C Yi, and H-J Li, "ZnO nanorod logic circuits", *Adv. Mater*, vol. 17, pp. 1393, 2005. 1

[10] M S Arnold, P Avouris, Z W Pan, and Z L Wang, "Field-Effect Transistors Based on Single Semiconducting Oxide Nanobelts", *J. Phys. Chem*, vol. 107, pp. 659, 2003. 1

[11] S M Frolov, S R Plissard, S Nedj-Perge, L P Kouwenhoven, and E P A M Bakkers, "Quantum computing based on semiconductor nanowires", *MRS Bulletin*, vol. 38, pp. 809, 2013. 1

[12] A K Sharma, J Narayan, J F Muth, C W Teng, C Jin, A Kvit, R M Kolbas, and O W Holland, "Optical and structural properties of epitaxial $Mg_xZn_{1-x}O$ alloys", *Appl. Phys. Lett.*, vol. 75, pp. 3327, 1999. 1

[13] A Ohtomo, M Kawasaki, T Koida, K Masubuchi, H Koinuma, Y Sakurai, Y Yoshida, T Yasuda, and Y Segawa, "$Mg_xZn_{1-x}O$ as a II-VI widegap semiconductor alloy", *Appl. Phys. Lett.*, vol. 72, pp. 2466, 1998. 1

[14] C-L Hsu, C-W Su, and T-J Hsueh, "Enhanced field emission of Al-doped ZnO nanowires grown on a flexible polyimide substrate with UV exposure", *RSC Adv.*, vol. 4, pp. 2980, 2014. 2

[15] A Mavlonov, S Richter, H von Wenckstern, R Schmidt-Grund, J Lenzner, M Lorenz, and M Grundmann, "Doping efficiency and limits in (Mg,Zn)O:Al,Ga thin films with two-dimensional lateral composition spread", *Phys. Status Solidi A*, vol. 12, no. 12, pp. 2850, 2015. 2

[16] G Zimmermann, M Lange, B Cao, M Lorenz, and M Grundmann, "Resistivity control of ZnO nanowires by Al doping", *Phys. Status Solidi RRL*, vol. 4, no. 3-4, pp. 82, 2010. 2, 9, 77, 101

[17] Z Qiu, X Yang, J Han, P Zhang, B Cao, Z Dai, G Duan, and W Cai, "Sodium-doped ZnO nanowires grown by high-pressure PLD and their acceptor-related optical properties", *J. Am. Ceram. Soc.*, vol. 97, no. 7, pp. 2177, 2014. 2

[18] S Sedky, A Witvrouw, H Bender, and K Baert, "Experimental determination of the maximum post-process annealing temperature for standard cmos wafers", *IEEE TRANSACTIONS ON ELECTRON DEVICES*, vol. 48, no. 2, pp. 377, 2001. 2

[19] M Riaz, J Song, O Nur, Z L Wang and M Willander, " Study of the Piezo-electric Power Generation of ZnO Nanowire Arrays Grown by Different Methods", *Adv. Funct. Mater.*, vol. 21, pp. 628, 2011. 2

[20] X Wang, J Song, J Liu, and Z L Wang, "Direct-current nanogenerator driven by ultrasonic waves", *Science*, vol. 316, pp. 102, 2007. 2

[21] I S Nefedov, C A Valagiannopoulos, S M Hashemi, and E I Nefedov, "Total absorption in asymmetric hyperbolic media", *Scientific Reports*, vol. 3, no. 2662, pp. 1 – 6, 2013. 2, 9

[22] C Pan, L Dong, G Zhu, S Niu, R Yu, Q Yang, Y Liu, and Z L Wang, "High-resolution electroluminescent imaging of pressure distribution using a piezoelectric nanowire led array", *Nature Photonics*, vol. 7, pp. 752, 2013. 2, 7, 9, 11

[23] M Lorenz, E M Kaidashev, A Rahm, T Nobis, J Lenzner, G Wagner, D Spemann, H Hochmuth, and M Grundmann, "$Mg_xZn_{1-x}O$ nanowire arrays on sapphire grown by high-pressure pulsed-laser deposition", *Appl. Phys. Lett.*, vol. 86, no. 14, pp. 143113, 2005. 2, 14, 21, 22, 25, 27, 31, 50, 51, 52, 53

[24] M Lorenz, *Zinc oxide as transparent electronic material and its application in thin film solar cells*, Springer, 2006. 2, 15, 22, 28, 30, 36, 51, 52

[25] C P Dietrich and M Grundmann, *Wide Band Gap Semiconductor Nanowires: Low-Dimensionality Effects and Growth*, Wiley-ISTE, 2014. 2, 9, 15, 22, 31, 52, 53, 91

[26] A A Chernov, *Modern Crystallography III*, Springer-Verlag, 1984. 2, 3, 8, 14, 15, 16, 17, 19, 20, 21, 22, 39, 40, 42, 43, 44, 50, 51, 53, 56, 63, 69, 71, 73, 74, 82

[27] Roman Tsybukh, *A comparative study of platinum nanodeposits on HOPG (0001), MnO(100) and $MnO_x$ /MnO(100) surfaces by STM and AFM after heat treatment in UHV, $O_2$ , CO and $H_2$*, PhD thesis, Universiteit Leiden, 2010. 2, 3, 15, 16, 17

[28] M Förster and M Bohnet, "Influence of the interfacial free energy crystal/heat transfer surface on the induction period during fouling", *Int. J. Therm. Sci.*, vol. 38, pp. 944–954, 1999. 2, 3, 21, 49

[29] J S Horwitz and J A Sprague, *Pulsed Laser Deposition of Thin Films*, Wiley-Interscience, 1994. 2, 3, 13, 15, 16, 18, 19, 21, 22, 28, 31, 36, 49, 51, 52, 82

[30] A Shkurmanov, C Sturm, H Hochmuth, and M Grundmann, "Growth kinetics of the $Zn_xAl_{1-x}O$ and $Zn_xGa_{1-x}O$ nanowires in the PLD process - in preparation". 50

[31] A Shkurmanov, C Sturm, H Hochmuth, and M Grundmann, "Growth kinetics of ultrathin ZnO nanowires grown by pulsed laser deposition", *Procedia Engineering*, vol. 168, pp. 1156, 2016. 54

[32] A Shkurmanov, C Sturm, H Franke, J Lenzner, and M Grundmann, "Low temperature PLD-growth of ultrathin ZnO nanowires by using $Zn_xAl_{1-x}O$ and $Zn_xGa_{1-x}O$ seed layers", *Nanoscale Research Lett*, vol. 12, pp. 134, 2017. 9, 26, 27, 37, 39, 53, 72

[33] S Käbisch, M A Gluba, C Klimm, S Krause, N Koch, and N H Nickel, "Polarity driven morphology of zinc oxide nanostructures", *Appl. Phys. Lett.*, vol. 103, no. 10, pp. 103106, 2013. 3, 27, 37, 38, 39, 45

[34] R Schmidt-Grund, P Kühne, C Czekalla, D Schumacher, C Sturm, and M Grundmann, "Determination of the refractive index of single crystal bulk samples and micro-structures", *Thin Solid Films*, vol. 519, pp. 2777, 2011. 3, 9, 72, 102

[35] L Wischmeier, T Voss, I Rückmann, and J Gutowski, "Dynamics of surface-excitonic emission in ZnO nanowires", *PHYSICAL REVIEW B*, vol. 74, pp. 195333, 2006. 3, 72

[36] Z L Wang, "ZnO nanowire and nanobelt platform for nanotechnology", *Mater. Sci. Eng. R*, vol. 64, pp. 33, 2009. 3, 7, 9, 10, 25

[37] J Zúñiga-Pérez, A Rahm, C Czekalla, J Lenzner, M Lorenz, and M Grundmann, "Ordered growth of tilted ZnO nanowires: morphological, structural and optical characterization", *Nanotechnology*, vol. 18, pp. 195303, 2007. 3, 25

[38] R Yang, R Zhu, W Zhang, and C Li, "Uniform zinc oxide nanowire arrays grown on nonepitaxial surface with general orientation control", *Nano Lett.*, vol. 13, pp. 5171–5176, 2013. 3, 9, 25

[39] A Shkurmanov, C Sturm, J Lenzner, G Feuillet, F Tendille, P DeMierry, and M Grundmann, "Selective growth of tilted zno nanoneedles and nanowires by PLD on patterned sapphire substrates", *AIP Advances*, vol. 6, pp. 095013, 2016.

[40] V A Coleman and C Jagadish, *Basic Properties and Applications of ZnO*, Elsevier Limited, 2006. 7, 8

[41] A R Hutson, "Piezoelectric and conductivity in ZnO and CdS", *Phys. Rev. Lett.*, vol. 4, no. 10, pp. 505, 1960. 7

[42] T Gao and T Wang, "Catalyst-assisted vapor-liquid-solid growth of single-crystal CdS nanobelts and their luminescence properties", *J. Phys. Chem. B*, vol. 108, no. 52, pp. 20045, 2004.

[43] Z L Wang, "Nanostructures of zinc oxide", *Materials Today*, vol. 7, no. 6, pp. 26, 2004. 7, 8

[44] L Vayssieres, K Keis, A Hagfeldt, and S-E Lindquist, "Three-dimensional array of highly oriented crystalline ZnO microtubes", *Chem. Mater.*, vol. 13, no. 12, pp. 4395, 2001. 8

[45] X-H Zhang, S-Y Xie, Z-Y Jiang, X Zhang, Z-Q Tian, Z-X Xie, R-B Huang, and L-S Zheng, "Rational design and fabrication of ZnO nanotubes from nanowire templates in a microwave plasma system", *J. Phys. Chem.*, vol. 107, pp. 10114, 2003. 8

[46] J Elias, R Tena-Zaera, G-Y Wang, and C Lévy-Clément, "Conversion of ZnO nanowires into nanotubes with tailored dimensions", *Chem. Mater.*, vol. 20, pp. 6633, 2008. 8

[47] Y Ma, C P Wong, X T Zeng, T Yu, Y Zhu, and Z X Shen, "Pulsed laser deposition of ZnO honeycomb structures on metal catalyst prepatterned si substrates", *J. Phys. D: Appl. Phys.*, vol. 42, pp. 065417, 2009. 8, 18

[48] A Rahm, G W Yang, M Lorenz, T Nobis, J Lenzner, G Wagner, and M Grundmann, "Two-dimensional ZnO:Al nanosheets and nanowalls ob-

tained by Al$_2$O$_3$-assisted carbothermal evaporation", *Thin Solid Films*, vol. 486, pp. 191, 2005. 8, 13, 23

[49] H-J Choi, *Semiconductor Nanostructures for Optoelectronic Devices,NanoScience and Technology*, Springer-Verlag Berlin Heidelberg, 2012. 8, 13, 14

[50] Z L Wang and J Song, "Piezoelectric nanogenerators based on zinc oxide nanowire arrays", *Science*, vol. 312, pp. 242, 2006. 9

[51] S Nadj-Perge, S M Frolov, E P A M Bakkers, and L P Kouwenhoven, "Spin-orbit qubit in a semiconductor nanowire", *Nature*, vol. 468, pp. 1084, 2010. 9, 101, 102

[52] P Yang, L E Greene, M Law, D H Tan, M Montano, J Goldberger, and G Somorjai, "General route to vertical ZnO nanowire arrays using textured ZnO seeds", *Nano Lett.*, vol. 5, no. 7, pp. 1231, 2005. 9, 24, 26

[53] N Petkov, J Volk, R Erdelyi, I E Lukacs, T Nagata, C Sturm, and M Grundmann, "Contacting ZnO individual crystal facets by direct write lithography", *ACS Appl. Mater. Interfaces*, vol. 8, pp. 23891, 2016. 9

[54] Chih-Wei Chuang, *III-V Nanowires and Nanoneedles on Lattice Mismatched Substrates for Optoelectronic Device Applications*, PhD thesis, University of California, Berkeley, 2009. 10, 13, 101

[55] Y W Zhu, H Z Zhang, X C Sun, S Q Feng, J Xu, Q Zhao, B Xiang, R M Wang, and D P Yu, "Efficient field emission from ZnO nanoneedle arrays", *Appl. Phys. Lett.*, vol. 83, no. 1, pp. 144, 2003. 10, 13

[56] Y Qin, R Yang, and Z L Wang, "Growth of horizonatal ZnO nanowire arrays on any substrate", *J. Phys. Chem. C*, vol. 112, no. 48, pp. 18734, 2008. 25

[57] S Xu, C Xu, Y Liu, Y Hu, R Yang, Q Yang, J-H Ryou, H J Kim, Z Lochner, S Choi, R Dupuis, and Z L Wang, "Ordered nanowire array blue/near-UV light emitting diodes", *Adv. Mater.*, vol. 22, pp. 4749, 2010. 10

[58] Z L Wang, "Piezopotential gated nanowire devices: Piezotronics and piezo-phototronics", *Nano Today*, vol. 5, pp. 540, 2010.

[59] E Saoutieff, M Allain, Y-R Nowicki-Bringuier, A Viana, and E Pauliac-Vaujour, "Integration of piezoelectric nanowires matrix onto a microelectronics chip", *Procedia Engineering*, vol. 168, pp. 1638, 2016. 12

[60] A Bouvet-Marchand, M Loubat, A Graillot, J Volk, R Dauksevicius, E Saoutieff, A Viana, C Christian, V Lebedev, C Sturm and C Loubat, "UV-crosslinked polymeric materials for encapsulation of ZnO nanowires in piezoelectric fingerprint sensors ", *Procedia Engineering*, vol. 168, pp. 1135, 2016. 12

[61] Y Zhang and Z L Wang, "Theory of piezo-phototronics for light-emitting diodes", *Adv. Mater.*, vol. 24, pp. 4712, 2012.

[62] S Xu and Z L Wang, "One-dimensional ZnO nanostructures: Solution growth and functional properties", *Nano Res.*, vol. 4, no. 11, pp. 1013, 2011. 12

[63] X Chen, C K Y Wong, C A Yuan, and G Zhang, "Nanowire-based gas sensors", *Sensors and Actuators B*, vol. 177, pp. 178, 2013. 12

[64] H Wang, B Kang, F Ren, L Tien, P Sadik, D Norton, S Pearton, and J Lin, "Hydrogen-selective sensing at room temperature with ZnO nanorods", *Appl. Phys. Lett.*, vol. 86, pp. 243503, 2005. 12

[65] Z Fan and J G Lu, "Chemical sensing with zno nanowire field-effect transistor", *IEEE Transaction on nanotechnology*, vol. 5, no. 4, pp. 393, 2006. 12

[66] C J Lee, T J Lee, S C Lyu, Y Zhang, H Ruh, and H J Lee, "Field emission from well-aligned zinc oxide nanowires grown at low temperature", *Appl. Phys. Lett.*, vol. 81, no. 19, pp. 3648, 2002. 13

[67] Y B Li, Y Bando, and D Golberg, "ZnO nanoneedles with tip surface perturbations: Excellent field emitters", *Appl. Phys. Lett.*, vol. 84, no. 18, pp. 3603, 2004. 2, 13

[68] R S Wagner and W C Ellis, "Vapor-liquid-solid mechanism of single crystal growth", *Appl. Phys. Lett.*, vol. 4, no. 5, pp. 89, 1964. 13

[69] A Rahm, M Lorenz, T Nobis, G Zimmermann, M Grundmann, B Fuhrmann, and F Syrowatka, "Pulsed-laser deposition and character-

ization of ZnO nanowires with regular lateral arrangement", *Appl. Phys. A*, vol. 88, pp. 31, 2007. 13, 14

[70] S R Hejazi and H R Madaah Hosseini, "A diffusion-controlled kinetic model for growth of Au-catalyzed ZnO nanorods: Theory and experiment", *Journal of Crystal Growth*, vol. 309, pp. 70, 2007. 13

[71] Y Zhao, C Li, M Chen, X Yu, Y Chang, A Chen, H Zhu, and Z Tang, "Growth of aligned ZnO nanowires via modified atmospheric pressure chemical vapor deposition", *Physics Letters A*, vol. 380, pp. 3993, 2016. 13

[72] A Menzel, K Komin, Y Yang, F Güder, Vanessa Trouillet, P Werner, and M Zacharias, "Ultra-long zinc oxide nanowires and boron doping based on ionic liquid assisted thermal chemical vapor deposition growth", *Nanoscale*, vol. 7, pp. 92, 2015. 14, 60

[73] W Yang, F Wan, S Chen, and C Jiang, "Hydrothermal growth and application of ZnO nanowire films with ZnO and $TiO_2$ buffer layers in dye-sensitized solar cells", *Nanoscale Res. Lett.*, vol. 4, pp. 1486, 2009. 14

[74] M Zinke-Allmang, "Phase separation on solid surfaces: nucleation, coarsening and coalescence kinetics", *Thin Solid Films*, vol. 346, pp. 1, 1999. 16, 17

[75] H von Wenckstern, H Schmidt, C Hanisch, and C Czekalla M Brandt, G Benndorf, G Biehne, A Rahm, H Hochmuth, M Lorenz, and M Grundmann, "Homoepitaxy of ZnO by pulsed-laser deposition", *Phys. Stat. Sol. (RRL)*, vol. 1, no. 4, pp. 129, 2007. 17

[76] H Nishinaka and S Fujita, "Step-flow growth of homoepitaxial ZnO thin films by ultrasonic spray-assisted MOVPE", *Journal of Crystal Growth*, vol. 310, pp. 5007, 2008. 17

[77] M Willander, O Nur, Q X Zhao, L L Yang, M Lorenz, B Q Cao, J Zúñiga-Pérez, C Czekalla, G Zimmermann, M Grundmann, A Bakin, A Behrends, M Al-Suleiman, A El-Shaer, A Che Mofor, B Postels, A Waag, N Boukos, A Travlos, H S Kwack, J Guinard, and D Le Si Dang, "Zinc oxide nanorod based photonic devices: recent progress in growth, light emitting diodes

and lasers", *Nanotechnology*, vol. 20, no. 332001, pp. 332001–332040, 2009. 18, 53, 60, 96

[78] Y Li, R Jia, W Zhang, M Ni, and Z Wang, "Stranski-krastanov model grown ZnO thin films", in *International Conference on Manipulation, Manufacturing and Measurement on the Nanoscale (3M-NANO)*, 2015. 18

[79] Martin Lange, *Herstellung und Charakterisierung von planaren und drahtförmigen Heterostrukturen mit ZnO- und ZnCdO-Quantengräben*, PhD thesis, Universität Leipzig, 2012. 3, 21, 31, 50, 51, 52

[80] U Diebold, L Vogel Koplitz, and O Dulub, "Atomic-scale properties of low-index ZnO surfaces", *Applied Surface Science*, vol. 237, pp. 336, 2004. 21

[81] N T K Thanh, N Maclean, and S Mahiddine, "Mechanisms of nucleation and growth of nanoparticles in solution", *Chem. Rev.*, vol. 114, pp. 7610, 2014. 21

[82] A Cacciuto, S Auer, and D Frenkel, "Solid-liquid interfacial free energy of small colloidal hard-sphere crystals", *J. Chem. Phys.*, vol. 119, no. 14, pp. 7467, 2003. 21

[83] K F Kelton and A L Greer, *Nucleation in Condensed Matter: Applications in Materials and Biology*, Elsevier, 2010. 21, 22, 42, 53, 56, 63, 71, 73, 74

[84] E G Wolff and T D Coskren, "Growth and morphology of magnesium oxide whiskers", *J. Am. Ceram. Soc.*, vol. 48, no. 6, pp. 279, 1965. 23

[85] S Hayashi and H Saito, "Growth of magnesia whiskers by vapor phase reactions", *Journal of Cryst. Growth*, vol. 24/25, pp. 345, 1974. 23

[86] B D Yao, Y F Chan, and N Wang, "Formation of ZnO nanostructures by a simple way of thermal evaporation", *Appl. Phys. Lett.*, vol. 81, no. 4, pp. 757, 2002. 23

[87] M Lorenz, J Lenzner, E M Kaidashev, H Hochmuth, and M Grundmann, "Cathodoluminescence of selected single ZnO nanowires on sapphire", *Ann. Phys. (Leipzig)*, vol. 13, no. 1-2, pp. 39, 2004. 23, 36, 72

[88] J Y Lao, J G Wen, and Z F Ren, "Hierarchical ZnO nanostructures", *Nano Lett.*, vol. 2, no. 11, pp. 1287, 2002. 23

[89] R A McBride, J M Kelly, and D E McCormack, "Growth of well-defined zno microparticles by hydroxide ion hydrolysis of zinc salts", *J. Mater. Chem.*, vol. 13, pp. 1, 2003. 24

[90] C M García, E D Valdés, A M Paniagua Mercado, A F Méndez Sánchez, J A A Adame, V Subramaniam, and J R Ibarra, "Synthesis of aluminum-doped zinc oxide nanowires hydrothermally grown on plastic substrate", *Adv. in Mat. Phys. and Chem*, vol. 2, pp. 56, 2012. 24

[91] H E Unalan, P Hiralal, N Rupesinghe, S Dalal, W I Milne, and G A J Amaratunga, "Rapid synthesis of aligned zinc oxide nanowires", *Nanotechnology*, vol. 19, pp. 255608, 2008. 24

[92] H Hu, X Huang, C Deng, X Chen, and Y Qian, "Hydrothermal synthesis of zno nanowires and nanobelts on a large scale", *Materials Chemistry and Physics*, vol. 106, pp. 58, 2007. 24

[93] A Y Cho and j R Arthur, "Molecular beam epitaxy", *Progress in Solid-State Chemistry*, vol. 10, pp. 157, 1975. 24

[94] Y-W Heo, B S Kang, L C Tien, D P Norton, F Ren, J R La Roche, and S J Pearton, "UV photoresponse of single ZnO nanowires", *Appl. Phys. A*, vol. 80, pp. 497, 2005. 24

[95] D P Norton, Y W Heo, I P Ivill, K Ip, S J Pearton, M F Chisholm, and T Steiner, "ZnO: growth, doping & processing", *Materials Today*, vol. 7, pp. 34, 2004. 24, 26

[96] H Ghayour, H R Rezaie, S Mirdamadi, and A A Nourbakhsh, "The effect of seed layer thickness on alignment and morphology of ZnO nanorods", *Vacuum*, vol. 86, pp. 101, 2011. 3, 27, 36, 39, 40

[97] C Durand, C Dubourdieu, C Vallèe, V Loup, M Bonvalot, O Joubert, H Roussel, and O Renault, "Microstructure and electrical characterizations of yttrium oxide and yttrium silicate thin films deposited by pulsed liquid-injection plasma-enhanced metal-organic chemical vapor deposition", *J. Appl. Phys.*, vol. 96, no. 3, pp. 1719, 2004. 28, 29

[98] S N Das, J P Kar, J Xiong, and J-M Myoung, *Synthesis of ZnO Nanowire by MOCVD Technique: Effect of Substrate and Growth Parameter, Nanowires - Recent Advances*, InTech, 2011. 9, 28

[99] P-C Chang, Z Fan, D Wang, W-Y Tseng, W-A Chiou, J Hong, and J G Lu, "ZnO nanowires synthesized by vapor trapping cvd method", *Chem. Mater.*, vol. 16, pp. 5133, 2004. 28

[100] K-S Kim and H W Kim, "Structural characterization of zno thin film grown on si-based substrates by metal organic chemical vapor deposition", *Journal of the Korean Physical Society*, vol. 42, pp. S149, 2003. 28

[101] B Q Cao J Zúñiga-Pérez, N Boukos, C Czekalla, H Hilmer, J Lenzner, A Travlos, M Lorenz, and M Grundmann, "Homogeneous core/shell ZnO/ZnMgO quantum well heterostructures on vertical ZnO nanowires", *Nanotechnology*, vol. 20, no. 305701, 2009. 31, 60

[102] B K B H Krischner, *Röntgenstrukuturanalyse und Rietveldmethode*, Vieweg, 1994. 33

[103] L Spiess, R Schwarzer, H Behnken, and G Teichert, *Moderne Röntgenbeugung*, B. G. Teubner, 2005. 33

[104] Michael Bonholzer, *Magnetic Tunnel Junctions based on spinel $Zn_xFe_{3-x}O_4$*, PhD thesis, Universität Leipzig, 2016. 33, 34, 35

[105] Helena Franke, *PLD-grown ZnO-based Microcavities for Bose-Einstein Condensation of Exciton-Polaritons*, PhD thesis, Universität Leipzig, 2012. 33, 34, 72, 96, 102

[106] G Binnig, C F Quate, and C Gerber, "Atomic force microscope", *Phys. Rev. Lett*, vol. 56, pp. 930, 1986. 34

[107] Park Systems Corporation, *XE-150 User Manual*, 1.8.2 edition, 2009. 34

[108] D Nečas and P Klapetek, "Gwyddion: an open-source software for SPM data analysis", *Open Physics*, vol. 10, pp. 181, 2012. 34

[109] H Bethge, *Electron microscopy in solid state physics*, Elsevier, Amsterdam, 1987. 35

[110] B Q Cao J Zúñiga-Pérez, N Boukos, C Czekalla, H Hilmer, J Lenzner, A Travlos, M Lorenz, and M Grundmann, "Tuning the lateral density of

ZnO nanowire arrays and its application as physical templates for radial nanowire heterostructures", *J. Mater. Chem.*, vol. 20, pp. 3848, 2010. 36

[111] H Fujiwara, *Spectroscopic ellipsometry: Principles and applications*, Wiley, 2007. 36

[112] R Schmidt-Grund, "Labcourse semiconductor physics experimental methods in semiconductor physics and optoelectronic devices", Universität Leipzig. 36

[113] L Zhang, D Wett, R Szargan, and T Chassé, "Determination of ZnO (0001) surface termination by x-ray photoelectron spectroscopy at photoemission angles of $0^o$ and $70^o$", *Surf. Interface Anal.*, vol. 36, pp. 1479, 2004. 37, 44

[114] A N Mariano and R E Hanneman, "Crystallographic polarity of zno crystals", *J. Appl. Phys.*, vol. 34, no. 2, pp. 384, 1963. 38

[115] E P Warekois, M C Lavine, A N Mariano, and H C Gatos, "Crystallographic polarity in the ii-vi compounds", *J. Appl. Phys.*, vol. 33, pp. 690, 1962. 38

[116] M Mehta and C Meier, "Controlled etching behavior of O-polar and Zn-polar ZnO single crystals", *Journal of The Electrochemical Society*, vol. 158, no. 2, pp. H119, 2011. 38

[117] A L Patterson, "The scherrer formula for X-ray particle size determination", *Phys. Review*, vol. 56, pp. 978–982, 1939. 42

[118] A P Samantilleke, L M F Rebouta, V Garim, L Rubio-Pe na, S Lenceros-Mendez, P Alpuim, S Carvalho, A V Kudrin, and Y A Danilov, "Cohesive strength of nanocrystalline ZnO:Ga thin films deposited at room temperature", *Nanoscale Res. Lett.*, vol. 6, pp. 309, 2011. 42

[119] T Dieing and B F Usher, "Wafer curvature in molecular beam epitaxy grown heterostructures", *PHYSICAL REVIEW B*, vol. 67, pp. 054108, 2003.

[120] B Simović, A Golubović, I Veljković, D Poleti, J Zdravković, D Mijin, and A Bjelajac, "Hydro- and solvothermally-prepared ZnO and its catalytic effect on the photodegradation of reactive orange 16 dye", *J. Serb. Chem. Soc.*, vol. 79, no. 11, pp. 1433, 2014. 44

[121] G Perillat-Merceroz, R Thierry, P-H Jouneau, P Ferret, and G Feuillet, "Compared growth mechanisms of Zn-polar ZnO nanowires on O-polar ZnO and on sapphire", *Nanotechnology*, vol. 23, pp. 125702, 2012.

[122] Y-W Heo, S-Y Kim, J-H Lee, and J-J Kim, "Effects of temperature, target/substrate distance, and background pressure on growth of ZnO nanorods by pulsed laser deposition", *J. Nanosci. Nanotechnol.*, vol. 14, no. 12, pp. 9020, 2014. 60

[123] T Michalsky, H Franke, R Buschlinger, U Peschel, M Grundmann, and R Schmidt-Grund, "Coexistence of strong and weak coupling in ZnO nanowire cavities", *Eur. Phys. J. Appl. Phys.*, vol. 74, pp. 30502, 2016. 60

[124] B J Kwon, K M Lee, H-Y Shin, J Kim, J Liu, S Yoon, S Lee, Y H Ahn, and J-Y Park, "Synthesis of vertical arrays of ultralong ZnO nanowires on noncrystalline substrates", *Materials Science and Engineering B*, vol. 177, pp. 132, 2011. 60

[125] C Gu, L Shanshan, J Huang, C Shi, and J Liu, "Preferential growth of long ZnO nanowires and its application in gas sensor", *Sensors and Actuators B*, vol. 177, pp. 453, 2013. 60

[126] J Schmalian, "Lecture notes, statistical mechanics (Theory F)", Tech. Rep., Karlsruhe Institute of Technology, 2012. 18, 75

[127] B K Meyer, H Alves, D M Hofmann, W Kriegseis, D Forster, F Bertram, J Christen, A Hoffmann, M Strassburg, M Dworzak, U Haboeck, and A V Rodina, "Bound exciton and donor-acceptor pair recombinations in ZnO", *Phys. Stat. Solid. (b)*, vol. 241, no. 2, pp. 231, 2004. 72, 96

[128] J-P Richters, T Voss, D S Kim, R Scholz, and M Zacharias, "Enhanced surface-excitonic emission in $ZnO/Al_2O_3$ core-shell nanowires", *Nanotechnology*, vol. 19, pp. 305202, 2008. 72

[129] S K Lim, S H Hong, S-H Hwang, W M Choi, S Kim, H Park, and M G Jeong, "Synthesis of Al-doped ZnO nanorods via microemulsion method and their application as a CO gas sensor", *Journal of Materials Science & Technology*, vol. 31, pp. 639, 2015. 77

[130] J B Baxter and E S Aydil, "Epitaxial growth of ZnO nanowires on a- and c-plane sapphire", *Journal of Crystal Growth*, vol. 274, pp. 407, 2005. 91

[131] E R Dobrovinskaya, L A Lytvynov, and V Pishchik, *Sapphire: Material, Manufacturing, Applications*, Springer, 2009. 91

[132] F Tendille, P DeMierry, P Vennéguès, and S Chenot, "Defect reduction method in (11-22) semipolar gan grown on patterned sapphire substrate by mocvd: Toward heteroepitaxial semipolar gan free of basal stacking faults", *Journal of Crystal Growth*, vol. 404, pp. 177–183, 2014. 92

[133] P de Mierry, N Kriouche, M Nemoz, S Chenot, and G Nataf, "Semipolar GaN films in patterned r-plane sapphire obtained by wet chemical etching", *Appl. Phys. Lett.*, vol. 96, no. 213918, pp. 213918–1 – 213918–3, 2010. 92

[134] L Xu, X Li, Z Zhan, L Wang, S Feng, X Chai, W Lu, J Shen, Z Weng, and J Sun, "Catalyst-free, selective growth of ZnO nanowires on $SiO_2$ by chemical vapor deposition for transfer-free fabrication of UV photodetectors", *Appl. Mater. Interfaces*, vol. 7, pp. 20264, 2015. 92

[135] S Dag, S Wang, and L-W Wang, "Large surface dipole moments in ZnO nanorods", *Nano Lett.*, vol. 11, pp. 2348, 2011. 102